Dissolution improvement of albendazole by reconstitutable dry nanosuspension formulation

Ph.D. thesis

Dr. Viktor Fülöp

Semmelweis University
Doctoral School of Pharmaceutical Sciences

Supervisor: Dr. István Antal, D.Sc.

Official reviewers: Dr. Ildikó Bácskay, D.Sc.

Dr. Angéla Jedlovszky-Hajdú, Ph.D.

Chairman of the Final Examination Committee:

Dr. Klára Gyires, D.Sc.

Members of the Final Examination Committee:

Dr. Éva Szökő, D.Sc.

Dr. Miklós Vecsernyés, D.Sc.

Budapest
2020

Table of contents

List of abbreviations

Abbreviation	Explanation
ABZ	Albendazole
IR	Immediate release
BCS	Biopharmaceutics classification system
Log P	Lipophilicity, the octanol-water partition coefficient of a molecule
m. p.	Melting point
PEGs	Polyethylene-glycols
PVAs	Polyvinyl-alcohols
TPGS 1000	d-α-tocopherol polyethylene glycol 1000 succinate
(PEO-PPO-PEO)	poly-(ethylene oxide)-poly-(propylene oxide)
SLS	Sodium laurylsulphate
DOSS	Dioctyl sulfo succinate sodium
PEI	Poly-(ethylene imine)
RES	Reticuloendothelial system
HPLC-MS	High-performance liquid chromatography physical separation combined with mass spectrometry analytical method
NSAID	Non-steroidal anti-inflammatory drug
MPS	Mononuclear phagocytic system
scAbCD3	single chain T–cell specific CD3 ligand
scAbCD3-PEG-g-PEI	Single chain T–cell specific CD3 ligand binded to the distal end of the Poly-(ethylene glycol)-grafted polyethylene imine
SPIONs	Superparamagnetic iron oxide nanoparticles

Abbreviation	Explanation
MRI	Magnetic resonance imaging
IL-2	Interleukin-2
PLGA-PEO	Poly-(lactic-co-glycolic acid)
LD50	Median lethal dose
NOEL	Non observed effect level
MRLs	Maximal residue limit
FASSIF	Fasted state simulated intestinal fluid
FESSIF	Fed state simulated intestinal fluid
LD	Laser diffractometry
PCS	Photon correlation spectroscopy
DLS	Dynamic light scattering
ELS	Electrostatic light scattering
XRD	X-ray diffraction analysis
PXRD	Powder X-ray diffractometry
DSC	Differential scanning calorimetry
FT-IR	Fourier transform infrared spectroscopy
SEM	Scanning electron microscopy
AFM	Atomic force microscopy
TEM	Transmission electron microscopy
IPA	Isopropanol
NMP	N-methylpyrrolidone
PGs	Propylene glycols
S	Solvent
AS	Antisolvent
HGCP	High-gravity controlled precipitation
RPB	Rotating packed bed
SCF	Supercritical fluid
RESS	Rapid expansion of supercritical solution
RESS-SC	Rapid expansion of supercritical solution with solid cosolvent

Abbreviation	Explanation
RESOLV	Rapid expansion of a supercritical solution into a liquid solvent
RESAS	Rapid expansion from supercritical to aqueous solution
SAS	Supercritical anti-solvent
CLIJ	Confined liquid impinging jets
HFAs	Hydrofluoroalkanes
SFL	Spray freezing into liquid
HPH	High pressure homogenization
IDD-T™ technology	Insoluble drug delivery technology
HPMC	Hypromellose
[CLH]	Hepatic clearance
CYP enzymes	Cytochrome P450 enzymes
CYP1A2	1A2 isoenzyme of the cytochrome P450 enzymes
CYP3A4	3A4 isoenzyme of the cytochrome P450 enzymes
CYP1A1	1A1 isoenzyme of the cytochrome P450 enzymes
API	Active pharmaceutical ingredient
Transcutol	Diethylene glycol monoethylether
AUC	Area under the plasma concentration curve
ABZSX/ABZSO	Albendazole sulfoxide
$ABZSO_2$	Albendazole sulfone
C_{max}	Maximal plasma concentration
MCC	Microcrystalline cellulose
DOE	Design of experiments
OVAT	One variable at a time

Abbreviation	Explanation
CMA	Critical material attributes
CQA	Critical quality attributes
CPP	Critical process parameters
WSSM	Wet stirred media milling
NIBS	Non-invasive-backscattering
Z AVG d	Intensity-weighted mean hydrodynamic diameter
PDI	Polydispersity index (width of particle size distribution measured by PCS/DLS)
D [4,3]	Volume-weighted mean particle size
Span	Width of a particle size distributions measured by LD method
LOD	Loss on drying
QbD	Quality by design
ARF	Artificial rumen fluid
NY	Nylon
DCR	Derived count rate
PTFE	Polytetrafluoroethylene
RH	Relative humidity
HLB	Hydrophilic-lipophilic balance

1. Introduction

Albendazole (ABZ) is a broad spectrum anthelmintic with poor aqueous solubility, which vastly inhibits its therapeutic effectiveness. In order to counter this undesirable biopharmaceutical property suitable formulation optimization is required for enhancing water solubility and dissolution rate. This study summarizes the development and formulation factors of albendazole containing nanosuspension, which was post processed by wet granulation and subsequent tray-drying to improve physical stability. Top-down bead milling method was applied for particle size reduction. Thermodynamic solubility, dissolution studies and solid state characterization of granules have been conducted comparing the behavior of the active substance with the dispersion containing unmilled and milled active.

1.1. Poorly water-soluble chemical compounds and classifications

There are many well know physicochemical factors limiting the bioavailability of orally administered solid dosage forms. One of the major obstacles of the development of highly potent new drug candidates is the poor water solubility of these compounds, which greatly hinders their therapeutic application [1]. Nowadays, about 40% of the marketed immediate release (IR) oral drugs are categorized as practically insoluble (< 100 µg/ml) [2]. The biopharmaceutics classification system (BCS) takes two of these limiting factors into consideration the solubility and the membrane permeability, distinguishing four classes of drug substances upon low and high values (**Table I)**.

Table I. *The biopharmaceutical classification system (BCS)* [3]

Membrane permeability	***Water solubility***	
	Low	***High***
Low	class IV	class III
High	class II	class I

Formulation of class II. and IV. candidates are the most challenging, where bioavailability is limited by either solubility or both solubility and permeability [4]. The poorly soluble "grease ball molecules" (BCS class II) represent highly lipophilic compounds with high log P values, which are not able to form bonds with water molecules, so solubility is limited by solvation, whereas "brick dust molecules" (BCS class IV.) usually have high melting point (m. p. >200 ^{0}C) and low log P values. "Brick dust molecules" have high lattice energy and their solubility in water and oils is restricted by the intermolecular bonds within the crystalline structure [5–7]. "Grease ball molecules" have easily passed through the drug development process procedure to reach the market by adopting appropriate commonly used formulation strategies. Application of these strategies on "brick dust molecules" however do not work effectively due to low encapsulation efficiency and low loading, so the "brick dust molecules" were readily withdrawn during the drug development stage until 1995, when Müller et al. (1998) firstly developed nanosuspensions, a sub-micro colloidal dispersion system, in order to overcome these limitations [8].

1.2. Pharmaceutical nanosuspensions

Pharmaceutical nanosuspension is defined as colloidal, biphasic systems, where solid drug particles (nanocrystals) are very finely dispersed in an aqueous vehicle, without any matrix material, stabilized by surfactants and/or polymers. Favorable for drug delivery purposes, where small doses are preferred, like oral, topical, parenteral, ocular and pulmonary routes of administrations [9]. The particle size of the solid particles (nanocrystals) in nanosuspensions is usually less than 1 μm with a mean particle size ranging between 200 and 600 nm [10].

1.2.1. Stability and stabilization principals of nanosuspensions

Ostwald-ripening (described previously by the Ostwald-Freundlich equation (Eq. (3)) determined for ultrafine dispersed systems and is responsible for crystal growth (aggregation and precipitation). These agglomerates have a higher settling rate according to the Stoke's law (Eq. (10)):

$$v = \frac{2 \times r^2 \times (\rho_1 - \rho_2) \times g}{9 \times \eta} \quad \textbf{(10)}$$

Where v is the settling rate of particles, with radius of r and true density of ρ_1, ρ_2 is the true density of dispersant, g is the gravitational acceleration and η is the viscosity of the dispersant. In order to slow the settling rate, increasing the viscosity of the dispersant and decreasing the density differences between phases can be achieved by the application of polymers with high molecular weight values. In addition increasing the uniformity of particle size distributions by removing large particles via centrifugation or filtering can also be taken into consideration [11,12].

The balance between attractive and repulsive forces among particles in suspensions has been quantitatively visualized by the classical Derjaguin, Landau, Verwey, Overbeek (DLVO) theory. This hypothesis assumes, that there is a balance between the repulsive interaction between the electrically charged and the attractive interactions arising from van der Walls forces between the particles. The thickness of the double layer is a major component in strongly affecting the shape of the function (**Figure 1**). The latter is dependent on the ionic strength of the system and on the presence of surface-modifying agents and/or adsorbed polymers.

When this double layer is thin, typically obtained by increasing the ionic strength, the function shows a secondary minimum at (relatively) large separation, typical to particles in the micron size range.

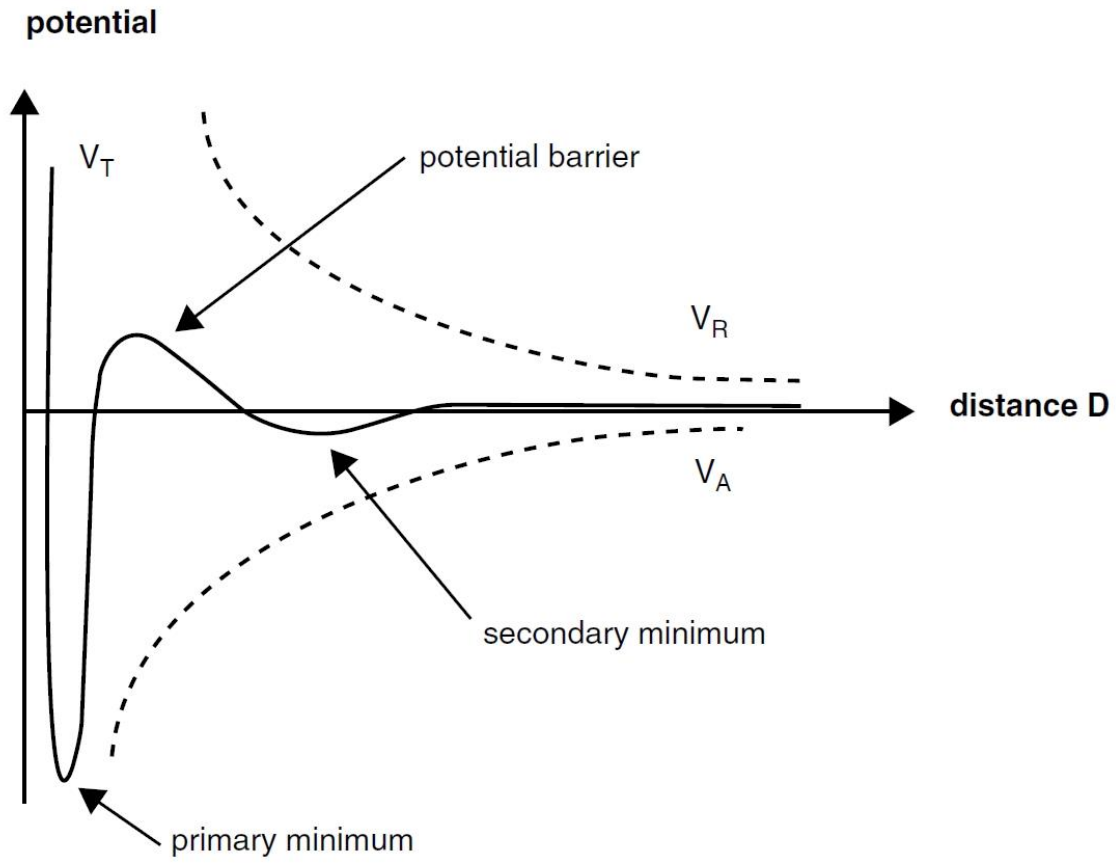

Figure 1. *DLVO theory, where V_A–Attractive (van der Waals) potential energy, V_R–Repulsive (electrostatic) potential energy, V_T–Total potential energy* [13]

Aggregation of the particles arising from the stabilizing effect of this secondary minimum is called "flocculation". Flocculated material can often be redispersed by simple agitation because the well (and the energy barrier) is normally very shallow. An irreversible aggregation of small particles into large aggregates (specified as coagulation) takes place when the distance between the particles is small and they enter the primary minimum of the potential energy curve, where the van der Walls forces are controlling the reaction [13–15].

During a milling process, selection of stabilizer(s) is the crucial step for successful accelerated breakdown of raw materials (Rehbinder effect) [16,17] and stabilization of newly formed nanocrystals, reported as the first step in the quality by design concept of nanosuspension development [18]. Therefore, the application of stabilizers is often necessary to avoid particle agglomerations and reduce the possibility of Ostwald-ripening [19]. Stabilizer surfactants prevent the aggregation of nanocrystals by either sterically (non-ionic surfactants) or electrostatically (ionic surfactants) [20]. Steric stabilization occurs, when polymers are absorbed onto the surfaces of nanoparticles and the thermal motion of polymer chain molecules create a dynamically rough surface, preventing coalescence by generating repulsive entropic forces [21].

The adsorption of nonionic surfactants on solid surfaces from aqueous solutions is important for controlling many properties including wetting, dispersion, and rheology. Nonionic surfactants are also advantageous because they can be mixed with other surfactants to enhance properties that are not easily attained without surfactant blends (e. g. stabilization of nanosuspensions). The adsorption of surfactants at the solid/liquid interface is strongly influenced by a number of factors including the nature of the structural groups on the solid surface, the molecular structure of the surfactant, and the environment of the aqueous phase (pH, temperature, electrolyte content, etc.). The wetting process is a three-phase equilibrium that is described by Young's equation (Eq. (11)):

$$\cos\theta = \frac{\gamma_{SV} - \gamma_{SL}}{\gamma_{LV}} \qquad \textbf{(11)}$$

where θ is the contact angle, γ_{SV} is the surface tension at the solid/vapor interface, γ_{SL} is the surface tension at the solid/liquid interface, and γ_{LV} is the surface tension at the liquid/vapor interface. Complete wetting occurs when $\cos\theta = 1$ [22].

Wenzel modified Young's equation (Eq. (12)) and proposed a well-known equation for the contact angle of liquids on a rough homogeneous surface θ_w, which is as follows:

$$\cos\theta_w = r \times \frac{\gamma_{SV} - \gamma_{SL}}{\gamma_{LV}} = r \times \cos\theta \quad \textbf{(12)}$$

where *r* is the roughness factor defined as the ratio of the actual surface area of the rough surface to the geometric projected area. The wetting for heterogeneous surfaces is traditionally described by the Cassie equation (Eq. (13)):

$$\cos\theta_c = f_1 \times \cos\theta_1 + f_2 \times \cos\theta_2 \quad \textbf{(13)}$$

where θ_c is the Cassie contact angle; f_1 and f_2 are the fractions of materials 1 and 2 on the surface, respectively. θ_1 and θ_2 represent the intrinsic contact angles of the liquid solid interface for materials 1 and 2, that can be calculated from the Young's equation (Eq. (11)). Quéré et al. studied rough hydrophobic surfaces (Eq. (14)), to understand the wetting behavior of such surfaces, they combined equations (12) and (13):

$$\cos\theta_{cr} = \frac{f-1}{r-f} \quad \textbf{(14)}$$

where θ_{cr} is the critical intrinsic contact angle, *f* the fractions, *r* is the roughness factor of surfaces [23].

Most commonly used non-ionic (steric) stabilizers for the formulation of nanosuspensions include polysorbates, polyethylene-glycols (PEGs), polyvinyl-alcohols (PVAs), povidones, poloxamers, lecithins, polyoleates, d-α-tocopherol polyethylene glycol 1000 succinate or TPGS 1000 (vitamin E), block copolymers of poly-(ethylene oxide)-poly-(propylene oxide) (PEO-PPO-PEO) (Pluronics®) and cellulose derivates [9,19,20,24,25]. Ionic stabilizers, like sodium laurylsulphate (SLS), dioctyl sulfo succinate sodium (DOSS), poly-(ethylene imine) (PEI) and chitosan generate electrostatic repulsions between nanoparticles by creating charged surfaces. Zeta-potential provides information about the surface charge properties and further the long-term physical stability of colloidal dispersions.

In order to obtain an electrostatically stabilized nanosuspension, a minimum zeta potential of ± 30 mV is required. Combination of steric and ionic surfactants often preferred [20,24,26]. In case of a combination of electrostatic and steric stabilization, a minimum zeta potential of ± 20 mV is desirable [20,27,28].

Post processing nanosuspensions into solid dosage forms in order to improve physical stability and shelf life has also shown great interest e. g. spray-drying [29,30], freeze-drying [31], fluid bed coating [32], electro spraying [33] and hot melt extrusion [34] techniques have been successfully applied developing various formulations containing redispersable nanocrystals.

1.2.2. Surface modifications of nanocrystals

Rapid, or burst release of drugs from nanosuspensions may cause toxicity and severe side effects. Therefore, surface modification is advised in order to control drug release and/or achieving prolonged residence of the actives at the site of action [35–37]. Targeted drug delivery can also be achieved, by modifying the surfaces of nanoparticles, e. g. PEG is commonly used to reduce immune response and degradation (e. g. protein adsorption and opsonization of nanoparticles), that leads to prolonged systemic circulation time (half-life) [38]. Longer circulation time allows nanoparticles to easily leak out from highly vascularized infective and inflammatory tissues, including cancer tissues [39,40]. Carefully engineered nanoparticles surfaces can also effectively target the diseased tissues and cross specific barriers, e. g. nanoparticles coated by classical steric stabilizers (Tween 20, 40, 60, and 80) can effectively deliver peptide dalargin across the blood-brain barrier [41].

1.2.3. Benefits and disadvantages of the utilization of nanocrystals

The potential benefits of the nanosuspension technology for poorly soluble drug delivery are increased drug dissolution rate, increased rate and extent of absorption, hence refined pharmacokinetics of an active (area under plasma concentration versus time curve, onset time, peak plasma level), reduced variability and reduced fed/fasted effects. They have low incidence of side effects caused by the excipients, increased resistance to hydrolysis, oxidation and increased physical stability to settling. Reduced administration volumes are essential for intramuscular, subcutaneous, and ophthalmic delivery.

By surface modifications they can also provide the passive targeting [26,42,43].

The vulnerable structures of protein/peptide biologically active compounds create challenges for formulation development. Maschke et al. (2006) attempted to micronize crystalline bovine insulin in the medium of Myglyol 812 with high pressure homogenization method. 100% of the particles were nanosized at 1500 bar applied homogenization pressure after 6 cycles. The influence of high pressure homogenization (HPH) on insulin stability and bioactivity was investigated by HPLC-MS analysis as well as in a chondrocyte proliferation assay and reported, that despite of the harsh HPH process conditions the stability and bioactivity of the insulin were maintained [44].

Merisko-Liversidge et al. (2004) also noticed retained stability and bioactivity of the non-crystalline zinc-insulin nanosuspensions, that were produced through a wet-milling process in presence of Pluronic® F68 and sodium deoxycholate. Chemical stability data were acceptable when compared the HPLC chromatograms of freshly prepared insulin to a nanoparticle formulation stored for 2 months under refrigeration conditions. There were no significant changes detected. In addition, the absence of significant degradation following heat treatment of the nanoparticle formulation suggested, that formulating insulin as a peptide nanoparticle dispersion shields the molecule from insults, that could significantly impact its chemical integrity [45].

Merisko-Liversidge et al. (2003) compared the maximal tolerated doses of various intravenously administered formulations of anticancer agents (Camptothecin, Etoposide, Paclitaxel) and the human pharmacokinetical parameters of the non-steroidal anti-inflammatory drug (NSAID) naproxen in marketed IR tablet, suspension and nanosuspension formulations [46].

The authors reported, that no death cases were observed, even at higher doses of administered nanocrystalline particles of anticancer agents compared to marketed products and solubilized (ethanol/Tween 80) formulations during the investigation. The authors also mentioned, that for intravenous delivery maximum tolerated dose can be increased by five- to ten-fold in comparison to solubilized formulations with the aid of solvent, surfactants and cyclodextrins. The authors were trying to explain this phenomenon by two separate theories. Regarding the first scenario, the population of nanoparticles, that avoids sequestration by the mononuclear phagocytic system (MPS) is capable to deliver a sufficient amount of active to the site of action [47–49]. Alternatively, the Kupffer cells of the liver can act as a controlled release vehicles (depot) of the nanonized active compound [50,51].

Application of the nanocrystalline formulation of naproxen approximately halved the T_{max} value and improved $AUC_{0\text{-}1\ h}$ value by 2.5 and 4.52 times compared to naproxen suspension (Naprosyn®) and IR tablet (Anaprox®) formulations, respectively [46].

Comparing with microparticles, drug nanocrystals have another outstanding feature because they can distinctly increase adhesiveness to surface/cell membranes. An increased adhesiveness of nanomaterials is usually due to an increased contact area of small particles versus large particles (at identical total particle mass). Similar to other nanoparticles, drug nanocrystals show an increased adhesiveness to tissues, which lead to an improvement of oral absorption and penetration capability in case of topical routes of administrations [52].

The ease of scale-up and low bath-to-batch variability could be mentioned as the main advantages of the production of nanosuspensions, while the most common disadvantages are high energy investment during manufacturing, immunotoxicity and non-specific uptake in reticuloendothelial system (RES) organs [26,42,43,53]. The latter can reduce the plasma concentration of actives, although it is not a clear disadvantage because these cells can act as depot of the nanoparticles, especially in case of prodrugs, mentioned above. Nevena S. Zogovic et al. (2009) reported the opposite effect of nanocrystalline fullerene (C_{60}) on tumor cell growth in vitro and in vivo.

The authors have drawn attention to immunosuppression as a potential side-effect of nanocrystalline fullerene-based therapeutic approaches, although these data at the same time supported investigation of C60-mediated immunoregulation in controlling excessive immune responses such as those in autoimmune and hypersensitivity disorders [54].

Jana Tulinska et al. (2013) have investigated the immunotoxicity and genotoxicity of poly-(Lactic-co-Glycolic Acid) (PLGA-PEO) nanoparticle on human blood cell models. Results have concluded that there was a dose dependent toxicity. Up to a dose of 3 μg/cm^2, no cytotoxicity was observed, however significant stimulation of phagocytic activity of granulocytes (119%) > monocytes (117%) and respiratory burst of phagocytes (122%) was recorded. At above 75 μg/cm^2 (424 μg/ml) dose however, significant decrease in [3H]-thymidine incorporation into DNA of proliferating cells after 4 h (70% of control) and 48 h (84%) exposure to nanoparticles were reported. In middle dosed cultures (3 μg/cm^2–75 μg/cm^2) the inhibition of proliferative function was the most significant in T-cells stimulated with CD3 antigen (up to 84%). Cytotoxicity of NK-cells was suppressed moderately (92%), but significantly after 4 h of exposure. After 24 h of exposure, cytotoxic activity did not differ from the controls, so the induced dose dependent cytotoxicity was reversible. Genotoxicity assessment has revealed no increase in the number of micro nucleated binucleated cells and no induction of SBs or oxidized DNA bases in PLGA-PEO nanoparticle treated peripheral blood cultures [55].

There are also nanocrystals designed especially for immunosuppressive therapies. Chen Guihua et al. (2009) have developed a non-viral vector, that effectively transports genes into T-cells by attaching a T-cell specific ligand, the CD3 single chain antibody (scAbCD3), to the distal ends of poly-(ethylene glycol)-grafted polyethylene imine (scAbCD3-PEG-g-PEI). This polymer was first complexed with superparamagnetic iron oxide nanoparticles (SPIONs) and was then used to condense plasmid DNA into nanoparticles. This delivery system has led to a 16-fold of enhancement in the gene transfection level in HB8521 cells, a rat T-lymphocyte line. This targeting event in cell culture was successfully imaged by MRI scan and resulted in a 43% inhibition in the stimulated proliferation of HB8521 cells as well as a 38% inhibition in the expression of a major functional cytokine interleukin-2 (IL-2), indicating the effective T-cell anergy induced by gene therapy.

The results revealed a great potential of this compound nano-system as a MRI-trackable and T-lymphocyte-targeted gene carrier in post transplantation immunotherapy [56].

1.2.4. Physicochemical characteristics of nanocrystals

The mean particle size, width of particle size distribution (span or polydispersity index PDI), the crystalline state, particle morphology, along with zeta potential are the main critical quality attributes (CQA) of nanosuspensions.

The mean particle size and the width of particle size distributions could be measured by several techniques such as laser diffractometry (LD), photon correlation spectroscopy (PCS) or dynamic light scattering (DLS).

Zeta-potential usually measured by electrostatic light scattering (ELS) provides information about the surface charge properties and can predict the long-term physical stability of colloidal dispersions.

The determination of the crystalline state and particle morphology together helps in understanding the polymorphic/amorphous or morphological changes that a drug might undergo when subjected to nanosizing. These techniques can offer invaluable information on the assessment of stability, detecting any changes, which can have a distinct impact on manufacturing, storage, bioavailability and/or safety.

To track the crystalline amorphous transformation x-ray diffraction analysis (XRD), FT-IR and Raman spectroscopies, differential scanning calorimetry (DSC) are the most commonly used methods.

Scanning electron microscopy (SEM), atomic force microscopy (AFM) and transmission electron microscopy (TEM) are routinely used to characterize the size and morphology of nanoparticles [57].

Table II summarizes the nanocrystal containing products currently available on the market.

Table II. *Examples of nanocrystal products on the market* [58–60]

Trade name (API)	**Therapy**	**Applied technology**	**Pharma company**
Rapamune (Rapamycin, Sirolimus)	Immunosuppressive	Top-down, wet media milling	Wyeth Pharmaceuticals
Emend (Aprepitant)	Antiemetic	Top-down, wet media milling	Merck & Co.
Tricor (Fenofibrate)	Hypercholesterolemia	Top-down, wet media milling	Abbot Laboratories
Triglide (Fenofibrate)	Hypercholesterolemia	Top-down, high pressure homogenization	SkyePharma
Megace ES (Megestrol acetate)	Antianorexic Anticachexic	Top-down, wet media milling	Par Pharmaceutical Companies Inc.
Avinza (Morphine sulfate)	Antidoloric	Top-down, wet media milling	King Pharmaceuticals
Focalin XR (Dexmethylphenidate HCl)	Antipsychotic	Top-down, wet media milling	Novartis
Ritalin LA (Methylphenidate HCl)	Antipsychotic	Top-down, wet media milling	Novartis
Zanaflex Capsules (Tizanidine HCl)	Muscle relaxant	Top-down, wet media milling	Acorda
Herbesser (Diltiazem)	Antianginal	Top-down, wet media milling	Mitsubishi Tanabe Pharma

Trade name (API)	Therapeutic use	Applied technology	Pharma company
Naprelan (Naproxen sodium)	NSAID	Top-down, wet media milling	Wyeth Pharmaceuticals
Theodur (Theophylline)	Bronchial dilatation	Top-down, wet media milling	Mitsubishi Tanabe Pharma
Invega Sustenna (Paliperidone palmitate)	Antidepressant Antipsychotic	Top-down, wet media milling	Janssen Pharma
Ilevro (Nepafenac)	NSAID	Top-down, wet media milling	Novartis

1.3. Biopharmaceutical aspects of particle size reduction

The first major ascertainment related to solubility and dissolution rate, where the physicochemical properties of the drug substance were taken into consideration was described by the Noyes-Whitney equation (Eq. (1)) (1897) later modified by Nernst and Brunner (1904) [61–64]:

$$\frac{dX_d}{dt} = \frac{A \times D}{h_H} \times \left(C_s - \frac{X_d}{V}\right) \quad \textbf{(1)}$$

Where *D* is the diffusion constant of the drug, *A* is the active surface of the drug particles, h_H is the hydrodynamic thickness of the diffusion (boundary) layer, C_s is the saturation solubility of the drug among physiological circumstances, *V* is the volume of the dissolution medium, X_d is the mass of the dissolved compound. It basically describes the effect of particle size to the Fick diffusion law. The particle size reduction leads to an increased specific surface area, which in turn stimulate dissolution.

Furthermore, the size reduction to nanocrystals (nanonization) leads to an improved saturation solubility, which amplifies the concentration gradient between gut lumen and blood further; therefore, promoting permeation. This incident can be explained by the Kelvin and the Ostwald-Freundlich equations. The Kelvin equation (Eq. (2)) is originally used to describe the vapor pressure over a curved surface of a liquid droplet in gas (aerosol). A decrease in the particle size of liquid droplet contributes to an increase in curvature of the surface and the raising vapor pressure. The situation of a transfer of molecules from a liquid droplet to a gas is comparable to the transfer of molecules from a solid nanocrystal to a liquid dispersion medium. Hence, the Kelvin equation is also applicable to explain the relation between the dissolution pressure and the curvature of the solid particles in liquid. The dissolution pressure is the equivalent of the vapor pressure. The dissolution pressure can be expanded by building up the curvature (decreasing particle size). Therefore, the equilibrium is shifted toward dissolution, and thus the saturation solubility increases [52].

$$ln\ \frac{P_r}{P_\infty} = \frac{2\ \times\ \gamma\ \times M_r}{r\ \times\ R\ \times T\ \times \rho} \qquad \textbf{(2)}$$

Where P_r is the dissolution pressure of a particle with the radius r, P_∞ is the dissolution pressure of an infinitely large particle, γ is the surface tension, R is the gas constant, T is the absolute temperature, r is the radius of the particle, M_r is the molecular weight, ρ is the density of the particle. The Ostwald-Freundlich equation (Eq. (3)) directly describes the relation between the saturation solubility of the drug and the particle size [52,65]:

$$log\ \frac{C_s}{C_\alpha} = \frac{2\ \times\ \sigma\ \times\ V}{2.303\ \times\ R\ \times\ T\ \times \rho\ \times\ r} \qquad \textbf{(3)}$$

Where C_s is the saturation solubility, C_α is the solubility of the solid consists of large particles, σ is the interfacial tension of substance, V is the molar volume of the particle material, R is the gas constant, T is the absolute temperature, ρ is the density of the solid, r is the radius. The formula shows that the saturation solubility C_s of drug increases by decreasing its particle size r. However, this effect is not substantial for larger particles, but will be pronounced for materials that have a mean particle size of less than 1-2 µm,

especially well under 200 nm [52]. Another important factor is the diffusional distance h_D, as a part of the hydrodynamic boundary layer h_H, which is also strongly dependent on the particle size as shown by Prandtl equation (Eq. (4)):

$$h_H = k \times \left(\frac{L^{\frac{1}{2}}}{V^{\frac{1}{3}}} \right) \quad \textbf{(4)}$$

Where h_H is the thickness of the hydrodynamic boundary layer, k is a constant, L is the length of the particle surface in the direction of the flow, V is the relative flow rate of the liquid phase surrounding the particle.

In accordance with the Prandtl equation, the particle size reduction leads to a decreased diffusional distance h_H and consequently, an improved dissolution rate, as described by the Noyes-Whitney equation [52,65]. In addition, the thickness of the diffusion boundary layer is also influenced by the shape of the particles and therefore the dissolution rate. Mitra Mosharraf and Chryster Nyström, (1995) have found out, that spherical particles have a higher dissolution rate, than irregular ones [66].

The BCS defines three dimensionless numbers, dose number D_o, dissolution number D_n and absorption number A_n, to characterize drug substances. These numbers are combinations of physicochemical and physiological parameters illustrating gastrointestinal drug absorption. First, the absorption number is the ratio of permeability P_{eff} and the gut radius R times the residence time T_{si} in the small intestine, which can be written as the ratio of residence time and absorptive time T_{abs} (Eq. (5)).

$$A_n = \frac{P_{eff}}{R} \times (T_{si}) = \frac{T_{si}}{T_{diss}} \quad \textbf{(5)}$$

Second, is the dissolution number D_n which is the ratio of the residence time to the dissolution time T_{diss}, which includes solubility C_s, diffusivity D, density ρ, and the initial particle radius r of a compound and the intestinal transit time T_{si} (Eq. (6)).

$$D_n = \left(\frac{3 \times D}{r^2} \right) \times \left(\frac{C_s}{\rho} \right) \times (T_{si}) \quad \textbf{(6)}$$

Finally, there is the dose number D_o, which is defined as the ratio of dose concentration to drug solubility (Eq. (7)).

$$D_0 = \frac{M/V_0}{C_s} \quad \textbf{(7)}$$

Where C_s is the solubility, M is the dose, and V_0 is the volume of water taken with the dose, which is generally set to be 250 ml.

The fraction absorbed F of a solution follows an exponential function, and can be calculated by (Eq. (8))

$$F = 1 - e^{-2 \times A_n} \quad \textbf{(8)}$$

For class II., poorly soluble compounds, where the maximum flux due to absorption is equal to the solubility times the permeability [67]. For such drugs, dissolution is important because it changes the actual drug concentration in solution over time. Consequently, dissolution is brought into the classification system since it impacts the concentration of drug at the membrane surface. The dissolution of a poorly soluble compound is normally low ($D_n < 1$), while for many poorly soluble compounds A_n and D_o are usually high. If A_n and D_n are low, then the drug will be considered as a class IV., assuming that dissolution is not limited [67], the fraction dose absorbed of a suspension can be calculated as (Eq. (9)) [68].

$$F = \frac{2 \times A_n}{D_0} \quad \textbf{(9)}$$

In conclusion, particle size reduction is effectively increasing the absorption of drugs applied in lower doses, where D_o is relatively low [69].

1.4. Preparation and formulation factors of pharmaceutical nanosuspensions

There are two converse methods available for manufacturing nanosuspensions: the 'bottom-up' and the 'top-down' technologies. The 'bottom-up' type is an assembling method from molecules to nano-sized particles. The 'top-down' variant is a disintegration approach from large particles, microparticles to nanoparticles. There are also newly developed combination techniques available, merging the advantages of already employed production methods [70,71] **Table III**.

1.4.1. 'Bottom-up' techniques

The bottom-up process is broadly called precipitation processes because the foundation of these methods is to precipitate drug particles from its supersaturated solution. Crystallization can be induced by further increasing supersaturation in the system, such as evaporation of the solvent, reduction of temperature or by mixing it with an antisolvent. With further modification, 'bottom-up' processes can be used in combination with 'top-down' ones to generate smaller nanoparticles [72].

Table III. *Overview of nanocrystal production techniques*

Basic approach	Technique group	Sub variations	Specialized versions
Bottom-up	Precipitations	by liquid solvent-antisolvent addition	NanoMorph® technology
		in presence of supercritical fluid	RESS-SC RESOLV RESAS
		by removal of solvent	Spray-drying Freeze-drying with atomization
		in presence of high energy processes	Sonoprecipitation HGCP CLIJ Electro-spraying
Top-down	Pearl/bead milling	-	NanoCrystal™ technology
	High pressure homogenization (HPH) techniques	Insoluble Drug Delivery (IDD-T™ technology)	-
		Dissocubes® technology	-
		Nanopure® technology	-
Combination	NANOEDGE™	-	-
	smartCrystal technology	H42 H96 CT H69	Cavi-precipitation

1.4.1.1. Precipitation approaches for preparing nanocrystals

In the last 30 years several research studies have been conducted based on precipitation technologies for the preparation of nanosized active pharmaceutical ingredients. These investigations involved four different sub variations: precipitation by liquid solvent-antisolvent addition, precipitation in presence of supercritical fluid, precipitation by removal of solvent and precipitation in presence of high energy processes [72]. Particles in nanosized range can be obtained by rapid micro-mixing of reactants to facilitate nucleation while overcoming particle growth. Both parameters are dependent on the level of supersaturation. Solute concentration on the particle surface C_i is closely related to the level of micro-mixing (i. e. mixing on the molecular scale). Thorough micro-mixing leads to the same C_i for all the nuclei in the liquid, resulting in uniform growth and particle size distribution. There are two characteristic time parameters in crystallization: the induction time τ, which is to establish a steady-state nucleation rate (normally in μs to ms), is given by (Eq. (15)):

$$\tau = \frac{6 \times d^2 \times n}{D \times ln\left(\frac{C_i}{C^*}\right)} \quad \textbf{(15)}$$

where d is the molecular size, n is the number of molecules in a nucleus, D is the diffusion coefficient of the molecule, C_i is the solute concentration on the particle surface, C^* is the saturation concentration and the micro-mixing time t_m, which is needed to achieve uniform molecular mixing. When $t_m \ll \tau$, the nucleation rate will be nearly uniform [73].

1.4.1.1.1. Precipitation by liquid solvent-antisolvent addition

Among the various precipitation techniques, nanoprecipitation by liquid solvent-antisolvent addition has been the most reported due to its simplicity and cost effectiveness. In this process the active substance is dissolved in a water miscible organic solvent (acetone, ethanol, methanol, isopropanol (IPA), N-methylpyrrolidone (NMP) etc.) in which the drug has an appropriate solubility. Cosolvents (polyethylene glycols (PEGs), propylene glycols (PGs), and buffer systems can also be used to improve the solubility of the compound. Thereafter, this solution is added dropwise from a burette or nozzle to an antisolvent (aqueous based, in most of the cases), then mixed thoroughly with the solvent phase. The aqueous phase can often contain stabilizers (surfactants and/or polymers) to prevent the growth of nuclei. In case of polymers addition of cross-linking enhancers is advisable to fix the nanoparticle matrix. The degree of supersaturation, the selection of solvent (S) and antisolvent (AS), the volume ratios, the order of addition of solvent to antisolvent, the mixing process, mixer type, the feeding rates of phases, the temperature of the antisolvent and the quality and quantity of excipients added to the system are some of the critical process parameters of precipitation.

The type of the antisolvent used in the precipitation process not only controls the particle size of nanocrystals but also its physical properties, such as crystallinity and polymorphism. It has been reported that if water is used as an antisolvent rather than any organic solvent, the product is more crystalline.

A decrease in the antisolvent temperature offers many advantages, not only reduces the particle size, and narrows the particle size distribution, in addition it reduces the equilibrium solubility and increases the degree of supersaturation. Higher supersaturation accelerates the rate of nucleation. Moreover, reduction of the temperature increases the viscosity of the system. A higher viscosity hinders particle mobility in the liquid phase. This offers the stabilizers sufficient time to be adsorbed uniformly across the nascent surfaces. A lower particle mobility also reduces the collision rate among the particles greatly slowing the rate of aggregation (preventing the Ostwald-ripening) (**Figure 2**).

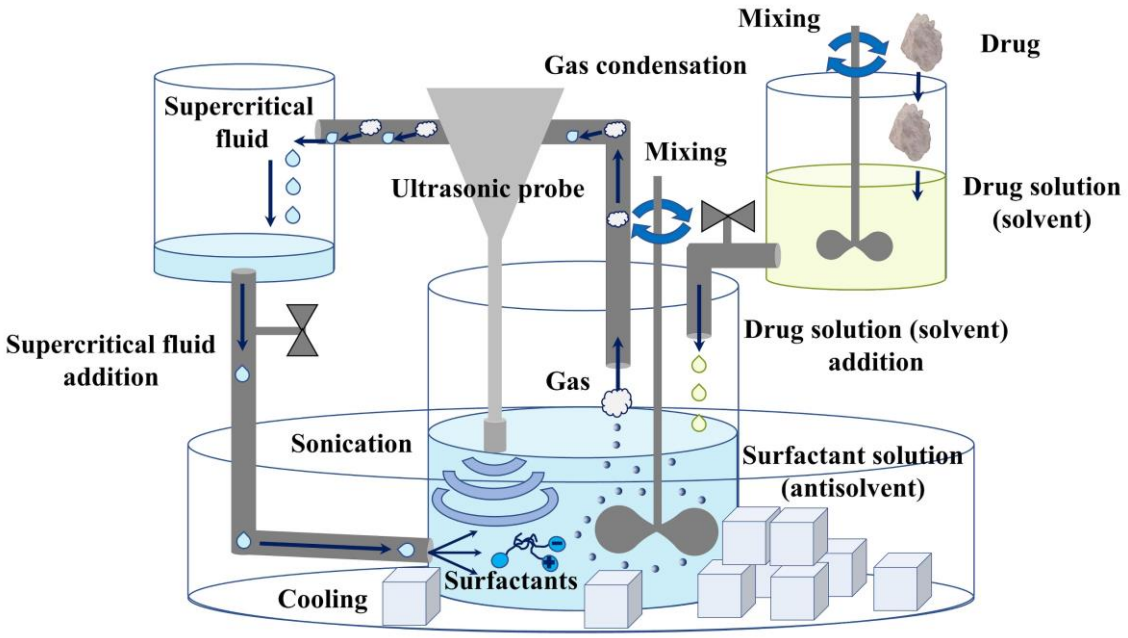

Figure 2. *Schematics of liquid solvent antisolvent, supercritical fluid (SCF) addition precipitation and sonoprecipitation methods*

List and Sucker in (1988) first reported preparation of "hydrosol" (nanosuspensions) by controlled precipitation method. Later, Soliqs (Abbott GmbH & Co.KG, Ludwigshafen, Germany) developed the NanoMorph® technology for the preparation of physically stabile nanosuspensions. This process involves preparing a heated solution of the drug in the mixing chamber, which is then rapidly mixed with a cooled aqueous blend of stabilizer(s) to induce rapid nucleation and form spherical amorphous nanosized particles [72,73].

1.4.1.1.2. Sonoprecipitation

Ultrasonic has been used by various researchers to prompt crystallization. The ultrasonic energy can be introduced simply by dipping a probe sonicator in a vessel kept under stirring or the ultrasonic source can also be fitted into a mixing device. Sonication increases micro-mixing, reduces particle growth and agglomeration by reducing contact between particles and controlling the number of nuclei. The particle size is dependent on the intensity, the energy of the ultrasound, the duration of sonication, horn length, horn tip size, its immersion depth, cavitation, and volume of the solution. Smaller particles are obtained by amplifying ultrasound power due to better mass transfer during mixing. In contrast, particle size will increase with larger batch sizes due to weaker penetration and cavitation. Immersion depth of the horn tip will affect the flow pattern but there is no set value and must be determined experimentally. While sonocyrstallisation has been successfully applied for the synthesis of micron-sized actives, its application for drug nanoparticles has been very limited and seemed more suitable for the production of amorphous molecules [72,73].

1.4.1.1.3. High-gravity controlled precipitation technology

High-gravity controlled precipitation (HGCP) is one of the most beneficial nanoprecipitation methods available at mass-production. This technique introduced a rotating packed bed, which maximizes mass and heat transfer in multiphase systems. The rotating packed bed (RPB) is a reactor in which two liquid streams can be administered, homogenized and directed to the center of the instrument, where high gravity is generated by the centrifugal force, causing the mixture to flow through, spread and split into thin layers then subdivided to fine droplets under the high shear initiated by the high gravity. The micro-mixing time (t_m) in this process minimized to around 10–100 μs. Two operation modes are available in HGCP, antisolvent and reactive. In the antisolvent mode, the liquid streams contain the drug solution and an anti-solvent causing precipitation of the active ingredient from interfacing phases. In the reactive mode, a chemical reaction is responsible for inducing crystallization. The rotation speed (high-gravity level), the reactant concentrations, the volumes and flow rate values of the liquid streams were identified as key factors affecting the particle size. As the rotating frequency of the packed bed was increased, the mean particle size had decreased rapidly, until 25 Hz. No particle size reduction was observed above this frequency [73].

1.4.1.1.4. Supercritical fluid (SCF) technologies

Compared to other methods a particular advantage of the SCF process is the rapid removal of the supercritical fluid and solvent without the need of a time consuming drying step (**Figure 2**). The most commonly used supercritical solvents include carbon dioxide, ammonia, fluoroform, ethane and ethylene. Although, the toxicity and flammability issue of some of these solvents may limit their pharmaceutical applications. Supercritical CO_2 is mostly favored because it can easily be converted into the supercritical state. Additionally, it is relatively cheap, easily available, non-toxic and non-flammable. Due to the low polarity of supercritical CO_2, hydrophobic drugs can be easily dissolved in it, then the solution is rapidly expanded in a low-pressured area from a narrow nozzle. The instantaneous reduction of pressure changes the density of the fluid. Hence, the rapid expansion of the supercritical fluid causes supersaturation, the solute nucleates and precipitates. This process is commonly called rapid expansion of supercritical solution (RESS). The major limitation of the RESS process, especially with supercritical carbon-dioxide is the limited solubility of the hydrophilic compounds in the supercritical fluid. However, this limitation was compensated to some extent by using a modified method called rapid expansion of supercritical solution with solid cosolvent (RESS-SC), where application of a potent cosolvent, such as methanol can improve the solubility of polar compounds. The RESS process was fine tuned to a process called rapid expansion of a supercritical solution into a liquid solvent (RESOLV), in which, the low-pressured are was filled with liquid phase instead of gas. The solvent can be an aqueous solution with or without stabilizers and the name of the process is changed to rapid expansion from supercritical to aqueous solution (RESAS). Another method applied supercritical CO_2 as an anti-solvent. This technique is called supercritical anti-solvent (SAS) process. In the SAS approach, the drug is dissolved in an organic solvent, which must be miscible with the supercritical antisolvent. Afterwards, the active substance is recrystallized from the solution by mixing it with a compressed fluid either at its supercritical or subcritical condition.

The supercritical antisolvent can be added directly into the solution of the compound (normal addition) or the drug solution can be sprayed into the antisolvent (reverse addition). The solvent rapidly diffuses into the antisolvent phase and the active precipitates due to its low solubility in the antisolvent. The effects of the different factors resulting in smaller particle sizes are increased pressure, decreased temperature of the supercritical solvent and by the utilization of a narrower expansion nozzle [72,73].

1.4.1.1.5. Flash nanoprecipitation

The sub variation called confined liquid impinging jets (CLIJ) has been used as a technique to produce colloidal particles. Precipitation takes place in a reactor, which is connected to nozzles from multiple sides due to extreme turbulence and intense mixing created by a jet stream of drug solution colliding a jet stream of anti-solvent coming through two opposing nozzles. The opposing nozzles allow precise flow rate control of the two jet streams, which is critical to prevent unbalanced flow and mixing. As the two liquid streams are homogenized, the antisolvent will cause the drug to precipitate as fine particles. The volume ratio of drug solution to antisolvent, the flow rates of liquid jet streams and drug concentration are important process parameters. Particle size was found to decrease with accelerated flow of jet streams or additional active content of solutions [73].

1.4.1.2. Methods based on solvent removal processes

Freeze-drying and spray drying are the two methods that fall into the solvent removal category. However, the purpose of these conventional techniques is not the production of nanosized products, rather gentle removal of moisture or solvent/dispersant from a system. In both cases, refined liquid atomization methodology is required to achieve small droplet sizes [72].

1.4.1.2.1. Spray drying processes

In spray drying, a drug solution (aqueous or organic) is atomized to fine droplets, which are evaporated in a heated air current to form dry particles. A lab-scale equipment is available (Büchi Nano Spray Dryer B-90), which can capture nanoparticles by an electrostatic collector. In addition, a piezo electrically driven vibrating mesh atomizer is employed, which allows production of finer droplets with homogeneous particle size distributions. The driving force for drying is controlled by the liquid content and the difference in the inlet and outlet temperatures of the drying air. A potential concern of spray drying is chemical degradation of the drugs due to the heat involved. However, the drying air temperature can be relatively high (e. g. > 100 ^{0}C), the actual temperature of the evaporating droplets is significantly lower due to cooling by the latent heat of vaporization. Thus, thermal degradation of the active ingredient is not so much a concern as it first appears. Drying time of the droplets depends on the residence time of the droplets in the spray dryer, which is determined by the dimensions of the spray dryer and the drying air flow rate. Higher air flow rate will evaporate the droplets more rapidly, resulting in a less crystalline product due to insufficient time allowed for crystallization. Thus, the usefulness of spray drying to prepare stable fine particles is limited. The drawbacks of the utilization of amorphous materials are hygroscopicity, increased cohesiveness, the difficulty of the dispersing process and their flowing properties are also questionable. Another limitation of spray drying is its unsuitability for substances sensitive to the mechanical stress of atomization. Application of an inert gas, instead of air or antioxidants can be a solution, but evaporation of an organic solvent (with low-boiling-point (< 20 ^{0}C, like hydrofluoroalkanes (HFAs) is more suitable for thermosensitive compounds such as proteins [73].

1.4.1.2.2. Precipitation using special freezing techniques

The first method developed in 2002 was the spray-freezing into liquid (SFL) process.
It was observed, that using a higher freezing rate or using an organic solvent with a higher freezing point generates smaller crystals, because of the rapid freezing. More concentrated solutions seemed to increase particle size, which can be explained by the higher viscosity of the solution, which caused larger micro droplets after atomization. A modified freeze-drying process was reported by De Waard et al., (2008) for preparation of nano-sized crystalline materials. The active substance was dissolved in an organic solvent and was mixed with an aqueous solution of a cryoprotectant, Thereafter the mixture was immediately frozen and freeze-dried. Suitable API candidates should have a low glass transition temperature T_g, because the freeze-drying was performed above the T_g, to induce formation of crystals. Faster freezing rate and lower water content induced higher nucleation rate, which reduced the size of the solvent crystals and thereby reduced the interstitial spaces among them. Smaller interstitial spaces restricted the growth of drug crystals [72].

1.4.1.2.3. Electro spraying

In this process, the liquid stream, which is flowing out from a capillary under the influence of an electric field, will acquire electrostatic charges close to the Rayleigh limit (the maximum amount of charge a droplet can carry). These charges will overcome the surface tension causing the liquid jet stream to break up into droplets. When coupled with a drying gas, the liquid will evaporate, and dry nanoparticles are formed. There are three major limitations of electro spraying. The first one is the surface tension of the liquid stream, which should not exceed 50 mN/m value, otherwise it will not be atomized. The second one is the conductivity of the solution, semi-conducting liquids (conductivity range10^{-4}–10^{-8} S/m) are feasible to spray. This can limit the processability of some water soluble drugs. Finally the low productivity of this technique, which can be compensated with the application of multiple nozzles [73].

1.4.2. 'Top-down' techniques

There are two basic disintegration technologies available for drug nanocrystal productions: pearl/ball milling and high pressure homogenization with different homogenizer types/homogenization principles [74].

1.4.2.1. Pearl/bead/ball milling

Dry milling (e. g. jet milling) is not efficient to obtain crystal sizes in the nanometer range; therefore, wet-milling is applied. Wet-milling means, that the drug particles are dispersed in a surfactant/stabilizer solution; the obtained macro suspension is then subjected to milling energy [71]. In pearl milling, the drug macro suspension is filled into a milling container, containing smaller or larger coated milling pearls as milling media (typically in the size of 0.2 mm or 0.4–0.6 mm) made of ceramics (cerium or yttrium stabilized zirconium-dioxide), stainless steel, or glass. A general problem of pearl mills is potential erosion of milling pearls leading to product contamination. Crosslinked polystyrene coatings proved to minimize the erosion of beads [58,74]. The pearls are moved by an agitator, the drug is ground to nanocrystals in between the pearls. This is the basic technology developed by G. Liversidge et al. (1992). The technique is recognized as NanoCrystal™ technology and it is a low-energy milling process [58,71,74]. Typically, lab scale production can be carried out at 100 mg or less amounts of API by applying the Nanomill® system and utilizing the neutral form of the chemical compounds [58]. The milling time can vary from about 30 min to hours or several days, dependent on several factors, such as physicochemical properties and quantity of the ground materials, applied surfactants/polymers, etc. There are numerous interfering critical process parameters responsible for optimal end-product quality. Including the type of the milling instrument, hardness of the compound subjected to milling, viscosity of the dispersion, composition of the milling medium and the inner wall of the milling container, size of the milling medium, milling speed, milling time, energy input, balls/beads to powder mass ratio, volume of the loading, milling atmosphere, milling temperature etc. [58,74,75]. Scaling up with pearl mills is possible; however, there is a certain limitation in the size of the mill due to its weight.

Up to about 2/3 of the container capacities are usually filled by the beads, leading to a heavy weight of the machinery, thus limiting the maximal batch size. The batch size can be increased above the void volume, introducing an instrument with suspension circulation mode. During the process, the suspension is contained in a product container and continuously pumped through the mill in a circle. This increases the batch size, however the milling time as well [58,74]. Batch sizes of more than 5 l (flow through mode) can be produced applying the Dynomill (Glen Mills, Inc. Cliffton, NJ, USA) with chamber size of 300 and 600 ml (**Figure 3**). There are also larger sized mills available (e. g. Netzsch mills (Netzsch Inc., Exton, PA, USA)), with e. g. in 2 l, 10 l and 60 l chamber capacities [58].

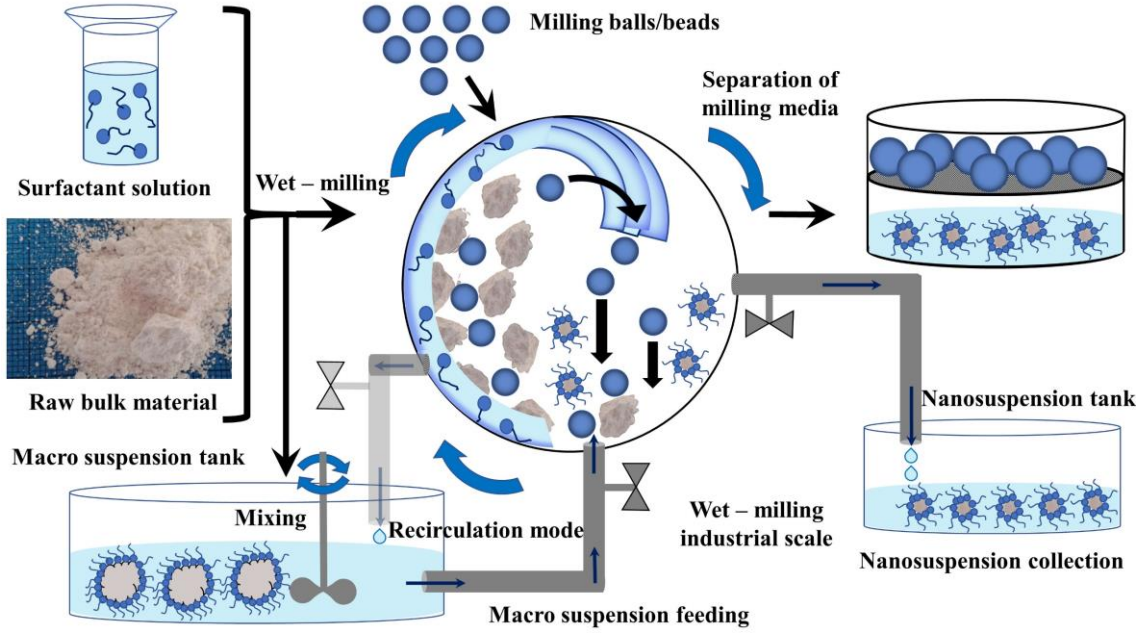

Figure 3. *Schematics of laboratory-and industrial scale wet-milling processes*

1.4.2.2. High pressure homogenization (HPH) technologies

The other most frequently used disintegration method is the high pressure homogenization. There are three homogenization principles/homogenizer types available:

1. Microfluidization (Microfluidics, Inc.) or insoluble drug delivery technology (IDD-T™ technology) based on the jet stream principle
2. Piston-gap homogenizers (e. g. APV Gaulin, Avestin, etc.) utilized in aqueous media, called the Dissocubes® technology, (SkyePharma)
3. Piston-gap homogenizers (e. g. APV Gaulin, Avestin, etc.) utilized in water-reduced or non-aqueous media, called Nanopure® technology, (previously PharmaSol GmbH., now Abbott Laboratories) [58,71,74]

1.4.2.2.1. Insoluble drug delivery technology (IDD-T™)

The Microfluidization technology can generate small particles via accelerating the stream of the macro suspension, which passes through a specially designed Z-shaped or Y-shaped homogenization chamber at high flow rate values. In the Z-type chamber, the suspension changes the direction of its flow leading to particle collisions and the generation of shear forces between walls and particles. In the second type of chamber, the Y-type, the suspension stream is divided into two streams, which then collide frontally generating up to 1700 bar pressure. It is considered as a time consuming, long operation, with low productivity, because sometimes high number of passing cycles (up to 75) is required through the microfluidizer to reach the desired particle sizes. In addition, the end-product can contain a relatively large fraction of undesired microparticles especially in case of hard compounds. [58,74].

1.4.2.2.2. Dissocubes® technology

Learning from the potential problems and limitations of pearl milling and microfluidization, as an alternative nanocrystal production technique, based on piston-gap homogenizers has been introduced in the middle of the 1990s by Müller et al. (**Figure 4**). At first the technology was based on homogenization of particles in pure aqueous solutions (Dissocubes® technology).

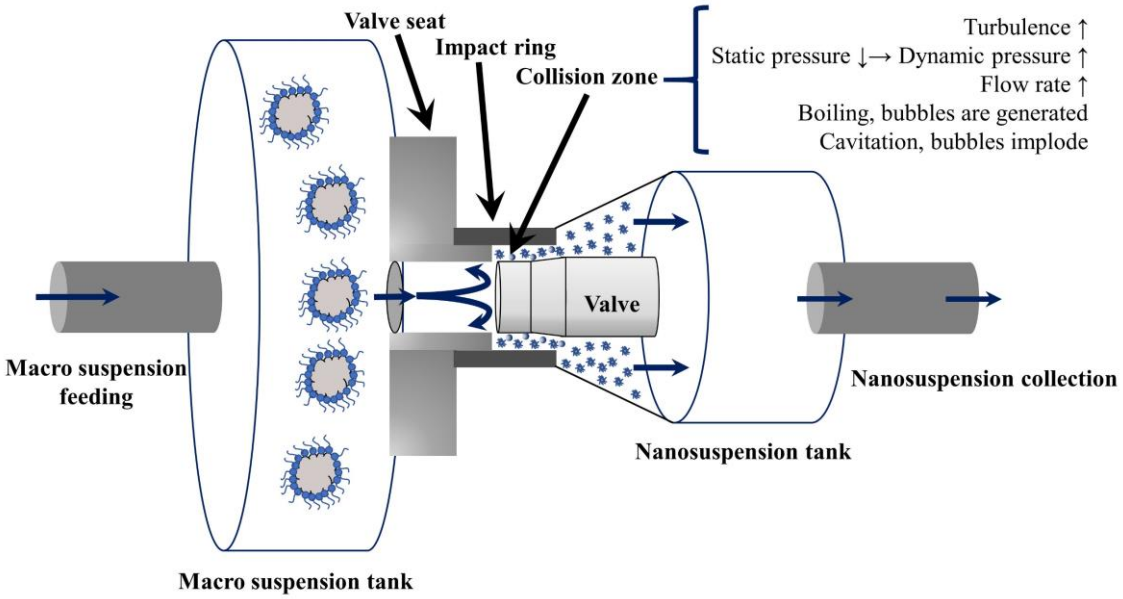

Figure 4. *Schematics of the piston–gap-type high pressure homogenizer*

In these homogenizer types, the dispersion (emulsion or suspension) pumped through a very thin gap (with a height of 5-20 µm) with an extremely high flow rate (e. g. 500 m/s). The reduction of the cavity diameter mounted into the wall of the collision zone leads to a tremendous increase in the dynamic pressure and simultaneously a decrease of the static pressure flowing through this area. Consequently, the liquid starts boiling, forms gas bubbles, which implode after leaving the homogenization zone and being under normal air pressure conditions again. Thus, the cavitation is considered to be the main driving factor of particle diminution for this high-energy process [58,71,74]. Parameters determining the final dispersity are power density (homogenization pressure), number of homogenization cycles applied and hardness/softness of the drug.

Quality and quantity of applied stabilizers for dispersion influences the long-term stability (preventing aggregation), but had no effect on maximum dispersity and on the shape of the nanocrystals. Contamination from the production equipment was reported to be below 1 ppm [74].

1.4.2.2.3. Nanopure® technology

For some administration routes or formulation purposes, it is more convenient to have drug nanocrystals dispersed in non-aqueous media (e. g. in oils or alternatively in liquid PEG 400 or 600 solutions for filling soft gelatin or hypromellose (HPMC) capsules). Highly chemically unstable, water sensitive drugs could be formulated in such non-aqueous media and diluted prior to, e. g. intravenous injection with water to get an isotonic suspension (e. g. water–glycerol mixtures). For solidification of nanosuspensions it can also be desirable to have suspensions with reduced moisture content values or dispersions with easily removable volatile components, e. g. water–ethanol mixtures [58,71,74]. In contrast to water, oils and fatty acids have a very low vapor pressure at room temperature. In case of the application of dispersants, having a much lower vapor pressure than water, may lead to an insufficient drop in the static pressure to initiate cavitation. Based on this, particle diminution should be not very efficient or distinctly less pronounced than in water [74]. Even without cavitation, the particle size diminution is sufficient enough because of shear forces, particle collisions and turbulences [58].

In addition to homogenization at room temperature, the process was performed at 0 ^{0}C and well below freezing point (e. g. -20 ^{0}C), the so called ‘deep-freeze homogenization’ [74]. The optional low temperatures allow the processing of temperature sensitive drugs, in addition materials are more fragile at lower temperatures [58].

1.4.3. Combination techniques

1.4.3.1. The NANOEDGE™ technology

The combination technologies combine generally a pre-treatment step followed by a high energy process, typically high pressure homogenization [71]. The NANOEDGE™ technology by Baxter International, USA utilizes a classical precipitation as a pre-treatment step with a subsequent annealing step by applying high energy, e. g. high pressure homogenization Kipp et al. (2001). According to the patent claims, the annealing step prevents the growth of the precipitated nanocrystals. Annealing is defined in this invention, as the process of converting thermodynamically unstable matter into a more stable form, by single or repeated exposure to energy (direct heat or mechanical stress), followed by thermal relaxation. Energy dissipation may be achieved by conversion of the solid form from a less ordered to a more ordered lattice structure. Alternatively, this stabilization may occur by a reordering of the surfactant molecules at the solid–liquid interface [58,76].

1.4.3.2. The smartCrystal technology

The smartCrystal technology was developed by PharmaSol, Germany in 2007, this technology is owned by Abbott Laboratories, US and marketed by Soliqs Drug Delivery Business Unit, Germany. This technique comprises different patent families for refined production of optimized nanocrystals for various applications. This fusion of processes either accelerate manufacturing by reducing e. g. the number of homogenization cycles or capable of generating very small nanocrystals, size below 100 nm [71]. Nanocrystals created by the smartCrystal technology are usually referred as second generation nanocrystals [58,77]. The method H42 is a combination of spray-drying with subsequent high pressure homogenization.

At the end of the synthesis of the drug, no crystallization is performed, but spray-drying of the drug solution instead. The obtained micrometer sized product is then dispersed under stirring in a surfactant solution and this suspension passed through a homogenizer. The H96 process is a combination of freeze-drying and high pressure homogenization. Here, during the last step of the synthesis of the active substance, the obtained solution is lyophilized. After dispersing the freeze-dried product into surfactant solution, it immediately passed through a homogenizer. This yielded nanocrystals with a mean size of about 50 nm. In the technique called "CT" the macro suspension is premilled applying a ball milling technique, then through the upcoming homogenization step, further size reduction is achieved with increased uniformity of the size distribution, an important factor for avoiding Ostwald-ripening. The obtained nanosuspensions showed an increased long-term physical stability during storage and in electrolytes [58,71,77]. The combination process H69 is a parallel flow precipitation and subsequent high pressure homogenization, where the precipitation takes place in the cavitation zone or just before the cavitation zone of the homogenizer (cavi-precipitation) [58,71].

Summarizing the production methods of nanocrystals, we can conclude, that 'bottom-up' processes pose many challenges due to careful evaluation of the critical parameters influencing the micro-mixing time (t_m), which is needed to achieve uniform molecular mixing. When the micro-mixing time is lower than the induction time by multiple orders of magnitudes ($t_m \ll \tau$), the nucleation rate will be nearly uniform. In addition, controlling crystal growth rate is another challenge, which has a major impact on the PSD of the final product. In contrast to 'bottom-up' techniques, 'top-down' approaches, can offer fewer process parameters to optimize, more precise control of PSDs, less complex machinery to work on. Therefore, 'top-down' variants are more widely spread and most commonly used to produce nanocrystals on industrial scales (**Table III**). However, combination techniques merge the advantages of both methods and propose many opportunities for tailor making nanocrystals for highly regulated future demands.

1.5. Characterization of model drug albendazole

1.5.1. Pharmacodynamical effects

Albendazole (ABZ) (CAS: 54965-21-8) is a benzimidazole carbamate-type, broad-spectrum anthelmintic for the treatment of intestinal helminth infections. According to product monographs, it has shown effectiveness in the treatment of ascaris lumbricoides (roundworm), trichuris trichiura (whipworm), enterobius vermicularis (pinworm/threadworm), ancylostoma duodenale and necator americanus (hookworms), strongyloides stercoralis (threadworm), hymenolepsis nana (dwarf tapeworm), taenia solium (pork tapeworm), taenia saginata (beef tapeworm) and the liver flukes opisthorchis viverrini and clonorchis sinensis.

It also has systemic anti-hydatid activity and is now recognized to have important application in treatment of human cystic and alveolar echinococcosis caused by infestation of echinococcus granulosus and echinococcus multilocularis, respectively. Albendazole is also effective in the treatment of neurocysticercosis caused by larval infestation of taenia solium [78,79].

During the clinical trials albendazole has eradicated cysts or significantly reduced cyst size up to 80% of treated patients with echinococcus granulosus cysts. Cysts have been investigated for viability following treatment with albendazole, 90% have been non-viable in laboratory or in animal studies. In the treatment of cysts by echinococcus multilocularis infestation, a minority of the patients were cured, and the majority had an improvement or stabilization in their conditions due to albendazole therapy. Also showed good results in eradication of the protozoan parasite giardia lamblia (intestinalis or duodenalis).

Common undesirable effects of the albendazole therapy are headaches, dizziness, gastrointestinal disturbances (abdominal pain, nausea, vomiting), mild to moderate elevations of hepatic enzymes, reversible alopecia (thinning of hair, moderate hair loss) and fever [78].

Albendazole is binded to the same site as colchicine on β-tubulin molecules and inhibits tubulin polymerization, preventing the formation of microtubules. As a result, fumarate reductase enzyme and glucose uptake inhibition cause paralysis and starvation to helminths [80,81].

1.5.2. Toxicology

1.5.2.1. Acute toxicity

Acute toxicity evaluations have demonstrated that this compound is relatively well tolerable. The median lethal doses (LD50) were found to be high in animal studies. The oral LD50 value for mice is > 3000 mg/kg, for rats it is between 1320–2400 mg/kg and rabbits are the most sensitive to ABZ with an LD50 value of 500–1250 mg/kg. Signs of autopsies demonstrated some common intestinal hemorrhage in rats and intestinal fluid in rabbits [82]. One overdosage has been reported with ALBENZA® in a patient who took at least16 grams over 12 hours [83].

1.5.2.2. Repeated dose toxicity evaluations

Comprehensive oral studies with doses of 30–40 mg/kg for 4-90 days long administration periods of murine, rat and dog models reported, some retardation of weight gain, reversible anemia, slight leucopenia, hypercholesterolemia, other non-specific and variable changes in clinical chemistry test results and slight proteinuria in the rats.

Autopsy and histopathological examination revealed relative enlargement of the liver in rats and dogs in doses above 40–60 mg/kg/day with some enlargement of centrilobular hepatocytes, and testicular hypoplasia in mice receiving a 400 mg/kg/day dose for 104 weeks. The non observed effect level (NOEL) has been established for rats at 7 mg/kg/days [82].

1.5.2.3. Genetic toxicity investigations

Negative results have been obtained in Ames, CHO chromosome aberration and 3T3 cell transformation tests in vitro; but a positive result was obtained in in vivo murine bone marrow micronucleus test. It has been recognized that there is a threshold concentration below this value aneuploidogenesis will not occur, so assessment of the risk of exposure to an aneugenic substance must also be taken in account of the dose and residue involved [82]. Therefore, EMA Committee for medicinal products for veterinary use has established maximal residue limits (MRLs) of albendazole and its metabolites recommended for foods of animal origins (EMEA/CVMP/457/03-FINAL) guidance modified by entry (EEC) No 2377/90 (**Table IV)** and for minor animal species (EMEA/CVMP/153a/97-FINAL) [84].

Table IV. *Recommended maximal residue limits of albendazole and its metabolites in foods of animal origins according to (EMEA/CVMP/457/03-FINAL) guidance modified by entry (EEC) No 2377/90* [84]

Pharmacologically active substance(s)	***Marker residue***	***Animal species***	***MRLs***	***Target tissues***
Albendazole	Sum of albendazole-sulphoxide, albendazole-sulphone and albendazole 2-amino sulphone expressed as albendazole	All ruminants	100 μg/kg 100 μg/kg 1000 μg/kg 500 μg/kg 100 μg/kg	Muscle Fat Liver Kidney Milk

1.5.2.4. Reproduction toxicity investigations

ABZ is teratogen and caused fetal toxicity in doses above 7.5 mg/kg/day in rat models, producing craniofacial, skeletal and visceral defects in segment II tests; therefore, non observed effect level (NOEL) should be corrected from 7 mg/kg/day to 5 mg/kg/day including the results of reproduction toxicity investigations. Maternal and fetal toxicity results were negative in murine models up to a dose of 30 mg/kg/day. Segment II tests in rabbits, showed maternal and non-specific fetal toxicity at doses of 10–30 mg/kg/day. A NOEL of 5 mg/kg/day was established. There is extensive review of albendazole reproduction toxicity in food animals in which doses of 10 mg/kg/day have caused fetal death and teratogenic effects. JECFA (1989b) has reported, that fetal effects have been noticed between the maximal plasma concentrations (C_{max}) of albendazole-sulphoxide 2.5–6.6 μg/ml [82]. Human trials with 17 women in first trimester of pregnancy were given 400 mg/day doses of albendazole and no adverse effects on mother or child was observed [84]. A pregnancy category C was reported, administer with caution, but it has a positive benefit/risk ratio [83].

1.5.2.5. Carcinogenicity evaluations

In a three generation test with rat and murine models up to doses of 400 mg/kg/day (twice the human dose/m^2) for 24 month of treatment, negative results were obtained [82].

1.5.2.6. Irritancy tests

The main metabolite albendazole–sulphoxide was tested for irritancy, results diverted between rabbits and guinea pigs. Eyes of rabbits were not sensitized by the metabolite in comparison to guinea pigs [84].

1.5.3. Pharmacokinetics

The main targeted animals are cattle (dosage: 7.5-10 mg/kg) and sheep (dosage: 5 mg/kg) in animal healthcare [85,86]. Oral absorption of ABZ is about 20-30% in mice and rats, 50% in cattle [82]. In humans albendazole is poorly absorbed (< 5%) following oral administration of a single dose of 400 mg from the gastrointestinal tract; however, absorption increased fivefold, when administered with a fatty meal. The pharmacologically active metabolite, albendazole-sulfoxide (ABZSO/ABZSX), has been reported to achieve plasma concentrations from 1.6 to 6.0 µmol/l (0.42–1.59 µg/ml), when taken with breakfast and has a half-life ($T_{½}$) of 8.5 hours [78]. Effective peak plasma concentrations (C_{max}) of albendazole-sulfoxide in cystic echinococcosis therapy was found to be 0.34-0.37 µg/ml in murine models [87], a mean of 1.7 µg/ml was observed in human trials after the peroral administration of 30 mg/kg/day doses for 8 days [88]. In murine trichinella larval infestations 3.4–3.8 µg/ml seemed to be the effective plasma level [89].

ABZ undergoes extensive first-pass metabolism to the point, that it is not usually detected in the plasma. Research with human liver microsomes identified albendazole as a high-clearance medication (hepatic clearance [CLH] = 18.2 ml/min/kg) with metabolism primarily though cytochrome P450 CYP1A2 and CYP3A4, with some involvement from CYP1A1 [82,90]. Albendazole's metabolite, albendazole sulfoxide, is thought to be the primary active moiety and is principally formed by CYP enzymes [(–) albendazole sulphoxide] and flavin enzymes [(+) albendazole sulphoxide]. Subsequent oxidation to a sulphone is dependent on the CYP isozymes with further elimination in the bile with only a small proportion appearing in the urine [78,82].

1.5.4. Physicochemical properties

This compound has a pH dependent, poor water solubility profile, a minimal of 0.016 mg/ml in pH = 6.0 buffers and a maximal of 0.376 mg/ml in medium at pH = 1.2, reported by Torrado et al. (1996) (**Figure 5**) [91].

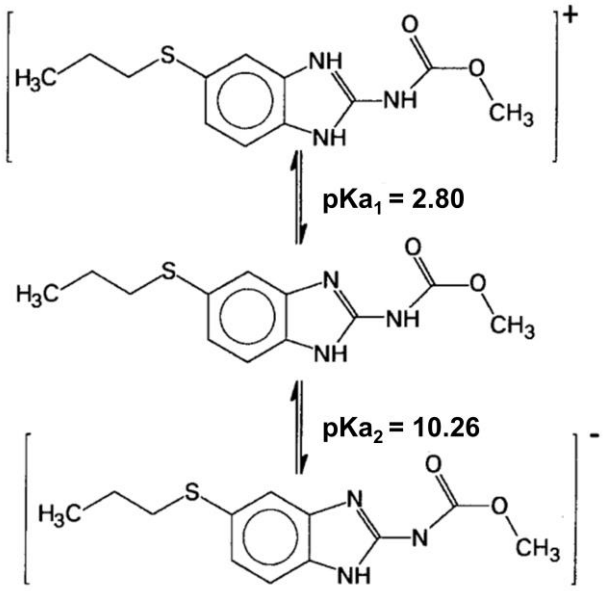

Figure 5. *Acid–base status of Albendazole* [92]

It is a weak alkaline chemical entity with molecular weight of 265.33 g/mol [93].

It has an octanol-water partition coefficient (*log P*) value of 3.83 [94], which is high, according to the BCS drug permeability classifications [95]. With low water solubility and high membrane permeability, it is classified as a BCS Class II. drug [68].

Solubility of actives in lipids and oils are also a key factor in research and development. Liposomal formulation of ABZ from egg phosphatidyl choline, improved peak plasma concentration level (C_{max}) of ABZ in rats from 0.1 µg/ml to 1.7 µg/ml (17 times gain) [79]. Self-micro-emulsifying drug delivery system of ABZ containing Capmul PG-8, Cremophor EL, Tween 80 and acidified PEG 400, improved peak plasma concentration level (C_{max}) of ABZ compared to commercially available suspension form (Zentel®) from 2.8 µg/ml to 4.3 µg/ml (+ 53.6% gain) [96].

Mean apparent solubility of ABZ in fasted state simulated intestinal fluid at pH = 6.5 (FASSIF) with taurocholic acid and lecithin was reported to be 1.9 µg/ml, which was improved to 6.1 µg/ml in fed state simulated intestinal fluid at pH = 5.0 (FESSIF) (demonstrated a 3.21 times gain) [97].

The melting point of ABZ is high, 197.7 ^{0}C according to our investigations, in agreement with other findings in the literature, like 200-230 ^{0}C by Chattah et al. (2015). Considering the melting point, the high membrane permeability value and intermolecular bonds, ABZ represents a borderline physicochemical behavior between "grease ball" (BCS class II.) and "brick dust" (BCS class IV.) molecules [98,99].

An excellent review on recrystallizations, identification, stability and solubility evaluations of enantiotropically related albendazole polymorphs were performed by Pranzo et al. (2010). According to the authors there are two polymorphs available for ABZ, Form I (commercially available form) and From II (recrystallized from N, N-dimethylformamide). Both forms proved to be physically quite stable, likely due to a high-energy barrier for the activation of the interconversion. Temperature dependent solubility studies revealed, that on 25 ^{0}C solubility of Form I is better, than Form II. Solubility values of Form I show a saturation curve with increasing temperature and an exponential curve for Form II, until 80 ^{0}C, which is the interception of the solubility vs. temperature curves, where the solid–solid transition is beginning. This observation confirms that Form I represent the metastable polymorphs at ambient temperature. Application of a metastable Form I may be advantageous (e. g., for exploiting higher solubility in the gastrointestinal tract) only when the kinetics of conversion would be slow, namely when the energetic barrier Form I → Form II cannot be overcome during specific storage conditions. In this respect, the metastable phase should be kept cool and dry and should not be too finely subdivided. On the other hand, one should be aware, that many pharmaceutical operations may cause an undesired change from the metastable to the stable form. A progressive Form II → Form I transition was observed upon heating the Form II at 130 ^{0}C, with complete conversion in < 20 hours, especially in those, where the conversion could be mediated by solubilization [100].

1.5.5. Adopted formulation strategies

The low bioavailability of the active pharmaceutical ingredient (API) reduces the efficacy in hydatid. Pragmatic approaches for chemotherapy of hydatid patients necessitate to focus on improved transport, targeting, modulation of the physicochemical parameters and metabolic decomposition of benzimidazoles [79].

To overcome the drawbacks of the poor water solubility of ABZ, a great number of different formulation approaches have been adopted. In animal studies, the main strategy to enhance albendazole bioavailability was by increasing water and lipid solubility with the utilization of cosolvents, surfactants or incorporating albendazole into particles. The relative bioavailability of albendazole in mice increased 1.8-fold by combining it with the cosolvent Transcutol (diethylene glycol monoethylether) [101]. A solid dispersion formulation enhanced the relative bioavailability in rabbits threefold [102]. Albendazole coadministered with the surfactant sodium taurocholate or polysorbate enhanced the area under the plasma concentration curve (*AUC*) value for rats by 55-or 88%, respectively [103–105], whereas incorporation into liposomes increased the uptake in rats by more than twofold [79]. Inclusion complexes with cyclodextrin increased the *AUC* value for sheep by 37% [106].

For humans, various other strategies were investigated to enhance the bioavailability of ABZ. When combined with a fatty meal, administration of the active metabolite albendazole sulfoxide (ABZSX) increased the maximum concentration of the drug in serum (C_{max}) 4.5– to 9-fold [107–110]. To inhibit CYP3A4 isozyme related ABZSX degradation, albendazole was coadministered with cimetidine. However, this caused a 52% decrease in ABZSX C_{max} values (probably due to inhibition of gastric acid secretion) [110,111], suggesting that absorption is pH dependent. When coadministered with grapefruit juice, the ABZSX C_{max} was enhanced 3.2-fold, probably due to inhibition of the intraluminal degradation of albendazole by CYP3A4 enzymes [110].

In another human study, a soybean oil emulsion was used to enhance albendazole solubility and showed a 1.6-fold enhancement of relative bioavailability compared with tablets [112].

Several in vitro albendazole containing nanosuspension based formulations are also available in the scientific literature. An overview of these techniques has been summarized in **Table V**.

Table V. *Overview of albendazole containing nanosuspension based formulations available in the scientific literature*

Applied method	Utilized surfactant/polymer	Mean size or size range achieved (nm)	Reference
Top down HPH	Polysorbate 80 Poloxamer 188 HPMC	385.7 ± 4.3 nm 420.4 ± 6.7 nm 576.2 ± 4.8 nm	Kumar et al. (2007) [113]
Top down HPH	Poloxamer 188	430.2 ± 13.2 nm	Li et al. (2014) [114]
Bottom up Sonication High speed homogenization Top down HPH	Polysorbate 80 Poloxamer 188 SLS Cremophor RH 40 HPMC	365.6 ± 55.6 to 753.8 ± 74.8 nm dependent on formulation	Kumar et al. (2008) [115]
Top down Wet-media milling	Polysorbate 80	197.2 ± 0.2 nm to 200.4 ± 2.3 nm	Fülöp et al. (2018) [98]
Bottom up Modified emulsion crosslinking volatile	Chitosan Poloxamer 188	157.8 ± 2.82 nm	Liu et al. (2013) [116]
Bottom up Modified emulsion crosslinking volatile	Chitosan triphosphate Poloxamer 407	224.9 ± 10.1 nm	Torabi et al. (2017) [117]

2. Aims and objectives

This Ph.D. thesis illustrates the development of a redispersable solidified nanosuspension, containing ABZ nanocrystals. It is divided into four major sections.

The first section emphasizes the potential of the optimization of loading composition and formulation factors of the top down wet planetary bead milling method. Our goal was to prepare ABZ nanocrystals with size distribution parameters similar to those, produced by novel bottom up techniques like the modified variant of the so called emulsion crosslinking volatile method [116,117]. Process parameter optimization was performed by design of experiments (DOE) approach, which is a useful tool for the quality by design (QbD) concept [118]. Particle size distributions have been defined by dynamic light scattering and laser diffraction methods. Long-term physical stability determination of the optimized nanosuspension formula as a liquid dosage form was not investigated in this study, only a short 56 day long demonstration was included.

The second section focuses on the stabilization principal of the obtained milled albendazole nanosuspension, as well as the starting macro suspension by the post-processing solidification wet granulation method, applying microcrystalline cellulose (MCC) as carrier [98] (**Figure 6**). The particle size distribution after redispergation was studied in various dissolution media and zeta-potential in demineralized water.

The third part summarizes the in vitro solubility and dissolution studies, which describes the impact of the particle size reduction and the solubilization on the water solubility of albendazole along with the dissolution rate values in various aqueous-based pH buffer solutions.

Finally, the last chapter summarizes the solid state characterization and morphological studies. These experiments involved the investigation and comparison of raw material albendazole, this active processed in milled suspensions after drying and in granules absorbed by solid carrier.

The novelty of this is work is the identification of extreme milling conditions, where disadvantageous ABZ Form I → Form II conversion is realized, giving a hint to formulation scientists to avoid these conditions during ABZ nanosuspension development by wet planetary bead milling techniques.

The influence of process parameters (capacity of the milling container, size of the milling medium, milling speed, milling time) and drying on ABZ polymorphism were studied. It has already been reported that mechanical stress and other sources of excess energy such as heat are inherent to milling and often lead to significant changes on the physical and chemical properties of pharmaceutical crystalline solids. Partial or complete transformation to the amorphous form, polymorphic transformations, and changes in chemical reactivity are among the frequently encountered changes produced by milling [119]. The presence of solvent can have drastic influence on the outcome of the mechanical treatment and can greatly affect the nature of the resulting material [120–124]. Crystal defects are practically unavoidable in pharmaceutical processing. Fundamental understanding of milling induced disorder will lead to a better process control and more consistent product performance [119]. Differential scanning calorimetry (DSC), Fourier-transform infrared spectroscopy (FT-IR) investigations have been performed to compare the solidified nanosuspension to the unmilled dispersion, active substance and to the carrier. Atomic force microscopy (AFM) and scanning electron microscopy (SEM) were utilized to compare the surfaces of the raw material albendazole to the MCC carrier (Vivapur® 12), to their physical mixture and to the albendazole milled dispersion.

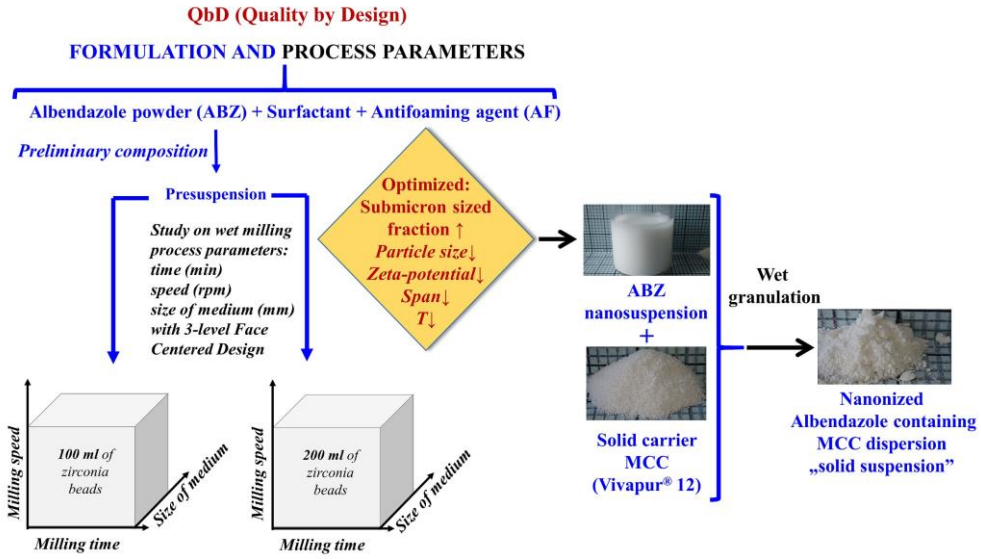

Figure 6. *Graphical abstract of the optimization of wet-milling for ABZ nanosuspension development and post processing solidification by wet granulation*

3. Materials and methods

3.1. Materials

Albendazole EP (micronized), (Sequent Scientific Ltd., India) was used as model drug. The effect of various surface-active agents on wet media milling have been compared such as polysorbate 80 (Tween 80) (Molar Chemicals Kft., Hungary), polysorbate 20 (Tween 20) (Molar Chemicals Kft., Hungary), sodium laurylsulphate (Molar Chemicals Kft., Hungary), hypromellose (Benecel™ E3 pharm) (Ashland Inc., USA), poloxamer 407 (Lutrol® F127), poloxamer 188 (Lutrol® F68) (BASF, Germany), polyoxyl 35 hydrogenated castor oil (Kolliphor® EL), polyoxyl 40 hydrogenated castor oil (Kolliphor® RH40) (Sigma-Aldrich, USA). Dimethylpolysiloxane (Foamsol) (Kokoferm Kft., Hungary) was applied as antifoaming agent (AF). Coarse grade microcrystalline cellulose (MCC) (Vivapur® 12), (JRS Pharma GmbH & Co. KG, Germany) with mean particle size and bulk density of 180 μm and 0.33 g/ml, respectively was applied as carrier of the solid suspension.

3.2. Instruments and pieces of equipment

All the instruments and pieces of equipment utilized for the experiments are summarized in **Table VI**.

Table VI. *Overview of the instruments and pieces of equipment utilized for the experiments*

Equipment/ Instrument	Manufacturer	Origin	Description	Application
ABT 320–4M	ABT–KERN & SOHN GmbH.	Germany	Analytical balance	Dispensing for dispersing, milling, wet granulation, solubility, and dissolution tests
MS-H-S10	DLAB Instruments Ltd.	China	Heatable magnetic stirrer	Dispersing for solubility tests and drug content evaluations

Equipment/ Instrument	Manufacturer	Origin	Description	Application
IKA RCT basic	IKA® Works Inc.	USA	Heatable magnetic stirrer	Dispersing for unmilled suspension preparation and drug content evaluations
PM 100	Retsch Technology GmbH.	Germany	Planetary ball mill	ABZ nanosuspension preparations by wet-milling method
Stainless steel milling container	Retsch Technology GmbH.	Germany	12 ml capacity	Loading composition optimization for wet-milling
Stainless steel milling container	Retsch Technology GmbH.	Germany	50 ml capacity	ABZ nanosuspension preparation for wet granulation
Stainless steel milling container	Retsch Technology GmbH.	Germany	500 ml capacity	Critical milling process parameter optimization
Stainless steel milling beads	Retsch Technology GmbH.	Germany	d = 1 mm sized	Loading composition optimization for wet-milling
Plastic milling beads	Retsch Technology GmbH.	Germany	d = 1 mm sized	Loading composition optimization for wet-milling
Zirconium-dioxide milling beads	Retsch Technology GmbH.	Germany	d = 1 mm sized	Loading composition and critical process parameter optimization for wet-milling
Zirconium-dioxide milling beads	Retsch Technology GmbH.	Germany	d = 0.3 mm sized	Critical milling process parameter optimization

Equipment/ Instrument	Manufacturer	Origin	Description	Application
Zirconium-dioxide milling beads	Retsch Technology GmbH.	Germany	d = 0.1 mm sized	Critical milling process parameter optimization
Stainless steel sieves	Retsch Technology GmbH.	Germany	mesh sizes of 800 μm 315 μm, 180 μm, 125 μm, 63 μm, 50 μm, and 32 μm	Separation of milling beads from milled suspensions, PSD determinations of granules and MCC
AS 200 control	Retsch Technology GmbH.	Germany	Vibrational sieve shaker	PSD determination of granules and MCC
Thermometer	Alla® France Sarl	France	Analog thermometer	At-line milling temperature registration
Smo 01	Scaltec Instruments GmbH.	Germany	LOD evaporator	Moisture content determination of granules
Labor-Innova	Labor-Innova Műszeripari Kft.	Hungary	Drying chamber	Drying of granules
AccuDry®	Dynatech Scientific Labs	USA	Drying chamber	Short-term stability test of nanosuspensions
Hydro SM	Malvern Instruments Ltd.	UK	Small volume dispersion unit	Dispersing suspensions for particle sizing
Mastersizer 2000	Malvern Instruments Ltd.	UK	Laser diffractometer	PSD determinations of suspensions
Zetasizer nano ZS™	Malvern Instruments Ltd.	UK	Two angle particle and molecular size analyzer	PSD and zeta–potential determinations of nanosuspensions

Equipment/ Instrument	Manufacturer	Origin	Description	Application
8453-type	Agilent Technologies	USA	Single beam UV-Vis spectrophotometer	Sample absorbance determinations prior to particle sizing, during drug content, solubility, and dissolution tests
MicroGen 16	Herolab GmbH	Germany	Centrifuge	Phase separation for solubility studies
Hanna pH 210	Hanna Instruments Inc.	Canada	Microprocessor pH meter	Adjusting pH values of various dissolution media
SR-8 Plus™	Teledyne Hanson Research Inc.	USA	Dissolution test station	In vitro dissolution studies
Autoplus Maximizer	Teledyne Hanson Research Inc.	USA	Sampling controller for dissolution station	Generating sampling programs for dissolution studies
Autoplus MultiFill	Teledyne Hanson Research Inc.	USA	Hydraulic pump for online and offline sampling	Offline sampling during dissolution studies
PANalytical X'Pert3	Malvern Panalytical B.V.	The Netherlands	Powder X-ray diffractometer	Comparisons of diffraction patterns of solidified samples
Exstar 6000/6200	Seiko Instruments Inc.	Japan	DSC apparatus	Comparison of DSC thermograms of solidified samples

Equipment/ Instrument	Manufacturer	Origin	Description	Application
FT/IR-4200 with ATR PRO470-H	Jasco Products Company	USA	FT-IR spectrophotometer equipped with single reflection accessory	FT-IR spectral comparisons of solidified samples
Cypher S	Asylum Research	USA	AFM instrument	Morphological studies of microparticulate systems
JSM 6380LA	JEOL Inc.	USA	SEM instrument	Morphological studies of microparticulate systems

3.3. Methods

3.3.1. Surfactant assisted media milling process

Determination of the preliminary composition of presuspension regarding to drug loading (albendazole concentration) and surfactants is one of the utmost importance during nanosuspension formulation development [18]. Then critical process parameter optimization of the wet planetary bead milling process was applied. PM 100 planetary ball mill, with stainless steel containers of 12 ml, 50 ml and 500 ml capacity and zirconium-dioxide beads with sizes of d = 0.1 mm, d = 0.3 mm, d = 1.0 mm were utilized for milling. Stainless steel sieves, with mesh sizes of d = 800 µm, d = 180 µm and d = 63 µm, were applied for separation of the beads from the milled suspensions by simply pouring the content of containers onto these sieves, avoiding aggregation by vibration. Milling temperature control was part of every milling experiment. At-line control was performed immediately after milling programs have ended, top of the milling container was removed, the analog thermometer was inserted directly into the container and maximal milling temperature values were registered.

3.3.2. Face centered composition design and desirability approach

Experimental design has been adapted to formulation development for process optimization and process validation. The manufacturing process can be optimized using the traditional ‘‘trial and error’’ method by evaluating one variable at a time keeping all others constant but this may lead to suboptimal results since the interaction effects of the process variables are ignored and therefore a better process can be discovered [125]. With recent quality initiatives and regulatory prospects, implementation of quality by design (QbD) has now become an integral part of pharmaceutical industry.

The fundamentals of DOE approach are detailed in the following five-steps:

- The first step begins with identification of critical material (CMA) and quality attributes (CQA) as independent variables, which can substantially influence the development and manufacturing processes (e. g. hardness, particle size distribution, polydispersity, polymorphy, aqueous solubility, lipophilicity, melting point, dose, and acid-base status of the raw bulk material, milling temperature and zeta-potential in case of nanosuspension formulations).
- The second step involves the selection of response variables, critical process parameters (CPP), that may have direct impact on the product quality (e. g. milling time, milling speed, size of milling media in case of nanosuspension development with planetary ball milling).
- In step three, a versatile experimental design should be configured based on the study objectives, number and type of factors, factor levels and responses being evaluated. Then the experiments are conducted guided by the corresponding design and the response variables are evaluated using mathematical models.
- In the fourth step, statistical significance of the model shall be assessed based on the experimental data. Optimal processes parameters are assessed using graphical or mathematical techniques.
- The validation of responses predicted by the design model shall be performed in the final step. This is done by conducting confirmatory trials using RSM (response surface methodology) and the results are critically evaluated.

Based on the trial results the optimal process parameters are selected for manufacturing of the product.

Out of all the experimental designs, central composite designs (CCD) have been extensively used to optimization of manufacturing and validation processes. CCD is a response surface design which provides information on direct effects, pair wise interaction effects and curvilinear variable effects and is widely used for formulation and process optimization in the field of pharmaceutical product development [125–128].

Desirability is an objective function that ranges from zero outside of the limits to one at the goal. The optimization module searches for a combination of factor levels that simultaneously satisfy the criteria placed on each of the responses and factors. To include a response in the optimization criteria it must have a model fit through analysis or supplied via an equation only simulation.

Numerical optimization uses the models to search the factor space for the best trade-offs to achieve or satisfy multiple goals. Graphical optimization uses the models to show the volume where acceptable response outcomes can be found. The numerical optimization finds a point that maximizes the desirability function. The characteristics of a goal may be altered by adjusting the weight or importance. For several responses and factors, all goals get combined into one desirability function. The value of desirability is completely dependent on how closely the lower and upper limits are set relative to the actual optimum. The goal of optimization is to find a good set of conditions that will meet all the goals, not to get to a desirability value of 1.0. Desirability is simply a mathematical method to find the optimum. An overlay plot can be generated depending upon the pre-set conditions highlighting an area of desired operability. For that, first we need to choose the desired goal for each factor and response. The possible goals are: maximize, minimize, target, within range, none (for responses only) and set to an exact value (factors only.) A minimum and a maximum level must be provided for each parameter included. A weight can be assigned to each goal to adjust the shape of the desirability function. The "importance" of each goal can be changed in relation to the other goals. The default is for all goals to be equally important at a setting of 3 pluses (+++). If we want one goal to be most important, we could change it to 5 pluses (+++++). The program seeks to maximize this function. Contour, 3D surface, and perturbation plots of the desirability function at each optimum can be used to explore the function in the factor space [129].

The desirability function can be applied for the optimization of multiple response processes finding the levels of the controllable independent factors, which provide the most desirable Y_i response values. *The* d_i *(*Y_i*)* uses numbers to the possible response Y_i, where d_i *(*Y_i*)* = 1 represents a completely desirable value and d_i *(*Y_i*)* = 0 demonstrates a completely undesirable value. After fitting response model equations for all *Y* variables and defining the goals, the individual desirabilities of the five responses are combined for the overall desirability (*D*), calculating (Eq. (16)) using the geometric mean in our case for five responses as follows:

$$D = (d_1 \times Y_1 \times d_2 \times Y_2 \times d_3 \times Y_3 \times d_4 \times Y_4 \times d_5 \times Y_5)^{\frac{1}{5}} \quad \textbf{(16)}$$

There are numerous DOE approaches available for nanosuspension development e. g. evaluation of one variable at a time (OVAT)–type [130], 2^2–type factorial [131], 3^2–type factorial [132,133], Box-Behnken–types [130,134].

Utilization of the microhydrodynamic models for milling parameter optimization, ideal milling beads selection and describing their fluctuating motion during high energy wet stirred media milling (WSSM) process [135] has also gained attention in recent years [136].

3.3.3. Ideal loading composition determination for wet media milling

Loading composition optimization evaluations were carried out in the smallest laboratory sized container (12 ml), with batch sizes of 20.00 g, at high milling speed (500 rpm), also with high volume of applied milling beads (4.8 ml), while various milling programs, continuous operations were compared to cyclic ones, comprised of equally long milling and cooldown cycles, (5-5 minutes and 10-10 minutes, on-off) total process time was 60 minutes. For determination of albendazole loadings 1.00% (w/w), 2.00% (w/w), 3.00% (w/w) and 4.00% (w/w) were investigated. The influence of the surface-active agents and polymers on wet-milling of albendazole were compared in concentrations of 0.40% (w/w). Best performed emulsifier concentration was screened between the ranges of 0.30% (w/w) to 1.00% (w/w), application of antifoaming agent dimethylpolysiloxane at higher concentrations (> 0.50% (w/w)) was also involved. Results were evaluated by the following criteria: maximizing submicron sized fraction (%), while minimizing volume-weighted mean particle size D [4,3]) (µm), and span values (polydispersity or width of particle size distributions).

3.3.4. Particle size distribution and zeta-potential analysis

Particle size distributions of milled albendazole suspensions have been determined by both laser diffractometry (LD) and dynamic light scattering (DLS). For that, 100 µl of milled suspensions were dispersed dropwise in 100 ml of demineralized water at a mixing speed of 1500 rpm, with Mastersizer Hydro SM small volume dispersion unit. Sample absorbances have been measured prior to every particle sizing on wavelength λ_{max} = 633 nm, which is the wavelength of both (He-Ne) red laser beams, found in instruments Mastersizer 2000 laser diffractometer and Zetasizer nano ZS™ two angle particle and molecular size analyzer. Laser diffraction measurement were performed based on Mie scattering theory. Preset measurement conditions for laser diffractometry included the refractive index of albendazole 1.634, refractive index of dispersant water 1.333 and true density of albendazole 1.3 g/ml. True density of materials is required for specific surface area calculations from size distribution parameters. General purpose measurement with enhanced sensitivity mode was utilized, which is useful for sample characterizations containing irregular shaped particles. Every sample was measured five times individually and the mean ± standard deviation values were reported in the results section.

Recorded parameters were the submicron sized fractions (%), volume-weighted mean particle sizes (*D [4,3]*) (µm)) to track aggregation, and span values (width of particle size distributions). Each measurement took 20 seconds to perform suggested by the Malvern diffraction application v.5.60.10.0 (Malvern Instrument Ltd., UK), to allow slow moving larger aggregates to pass through the detector array.

For volume weighted particle size distributions, such as those measured by laser diffraction, it is often convenient to report parameters based upon the maximum particle size for a given percentage volume of the sample [137]. In this work the volume weighted mean particle size (*D [4,3]*) has been chosen as one of the dependent variables in 3-factor 3-level central composite design (face centered of alpha 1) over *d50*, the median particle size, and *d90*, which is the particle size based on 90% of the cumulative undersize distribution. The volume weighted mean particle size or volume moment mean (De Brouckere mean diameter) is relevant for many samples as it reflects the size of those particles which constitute the bulk of the sample volume. It is most sensitive to the presence of large particulates in the size distribution [137,138]. The equation for defining the volume mean is shown below (Eq. (17)):

$$D\ [4,3] = \frac{\sum_1^n D_i^4\ \times v_i}{\sum_1^n D_i^3 \times v_i} \qquad \textbf{(17)}$$

Where the D_i value for each screened channel is the geometric mean, the square root of upper multiplied by the lower diameters. For the numerator, the geometric D_i should be taken to the fourth power and multiplied by the percentage in that channel, summed over all channels. For the denominator the geometric D_i should be taken to the third power times the percent in that channel, summed over all channels [139,140].

One of the common values applied for describing the width of particle size distributions measured by laser diffraction method is the span parameter (Eq. (18)):

$$Span = \frac{D_{v0.9} - D_{v0.1}}{D_{v0.5}} \qquad \textbf{(18)}$$

Where the $D_{v0.9}$ or *d90* and $D_{v0.1}$ or *d10* are the particle sizes based on 90% and 10% of the cumulative undersize distributions, $D_{v0.5}$ or *d50* is the median particle size [139].

Final, optimized nanosuspension formula has also been characterized by DLS method as well. For that, 1 ml of dispersed, diluted nanosuspension has been withdrawn from the small volume dispersion unit and were poured into a PCS 1115 glass, sizing cuvette with square aperture (Malvern Instruments Ltd., UK). DLS measurement settings included: Automatic, non-invasive-backscattering (NIBS) mode with laser angle of 173^0, 28–32 sub runs/measurement, run durations: 10 seconds. Sample chamber was heated to 25.0 ^{0}C, and equilibration time was 300 seconds.

Automatic laser positioning and attenuation have been predescribed for DTS Application v.7.11.07073 (Malvern Instruments Ltd., UK), also five individual measurements were performed, for every sample and the mean ± standard deviation values were reported for all the DLS parameters, including: intensity-weighted mean hydrodynamic diameter (Z AVG d) and polydispersity index (PDI) values in this work. Zeta-potential values were also recorded with electrostatic light scattering (ELS) method, based on laser doppler micro-electrophoresis by registering the mobility of a fine particle placed into an electric field using the Smoluchowski model (Eq. (19)):

$$U_E = \frac{4\pi\varepsilon_0\varepsilon_r\zeta + 4\pi\varepsilon_0\varepsilon_r\zeta\kappa r}{6\pi\eta} \quad \textbf{(19)}$$

Where U_E is the mobility of fine particles in the electric field, ε_0 is the dielectric constant, ε_r is the electrical permittivity of vacuum, η is the viscosity of the solution or dispersion, ζ is the zeta-potential, κ is the Debye-Hückel parameter, r is the particle radius [141].

The instrument was operated by automatic selection of voltage based on the measured conductivity values of diluted milled suspensions and dispersions. Sample preparations involved carefully pouring 750 µl of diluted milled samples into DTS 1070 capillary folded, disposable zeta cells (Malvern Instruments Ltd., UK) to avoid the formation of bubbles in capillaries, which can mislead measurement results. Zeta-potential distributions were registered in automatic mode from 5 parallels after 300 seconds equilibration time at 25 ^{0}C and the mean ± standard deviation values were reported. Dispersant viscosity correction was not necessary, because calculated surfactant concentration and milled active content of diluted samples was 0.0005% (w/w) and 0.00365% (w/w) respectively, which had no impact on dispersant viscosity.

3.3.5. Process parameter optimization of wet-milling

In order to characterize the relationship between formulation factors and their impact on the output variables response surface methodology based on face centered central composite design was utilized. The sizes of zirconia beads, the milling speed and the milling time values can significantly influence the quality performance of nanosuspensions. In this study these were the analyzed formulation variables. Milling experiments were carried out in 500 ml containers, with two different volumes of milling beads (100 ml and 200 ml) as category factors, where batch sizes were 425.5649 g and 476.1498 g, respectively. A three-level (+1, 0, -1) factorial design for the optimization of the independent variables with 32-32 runs (5-5 center points) was applied to each category.

Submicron sized fraction (%) (Y_1), volume-weighted mean particle size ($D\ [4,3]$) (µm) (Y_2), span of particle size distributions (Y_3), zeta-potential (mV) (Y_4) and milling temperature (^{0}C) (Y_5) values were selected as responses (dependent variables). Experiments were run in random order to increase the predictability of the quadratic models.

The following 3-level factorial polynomial equation (Eq. (20)) was fitted to the measurement data:

$$Y_n = b_0 + b_1 \times X_1 + b_2 \times X_2 + b_3 \times X_3 + b_{12} \times X_1 \times X_2 + b_{13} \times X_1 \times X_3 + b_{23} \times X_2 \times X_3 + b_{11} \times {X_1}^2 + b_{22} \times {X_2}^2 + b_{33} \times {X_3}^2 \quad \textbf{(20)}$$

where Y_n were the dependent variables; b_0 was the intercept, the arithmetic mean of all quantified outcomes of 32 runs; b_1, b_2 ,b_3 were the individual polynomial coefficients describing the influence of each parameter on the outcome; b_{12}, b_{13}, b_{23} were the coefficients of the interaction functions; and b_{11}, b_{22}, b_{33} were the coefficients of the quadratic functions. X_1, X_2, X_3 values were the independent variables, where X_1 represented the milling time (20, 40 and 60 minutes long programs were screened), X_2 represented the milling speed (effect of 200, 400 and 600 rpm on wet-milling were investigated) and X_3 represented the sizes of milling beads (effect of d = 0.1, d = 0.3 and d = 1.0 mm sized zirconia beads on wet-milling were compared).

The optimization and statistical experiments were designed and evaluated using the Design-Expert® software version 7.0.0 (Stat-Ease® Inc., USA). A quadratic polynomial 3-level factorial response surface design type has been predescribed, with no blocks.

Numerical optimization preset evaluation conditions included: maximizing submicron sized fraction, with target set to 100% importance (weighting) to 5 (+) maximal, minimizing volume-weighted mean particle size, where upper target was (*D [4,3]*) (µm) < 0.600 µm importance (weighting) 5 (+) maximal, minimizing span (width of particle size distributions) importance (weighting) 3 (+), minimizing zeta-potential (mV), where upper target was < -30 mV importance (weighting) 5 (+) maximal and also minimizing milling temperature (^{0}C) values, with upper target of < 40 ^{0}C importance (weighting) 5 (+) maximal (**Table VII/B**).

For end-product process parameter selection economical purposes were also taken into consideration, such as maximizing loading and yield, while minimizing energy consumption (milling speed and process time) importance (weighting) 5 (+) maximal. (**Table VII/A**).

Table VII. *(A) Independent variables with levels and goals for the construction of DOE (B) Preset nanosuspension criteria for the evaluation of dependent variables with numerical optimization of desirability function*

A

Volume of milling beads		**100 ml**			**200 ml**			
Independent variable	**Code**	**Levels**			**Levels**			**Goals**
		-1	0	+1	-1	0	+1	
Milling time (mins)	X_1	20	40	60	20	40	60	Min.
Milling speed (rpm)	X_2	200	400	600	200	400	600	Min.
Sizes of milling beads (mm)	X_3	0.1	0.3	1.0	0.1	0.3	1.0	None

B

Volume of milling beads		**100 ml**		**200 ml**	
Dependent variable	**Code**	**Target**	**Goals**	**Target**	**Goals**
Submicron sized fraction (%)	Y_1	Y_1 = 100	Maximize	Y_1 = 100	Max.
D [4,3] (µm)	Y_2	Y_2 < 0.600	Minimize	Y_2 < 0.600	Min.
Span	Y_3	None	Minimize	None	Min.
Zeta-potential (mV)	Y_4	Y_4 < -30	Minimize	Y_4 < -30	Min.
Milling temperature (^{0}C)	Y_5	Y_5 < 40	Minimize	Y_5 < 40	Min.

3.3.6. Maximizing albendazole yield after optimized milling process

Economic considerations necessitate the maximization of yield for cost effective manufacturing. In order to do so, several washing experiments have been performed and compared by an additional 16.66% (w/w) of suspension loading of surfactant solution added to separated beads in milling container with 500 ml capacity. Surfactant solution consisted of 0.50% (w/w) Tween 80 and 0.01% (v/v) of antifoaming agent dimethylpolysiloxane. The operation was repeated by the addition of two times of 16.66% (w/w) container mass loading, followed by one time of 33.33% (w/w), then two times of 33.33% (w/w).

An additional milling cycle was applied after every surfactant solution addition to separated beads on 300 rpm milling speed for 5 minutes followed by another separation on stainless steel sieve with mesh size of d = 63 μm. Collected and diluted nanosuspensions were mixed with milled ones on heatable magnetic stirrer MS–H-S10 at a stirring speed of 600 rpm, with a homogenization time of 5 minutes. Drug loading, particle sizing and zeta-potential determinations were performed after each washing experiment in order to study the effect of dilution on dosage, particle size distribution parameters and physical stability.

3.3.7. Short-term physical stability evaluations of nanosuspension

Physical stability of the optimized formula was tracked by registering particle size distribution parameters and zeta-potential values at predetermined storage intervals: 1, 2, 3, 24, 48, 72, 168, 336, 672, 1344 hours at 25 ^{0}C 60% (RH) and at 4 ^{0}C 60% (RH). Samples were stored in 25 ml volumetric, brown vials, protected from direct sunlight. Each sample was shacked manually for ten seconds prior to investigations. For particle size distribution and zeta-potential measurement settings, see section 3.3.4. Particle size distribution and zeta-potential analysis.

3.3.8. Nano- and macro suspension solidifications by wet granulation method

Based on preliminary loading composition optimization milling trials, freshly prepared ABZ nanosuspensions were immediately transformed to a solid form by wet granulation processes. Critical milling conditions were as following: batch sizes of 80 g with 20 ml of applied d = 0.1 mm sized zirconia beads in milling container of 50 ml capacity, milled at 400 rpm rotation speeds for 120 minutes in 5:5 cyclic mode.

It has already been reported that water is retained in a porous material during wet granulation of MCC as a result of absorption and capillary effects. The material was characterized by irreducible saturation, which refers to liquid, which remains in porous bed, regardless of any further increase in pressure applied. For MCC and water, irreducible saturation was 90% (w/w), this indicates high extent of solid liquid interaction [142]. In order to avoid supersaturation of MCC and maximizing drug content of granules, we have applied only 85% (w/w) of milled and unmilled suspension added to weighted amount of the dried MCC carrier, during wet granulation. Thus 11.45 g of dried MCC carrier (Vivapur® 12) was dispensed into a steel mortar, utilizing the analytical balance.

After every milling process 9.73 g of obtained ABZ nanosuspension was added to the carrier and mixed manually by kneading in steel mortar for 3 minutes, then sieved through a stainless steel sieve with mesh size of d = 180 μm and dried in a Labor-Innova drying chamber on 40 ^{0}C for 2 days. Dried granules were sieved again (regranulation) through the same sieve used for granulation. This process was repeated 8 times to achieve a desirably low dose. Solid suspension of unmilled albendazole was prepared the same way, but instead of milling, an IKA RCT basic, heatable magnetic stirrer was employed for dispersing of albendazole at 400 rpm mixing speed, for 120 minutes on 24 ^{0}C.

3.3.9. Moisture content and particle size determinations of dried granules

Determination of the moisture content values are a part of every solid dosage form preformulation study and batch to batch production influencing the processability and long-term stability of these products [143,144]. The moisture content values of the albendazole containing granules were measured by the loss on drying (LOD) method, with an evaporator. Predetermined temperature was set to 95 ^{0}C and batch sizes of 1.000 g of milled and unmilled solidified suspensions.

From quality by design (QbD) perspective, critical physical parameters of granules are particle size distribution, content uniformity, morphology and porosity [145,146]. Particle size distribution comparison of granules and MCC Vivapur® 12 powder was performed by sieve analysis method, utilizing stainless steel sieve series containing sieves with 315 μm, 180 μm, 125 μm, 50 μm, 32 μm mesh sizes mounted on a vibrational sieve shaker. Fractionation adjusted parameters, included: amplitude of vibration 1.5 mm and process time 5 minutes were applied. Cumulative undersize distributions (% (w/w)) were calculated from the masses of leftover fractions on sieves.

3.3.10. Reconstitution of nanocrystals from solidified nanosuspensions

Particle size distributions of milled suspensions and released ABZ nanocrystals from dry suspensions have been determined by dynamic light scattering (DLS) method.

Before dispersing the milled suspensions and dry suspensions in 100 ml of pH = 6.50 artificial rumen fluid (ARF), pH = 6.80 dissolution medium and demineralized water, the dispersants were prefiltered applying 0.22 µm pore sized nylon (NY) syringe membrane filters (Nantong FilterBio Membrane Co. Ltd., China).

Filtered media were heated to 37 ^{0}C by mixing them at 250 rpm rotation speeds, and with small magnetic stirrer bars, on heatable magnetic stirrer IKA RCT basic. A dose of dispersions, containing 200 mg of albendazole were then added to each filtered dispersant and mixed using the same 250 rpm mixing speed for 60 minutes until registered derived count rate (DCR) values showed sufficient number of released particles (> 25000 counts/second). From these solutions 5 ml of samples were taken with a syringe and filtered through 0.45 µm pore sized polytetrafluoroethylene (PTFE) membrane syringe filters Whatman® UNIFLO® (Sigma-Aldrich Co., USA) prior to measurements, in order to remove MCC carrier particles. For particle size and zeta-potential determinations, see section 3.3.4. Particle size distribution and zeta-potential analysis.

3.3.11. Thermodynamic solubility studies

Thermodynamic solubility studies were determined using a slightly modified version of the classical saturation shake-flask method in dissolution media at pH = 1.2 (0.1 N hydrochloric acid), pH = 4.5 (phosphate-buffer) and pH = 6.8 (phosphate-buffer) for optimized albendazole nanosuspension. For albendazole containing solid suspensions investigations were carried out in media at pH = 1.20 (0.1 N hydrochloric acid), pH = 6.50 artificial rumen fluid (ARF) and pH=6.80 (phosphate-buffer). Albendazole powder (10 mg), milled and unmilled surfactant dispersions containing 10 mg of albendazole were poured into volumetric vials with screwcaps and 10 ml capacity. An additional 5 ml of dissolution media were poured on top of the samples. The contents of the sealed vials were mixed at speed 800 rpm and heated to 37 ^{0}C with heatable magnetic stirrer MS-H-S10 and magnetic stirrer bars for 24 hours, then sedimentation was utilized for another 24 hours on 37 ^{0}C as well.

It has already been reported by Baka et al. (2008), that the safest way for phase separation is sedimentation, although diluted milled samples formed stable colloidal systems, where sedimentation was not enough for phase separation [147].

As a result, aliquots were taken and centrifuged at 14000 rpm for 15 minutes. For samples containing ABZ suspensions to avoid dissolved ABZ absorption of syringe mounted membrane filters and to increase precision and reproducibility, membrane filtering has been ignored, only centrifugation had been utilized for phase separation [148]. Complete phase separation has been confirmed by transmittance analysis and dynamic light scattering particle sizing methods. Three clean supernatants were taken and measured, the mean thermodynamic solubility values (μg/ml) ± SDs were calculated from the linear calibrations in each dissolution medium and were determined by spectrophotometry on the absorption maximum of albendazole at wavelength λ_{max} = 291 nm.

For samples containing solid carrier MCC particles, filtering was necessary after centrifugation. For that, 0.22 μm pore sized nylon (NY) syringe membrane filters (Nantong FilterBio Membrane Co. Ltd., China) were utilized prior to measurements.

3.3.12. Artificial rumen fluid (ARF) medium at pH = 6.50 preparation

Utilizing the analytical balance, the following constituents were dispensed: 9.80 g of sodium hydrogen carbonate (Molar Chemicals Kft., Hungary), 9.30 g of disodium hydrogen phosphate dodecahydrate (Molar Chemicals Kft., Hungary), 0.47 g of sodium chloride (Molar Chemicals Kft. Hungary), 0.57 g of potassium chloride (Molar Chemicals Kft., Hungary), 0.06 g of magnesium chloride anhydrate, (Sigma-Aldrich Co., USA) and were dissolved in 750 ml of demineralized water. Then 0.04 g of calcium chloride anhydrate (Sigma-Aldrich Co., USA) was dissolved in 10 ml of demineralized water and this solution was then added to the first solution. 20 ml of 5 M acetic acid solution was diluted with demineralized water from concentrated acetic acid (99.5%) (Molar Chemicals Kft., Hungary) and also added to the first solution. The volume was completed to 1000 ml with demineralized water. Finally, the pH should be in the range of 5.5 to 6.5. If it is not, 5 N hydrochloric acid or 5 N sodium hydroxide solutions should be used for pH adjustments [149]. The pH value of the solution was exactly 6.50, no pH adjustments were required.

3.3.13. Drug content determinations of liquid and solid samples

Since albendazole has pH dependent, poor water solubility, with a maximum at pH = 1.2 (mentioned in section 1. Introduction) as a weak base compound, it was evident to determine the amount of active content in highly diluted stock solutions at pH = 1.2 (Ph. Eur. 9). Three stock solutions have been prepared by adding 0.25 ml of milled ABZ suspension to 0.1 N hydrochloric acid in 250 ml volumetric flasks. Final volumes were completed to 250 ml (1000 times dilution) mixed on heatable magnetic stirrer MS-H-S10 (DLAB Instruments Ltd., China) at stirring speed of 1000 rpm, with a homogenization time of 60 minutes on 24 ^{0}C. Stock solutions were transparent and floating, undissolved particles were not registered. Mean administration volume values (ml) ± SDs of nanosuspensions containing 200.0 mg ABZ determined by UV-Vis spectrophotometry on the absorption maximum of albendazole at wavelength λ_{max} = 291 nm.

For solidified samples three stock 2000 ml stock solutions have been prepared by weighing in 1 g of dispersions into 2000 ml volumetric flasks and diluted with 0.1 N hydrochloric acid to 2000 ml, stirred at 1000 rpm speed with IKA RCT basic, heatable magnetic stirrer for 24 hours on 24 ^{0}C. Withdrawn samples were filtered through 0.22 µm pore sized nylon (NY) syringe membrane filters (Nantong FilterBio Membrane Co. Ltd., China) prior to measurements for the removal of MCC particles. Mean drug content values were calculated in % (w/w). Dose determinations of solid suspensions were based on studying the therapeutic efficacy, toxicity pharmacokinetics of albendazole and therefore a 200 mg dose was preferred [82] [150].

3.3.14. In vitro dissolution studies

Dissolution tests were performed by USP apparatus 2 (paddles) methods at 75 rpm rotation speed for suspensions and 100 rpm for solidified suspensions at $37 \pm 0.2\ ^{0}C$ bath temperatures. Dissolution kinetics of optimized nanosuspensions, albendazole containing surfactant dispersions and albendazole powders were investigated in 900 ml aqueous-based buffer solutions at pH = 1.2 (Ph. Eur. 9) (in doses of 200 mg), pH = 4.5 phosphate buffer solution (Ph. Eur. 9) (in doses 100 mg) and pH = 6.8 phosphate buffer solution (Ph. Eur. 9) (in doses 100 mg). Dissolution profiles of unmilled and milled Vivapur® 12 dispersions containing 200 mg of albendazole, compared to 200 mg of albendazole powder were studied in 900 ml of pH = 1.2 (Ph. Eur. 9), pH = 6.50 artificial rumen fluid (ARF) and pH = 6.8 phosphate buffer solution (Ph. Eur. 9).

At predetermined time-points 5 ml of samples were withdrawn from the vessels and filtered through P/N FIL10S-HR 10 µm pore sized full flow membrane filters (Quality Lab Accessories L.L.C., USA) placed on the e-probes. Samples were collected in offline mode to 16 x 100 type rack into test tubes. After every sampling, media replacement was accomplished by 5 ml of fresh buffer solutions.

Collected samples of liquid dosage forms were filtered through 0.1 µm pore sized polyether sulfonate (PES) syringe membrane filters (Nantong FilterBio Membrane Co. Ltd., China) prior to measurements, in order to remove undissolved particles. Dissolution studies were performed in triplicates and the cumulative drug release (%) mean values ± SDs were calculated from the linear calibrations in the defined dissolution media, determined by UV-Vis spectrophotometry on the absorption maximum of albendazole at wavelength λ_{max} = 291 nm.

Dissolution rate constants (k $[min^{-1}]$) have been calculated considering thermodynamic solubility values (M_∞) measured in appropriate media, lag times (t_0), shape parameter (β) and (τ_d) mean dissolution time values with the minimization of sum of square values between measured and calculated dissolution points, performed by smoothening fitting with Excel 2016, (Microsoft Corp., USA) solver plug-in followed by Weibull-model calculation, according to (Eq. (21)) (Langenbucher, 1976.):

$$M_t = M_\infty \times [1 - exp - (\frac{t-t_0}{\tau_d})^\beta] \quad \textbf{(21)}$$

Where M_t is the dissolution (%) at time 't' (min), M_∞ is the dissolution (%) at infinite time, t_0 is the lag-time (min) of the dissolution, β is the shape parameter of the fitted polynoms, τ_d is the mean dissolution time (min), when 63.2% of M_∞ has been dissolved [151].

3.3.15. Solid state characterization investigations of solidified samples

3.3.15.1. Diffraction pattern comparison of solids

Diffraction patterns were registered powder diffractometer using Cu Kα radiation with 45 kV accelerating voltage and 40 mA anode current over the range of 5–40^0 2θ with 0.0084^0 step size and 99.695 s times per step in reflection mode, spinning the sample holder by 1 s^{-1} rotation speed. Incident beam optics was as following: programmable divergence slit with 15 mm constant irradiated length, anti-scatter slit at fixed 2^0. Diffracted beam optics consisted of X'Celerator Scientific ultra-fast line detector with 0.02^0 soller slit and programmable anti-scatter slit with 15 mm constant observed length. Single crystalline silicon zero-background diffraction plates were utilized in case of diffraction pattern comparisons of starting material ABZ powder, albendazole processed in milled and in unmilled suspension forms after drying.

Milled and unmilled ABZ suspensions were poured into Petri dishes and dried slowly in AccuDry® drying chamber on 40.0 ^{0}C, for 2 days under air atmosphere and pressure. Dried powders were gently removed from dishes and sieved through a 30 μm mesh size stainless steel sieve before analysis. Data were collected by PANalytical Data Collector Application, version 5.5.0.505 (Malvern Panalytical B.V., The Netherlands).

3.3.15.2. DSC thermogram comparisons

Comparison of the phase transitions and thermoanalytical behaviors of solid samples were investigated by differential scanning calorimetry (DSC) method. 3 mg of solid samples were accurately dispensed into small aluminum pans and the empty pans were used as blanks to calculate the enthalpy (mJ/mg) values required for the phase transitions. Temperature of the sample chamber was fluctuated between 4 ^{0}C to 250 ^{0}C, heating rate was 10 ^{0}C/min and investigations were carried out under air atmosphere.

3.3.15.3. FT-IR spectral comparisons

Physicochemical properties of MCC carrier Vivapur® 12, albendazole powder, granules of unmilled solid suspension and milled solid suspension were examined and compared by FT-IR method in absorbance mode. The spectra were collected over a wavenumber range of 4000 to 800 cm^{-1}. After performing 50 scans, the measurements were evaluated with the software Spectra Manager-II, (Jasco Product Company, USA).

3.3.16. Morphological investigations of solid particulate systems

In order to get an actual understanding of particle morphology microscopic techniques are preferred. In search for milled albendazole nanocrystals on the surface of the milled dispersion, the surfaces of the albendazole powder, MCC carrier (Vivapur® 12), their physical mixture and the albendazole milled dispersion have been scanned and compared.

3.3.16.1. AFM imaging

Double sided tape was mounted on a metal AFM specimen disc (Ted Pella Inc., Redding, CA) and a small fraction of the microparticulate systems were poured on it. Unbound particles were removed with a stream of N_2 gas. AFM images were collected from the surfaces of individual particles in non-contact mode at 1–2 Hz line-scanning rate in air, using a silicon cantilever (OMCL AC-160TS, Olympus, Japan), typical resonance frequency 300–320 Hz. Temperature during the measurements was $29 \pm 1\ ^0$C. AFM amplitude contrast images are shown in this work.

3.3.16.2. SEM imaging

SEM images were collected from the surfaces of individual particles. Accelerating voltages varied from 5 kV to 10 kV and spot sizes from 8 to 10 depended on the electrostatic charge-up of microstructured surfaces. Images with 100–1500 times of magnifications have been taken from microparticulates for particle size determinations and 1000–3000 times for particle surface morphological comparisons.

4. Results and discussions

4.1. Ideal loading composition determination for wet media milling

When performing milling trials with d = 1.0 mm sized milling media, applying concentration of 0.40% (w/w) Tween 80 solutions as stabilizers at 3.00% (w/w) albendazole loading, zirconium-oxide beads seemed to be the ideal choice, according to predetermined criteria (see end of section 3.3.5. Process parameter optimization of wet-milling), although slightly increased polydispersity compared to the results of milling experiments with plastic and stainless steel beads. There was no difference in milling temperature values; it was 29 ^{0}C after each milling experiment (**Figure 7**).

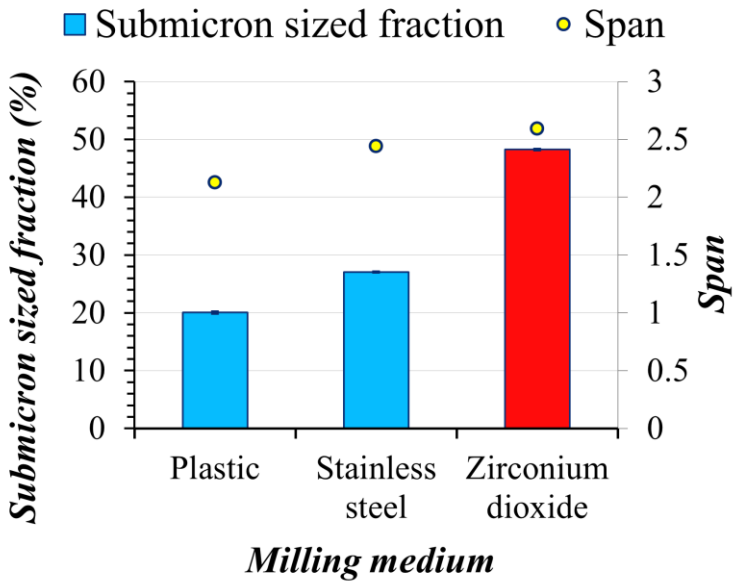

Figure 7. *Effect of the texture of milling media on wet media milling of albendazole, milling parameters: 8 ml loading, 500 rpm rotation speed, 60 minutes long operation, 4.8 ml applied d = 1.00 mm sized milling beads, n = 3, mean values ± SDs, where columns represent submicron sized fractions, o symbols: span values; red color the selected milling medium*

To increase performance by increasing the contact surface between suspension and the beads, we switched to d = 0.3 mm sized zirconia beads for further investigations. As expected, milling temperature values have massively increased on 500 rpm milling speed, with continuous operations. To offset this phenomenon, various cyclic operations have been introduced and compared, in order to keep the milling temperature as low as possible. We have registered the heating and cooldown rates of loadings and found out, that based on the utilized milling speed, milling time and container size, it took 30-80 minutes to cooldown to room temperature at 200 ml amount of applied beads. The slow cooldown rates were compensated by limited milling time, rotation speed to obtain ABZ nanosuspensions. We have compared shorter and longer programs, with equally long cooldown cycles (5:5 (mins), 10:10 (mins) on-off) and continuous operations. After 60 minutes of milling sessions, the milling temperature values were 31.0 ^{0}C, 38.0 ^{0}C and 60.0 ^{0}C, respectively. Both milling temperature values and particle size distribution evaluation results favored the selection of 5:5 (mins) (on-off) milling program. As a result, we have chosen this milling program, along with the same previously determined settings for further investigations (**Figure 8**).

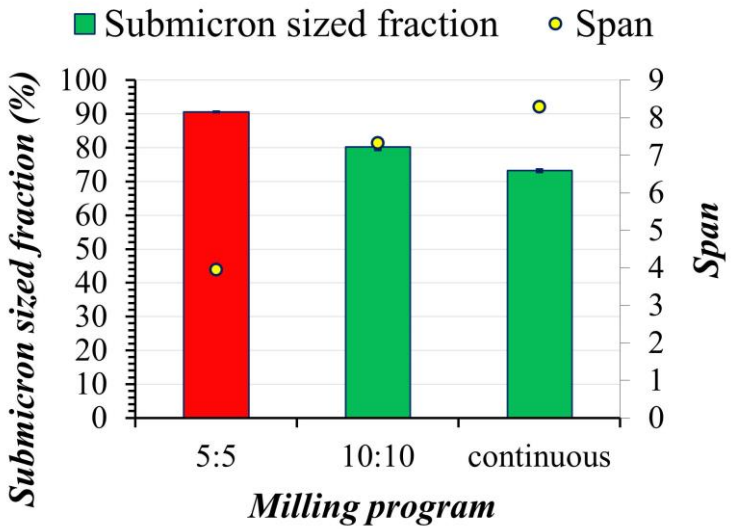

Figure 8. *Effect of milling program on wet media milling of albendazole, where columns represent submicron sized fractions, o symbols: span values; red color the selected milling program, n = 3, mean values ± SDs*

Applied milling parameters were as following: 8 ml loading in container with 12 ml capacity, 500 rpm rotation speed, 60 minutes long operation, 4.8 ml applied d = 0.3 mm sized zirconia beads. In order to compare surface-active agents, that were the most ideal for wet planetary bead milling of ABZ, two non-ionic (Tween 20 and 80), one anionic (SLS) emulsifiers, four triblock copolymers (Lutrol® F127, Lutrol® F68, Kolliphor® EL, and Kolliphor® RH40) and two water soluble polymers (Kollidon® K30, Benecel™ E3 pharm.) with low molecular weight values in concentrations of 0.40% (w/w) have been tested (**Figure 9/A**).

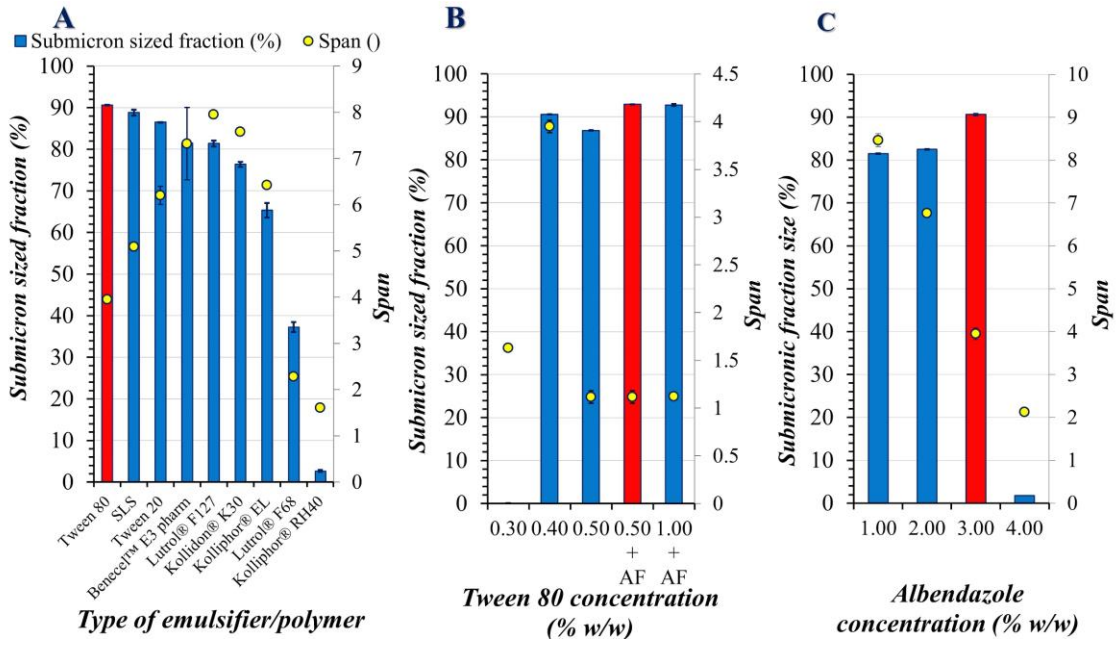

Figure 9. *Loading composition optimization for wet planetary bead milling of ABZ, A: Influence of the quality of surface-active agents and polymers, B: Influence of the quantity of Tween 80 and C: Influence of the ABZ loading on particle size distribution parameters of ABZ measured by laser diffraction n = 5, mean values ± SDs, where columns represent submicron sized fractions, o symbols: span values; red color the selected composition and AF = Antifoaming agent added to composition*

All types of surfactants, along with water soluble polymers Lutrol® F127, Kollidon® K30 and Benecel™ E3 pharm. showed promising results.

Best performed emulsifier however was Tween 80 considering 90% submicron sized fraction and lowest span value compared to suitable alternatives. Toxicity evaluations of surface active agents favor the selection of nonionic Tween 80 over anionic SLS and lower hydrophilic-lipophilic balance (*HLB*) value of Tween 80 ($HLB_{Tween\ 80}$ = 15.0) supports it over Tween 20 ($HLB_{Tween\ 20}$ = 16.7) in stabilization attempts of dosage forms containing lipophilic entity ABZ ($log\ P_{ABZ}$ = 3.14-3.83) [94,152,153]. It seemed emulsifier/polymer type had no impact on milling temperature values, 31.0 ^{0}C was measured in all cases. Ideal surface-active agent (Tween 80) concentration was also screened between the concentration rage of 0.30% (w/w) to 1.00% (w/w) with and without antifoaming agent dimethylpolysiloxane in 0.01% (v/v) at above 0.50% (w/w) emulsifier, suggested by the user's manual of Foamsol (**Figure 9/B**). Above 0.40% (w/w) Tween 80 submicron sized fractions were about 90%, highest value (92.89%) registered at 0.50% (w/w) Tween 80 + 0.01% (v/v) dimethylpolysiloxane solutions, increasing amount of Tween 80 had a positive impact on polydispersity (span) values. Application of antifoaming agent in this concentration slightly increased submicron sized fraction from 86.84% to 92.89% and had no impact on polydispersity, although significantly improved milled suspension average yield from 50.12% (w/w) to 60.53% (w/w) after the separation from beads. Ideal drug loading investigations involved the screening of 1.00-4.00% (w/w) ABZ at predetermined best performed conditions (**Figure 9/C**). Best-case scenario was the application of 3.00% (w/w), which yielded maximal submicron sized fraction, with minimal polydispersity values at highest drug loading. Milling temperature values were slightly different this time, 28.0 ^{0}C, 29.0 ^{0}C, 31.0 ^{0}C and 40 ^{0}C, respectively.

4.2. Effect of milling process parameters

The process parameters during laboratory scale bead milling process were optimized for the development of albendazole nanosuspensions using 3-factor 3-level central composite design (face centered of alpha 1) as the response surface methodology. A stepwise regression was used to build quadratic equations for each response variables. The optimization and statistical experiments were designed and evaluated with the Design-Expert® software version 7.0.0 (Stat-Ease® Inc., USA). For a design space containing $3^3 = 27$ trials, this software suggested, that alpha should be set to 1 and the utilization of 5 center points [154]. For all dependent variables (responses) (Y_n) quadratic model fittings were suggested and selected manually.

For dependent data analysis transformations were not utilized, the software suggested the highest ordered polynomial fitting selections, where additional terms were significant and the models were not aliased, results of lack-of-fit tests were insignificant, as well as adjusted R-squared and predicted R-squared values were maximized. The response variables listed in **Table VIII** are fitted to a third-order polynomial model and, the regression coefficients for each term in the regression model are summarized also in **Table VIII** along with R – squared values.

Table VIII. *Polynomial model coefficients and statistical results of analysis based on the 3-factor 3-level face centered composite design (alpha 1) (statistical significance of the observed parameter indicated by * symbol, where p-value < 0.05)*

Polynomial coefficients/volume of applied beads	**Y_1 Submicron sized fraction (%)**		**Y_2 D [4,3] (µm)**		**Y_3 Span**		**Y_4 Zeta-potential (mV)**		**Y_5 Milling temperature (^{0}C)**	
	100 ml	***200 ml***	***100 ml***	***200 ml***	***100 ml***	***200 ml***	***100 ml***	***200 ml***	***100 ml***	***200 ml***
b_0	+39.90	+51.13	+1.59	+1.29	+2.28	+2.05	-33.38	-34.47	+34.92	+32.15
b_1	***+4.13****	***+3.81****	***-0.31****	***-0.26****	***-0.22****	***+0.51****	***-0.83****	-0.08	+0.69	***+1.19****
b_2	+0.07	-0.93	***-0.18****	+0.23	-0.01	***+0.60****	***+0.66****	**+1.26***	***+12.44****	***+7.97****
b_3	***-34.78****	***-34.28****	***+1.25****	***+1.05****	***+0.24****	-0.28	***-1.88****	***-3.33****	***-1.56****	***+0.97****
b_{12}	+0.04	-1.69	***+0.14****	+0.06	+0.06	+0.60	***-0.48****	***+1.28****	+0.58	+0.62
b_{13}	+0.15	***+5.22****	***-0.35****	***-0.62****	***-0.14****	***-1.07****	-0.25	***+0.17****	+1.04	***+1.54****
b_{23}	***+2.01****	+1.16	***-0.27****	-0.03	***-0.21****	-1.21	***+1.43****	***-1.50****	***-2.25****	***+1.92****
b_{11}	-0.16	-1.32	+0.14	+0.19	+0.001	-0.28	***-1.68****	+3.78	-1.74	-0.50
b_{22}	***-4.12****	-2.16	***+0.22****	-0.16	+0.04	-0.60	***-1.65****	**+2.64***	+1.34	+1.00
b_{33}	***+19.81****	***+13.27****	+0.02	***+0.32****	***+0.21****	***+1.30****	***+1.18****	***+6.53****	***+2.68****	+0.83
P-value	<0.0001	<0.0001	<0.0001	<0.0001	<0.0001	<0.0001	<0.0001	<0.0001	< 0.0001	< 0.0001
R-squared	0.9941	0.9819	0.9739	0.9259	0.9673	0.8547	0.9652	0.9454	0.9347	0.9584
Adj. R-squared	0.9917	0.9744	0.9632	0.8956	0.9539	0.7953	0.9510	0.9230	0.9080	0.9414
Pred. R-squared	0.9861	0.9570	0.9272	0.7774	0.9222	0.5982	0.9113	0.8524	0.8370	0.8944
Adeq. Precision	57.686	33.752	36.226	20.840	37.552	17.615	35.516	22.450	19.258	28.451

Every design point was well fitted to the polynoms, demonstrated by the significance of fitted models (p-value < 0.05), high (> 0.85) coefficient of determination values and high (> 10) signal to noise ratios, which indicated that, the milling experiment have been performed precisely and results were reproducible. Statistical significance (p-value < 0.05) of the observed parameter was indicated by * symbol. The following subsections involve the in depth analysis of the impact of independent variables on dependent variables (responses).

4.2.1. Submicron sized fraction (Y_1)

Maximizing this parameter is desirable for formulation development of nanosuspensions, therefore any factor increasing its value considered as positive impact. At 100 ml of applied beads, significance of increasing milling time (X_1) had a positive impact (b_1), increasing diameter of zirconia beads (X_3) had a negative impact (b_3) on submicron-sized fraction (Y_1), interaction of milling speed and the size of milling medium ($X_2 \times X_3$) had a positive impact (b_{23}) on the observed parameter.

The quadratic function of milling speed ($X_2{}^2$) had a negative impact (b_{22}), while and the size of milling media ($X_3{}^2$) had a positive impact (b_{33}) on submicron-sized fraction (Y_1).

At 200 ml of applied beads, significance of milling time (X_1) positively (b_1), the increasing diameter of zirconia beads (X_3) negatively (b_3), their interactions ($X_1 \times X_3$) positively (b_{13}) and the quadratic function of the size of milling media ($X_3{}^2$) also positively (b_{33}) influenced the submicron-sized fraction (Y_1).

4.2.2. Volume-weighted mean particle size (Y_2)

Minimizing this parameter is desirable for formulation development of nanosuspensions, therefore any factor decreasing its value considered as positive impact. At 100 ml of applied beads, volume-weighted mean particle size (Y_2) reduction was positively (b_1, b_2) influenced by the increasing milling time (X_1) and milling speed (X_2), negatively (b_3) by the increasing size of the zirconia beads (C), negatively (b_{12}) by the interaction of the milling time and speed ($X_1 \times X_2$), positively (b_{13}, b_{23}) by the interaction of milling time and the size of milling media ($X_1 \times X_3$), as well as the interaction of milling speed and size of milling media ($X_2 \times X_3$). Negative (b_{22}) effect of the quadratic function of milling speed ($X_2{}^2$) can also be reported on mean particle size reduction.

At 200 ml of applied beads, volume-weighted mean particle size (Y_2) reduction was positively (b_1) influenced by the increasing milling time (X_1), negatively (b_3) by the increasing size of zirconia beads (X_3), interactions of milling time and size of milling media ($X_1 \times X_3$) had a slight positive impact (b_{13}), and the quadratic functions of the increasing size of milling media (X_3^2) had a negative (b_{33}) effect on mean particle size reduction.

4.2.3. Span (polydispersity) values of particle size distributions (PSDs) (Y_3)

Minimizing this parameter is desirable for formulation development of nanosuspensions, therefore any factor decreasing its value considered as positive impact. At 100 ml of applied beads, span values of particle size distributions (PSDs) (Y_3) were positively (b_2) influenced by the increasing milling speed (X_2), negatively (b_3) by the increasing size of zirconia beads (X_3), positively (b_{13}) by the interaction of milling time and size of milling media ($X_1 \times X_3$), positively (b_{23}) by the interaction of the milling speed and size of beads ($X_2 \times X_3$) and negatively (b_{33}) by the quadratic function of the increasing size of the milling media (X_3^2).

At 200 ml of applied beads, span values of PSDs (Y_3) were negatively (b_1, b_2) influenced by the increasing milling time (X_1) and milling speed (X_2), positively (b_{13}) by the interaction of milling time and size of milling media ($X_1 \times X_3$) and negatively (b_{33}) by the quadratic function of the size of beads (X_3^2).

4.2.4. Zeta-potential values (Y_4) of milled ABZ suspensions

Minimizing this parameter is desirable for formulation development of nanosuspensions, therefore any factor decreasing its value considered as positive impact. At 100 ml of applied beads, zeta-potential values (Y_4) were positively (b_1, b_3) influenced by the increasing milling time (X_1), and the increasing size of zirconia beads (X_3), negatively (b_2) by the increasing milling speed (X_2). The interactions of milling time and milling speed ($X_1 \times X_2$) had a positive impact (b_{12}), the interaction of milling speed and milling media size (X_2X_3) had a negative (b_{13}) impact on zeta-potential values. The quadratic function of size of beads (X_3^2) had a negative impact (b_{33}), the quadratic functions of milling time and milling speed (X_1^2 and X_2^2) had a positive impact (b_{11}, b_{22}) on zeta-potential values.

At 200 ml of applied beads, zeta-potential values (Y_4) were negatively (b_2) influenced by the increasing milling speed (X_2), positively (b_3) by the increasing size of zirconia beads (C). The interactions of milling time and milling speed ($X_1 \times X_2$) and the milling time and size of beads ($X_1 \times X_3$) had a negative impact (b_{12}, b_{13}), the interaction of milling speed and diameter of milling media ($X_2 \times X_3$) had a positive impact (b_{23}) on zeta-potential values. The quadratic functions of the milling speed and the size of milling media ($X_2{}^2$ and $X_3{}^2$) negatively (b_{22}, b_{33}) influenced the zeta-potential values of milled ABZ suspensions.

4.2.5. Milling temperature values (Y_5)

Minimizing this parameter is desirable for formulation development of nanosuspensions, therefore any factor decreasing its value considered as positive impact. At 100 ml of applied beads, milling temperature values (Y_5) were negatively (b_2) influenced by the increasing milling speed (X_2), increasing size of zirconia beads (X_3) although had a positive impact (b_3). The interaction of milling speed and size of beads ($X_2 \times X_3$) had a positive impact (b_{23}) on the observed parameter. Quadratic function of the size of zirconia beads ($X_3{}^2$) had a negative impact (b_{33}) on milling temperature values.

At 200 ml of applied beads, milling temperature values (Y_5) were negatively (b_1, b_2, b_3) influenced by the increasing milling time (X_1), milling speed (X_2), and the size of zirconia beads (X_3). The interactions of the milling time and size of milling media ($X_1 \times X_3$), along with the milling speed and size of milling media ($X_2 \times X_3$) negatively (b_{13}) influenced the milling temperature values.

When influence of zirconia beads with different sizes were compared on milled ABZ particle size distribution parameters and suspension zeta-potential values at 100 ml of applied zirconia beads, result showed improving performance on size reduction with the utilization of smaller beads, consequently showed inverse proportionality with the size of milling medium.

Nanosuspension criteria (see end of section 3.3.5. Process parameter optimization of wet-milling) were easily fulfilled with the application of d = 0.1 mm sized beads at low to mediocre milling speed intervals (200–434 rpm), with a wide range in process time (20-59.4 mins), however coarse programs at higher rotation speeds (500–600 rpm) seemed to deteriorate results (**Figure 10)**.

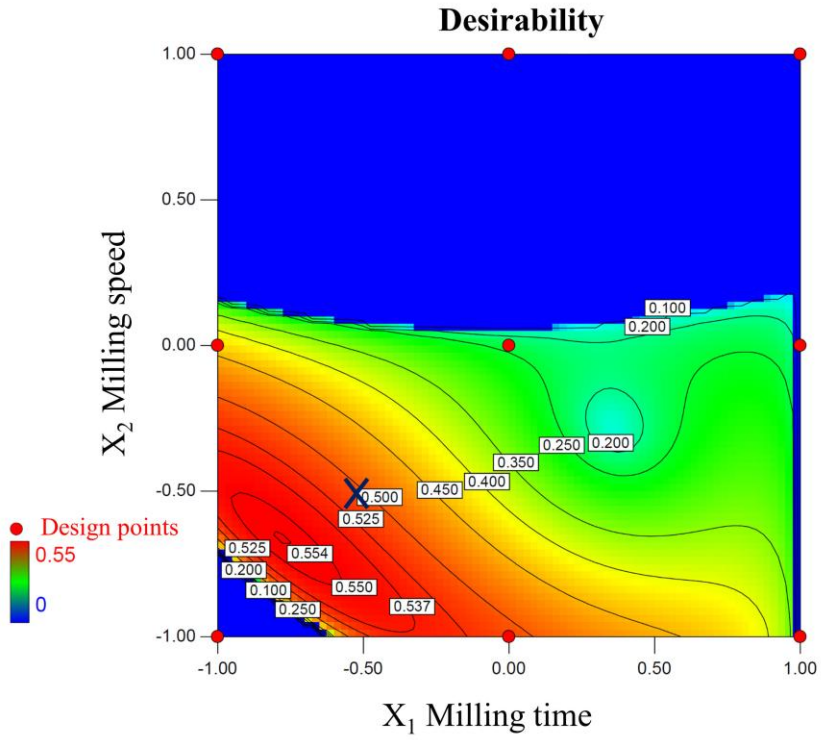

Figure 10. *Contour plot of the nanosuspension criteria by numerical optimization of desirability function, where x marks the chosen process parameters: 300 rpm rotation speed, 30 minutes long operation, with 100 ml of* X_3*: applied d = 0.1 mm sized zirconia milling beads*

For explanation we should look at the 3-Dimensional response surface plots (**Figure 11**). Low energy bead milling with 100 ml of applied amount of d = 0.1 mm sized zirconia beads was effective below 400 rpm, at this rotation speed value submicron sized fraction was maximal (100%) and volume weighted mean particle size (D [4,3]) was minimal (0.192 µm), due to maximal specific surface area of ABZ nanocrystals, this is also the point, where mean zeta-potential value was maximal (-30.5 mV). Above 400 rpm rotation speed, aggregation due to increased thermal motion at higher milling temperature values (36.0-39.0 ^{0}C), can be observed, probably due to growing bead-bead collisions.

Milling trials with d = 0.3 mm and d = 1.0 mm sized beads showed less promising results compared to d = 0.1 mm beads, even tendencies were different, unlike d = 0.1 mm sized ones, prolonged, coarse operations yielded the best results considering volume-weighted mean particle sizes 1.600 µm for d = 0.3 mm and 2.200 µm for d = 1.0 mm sized beads.

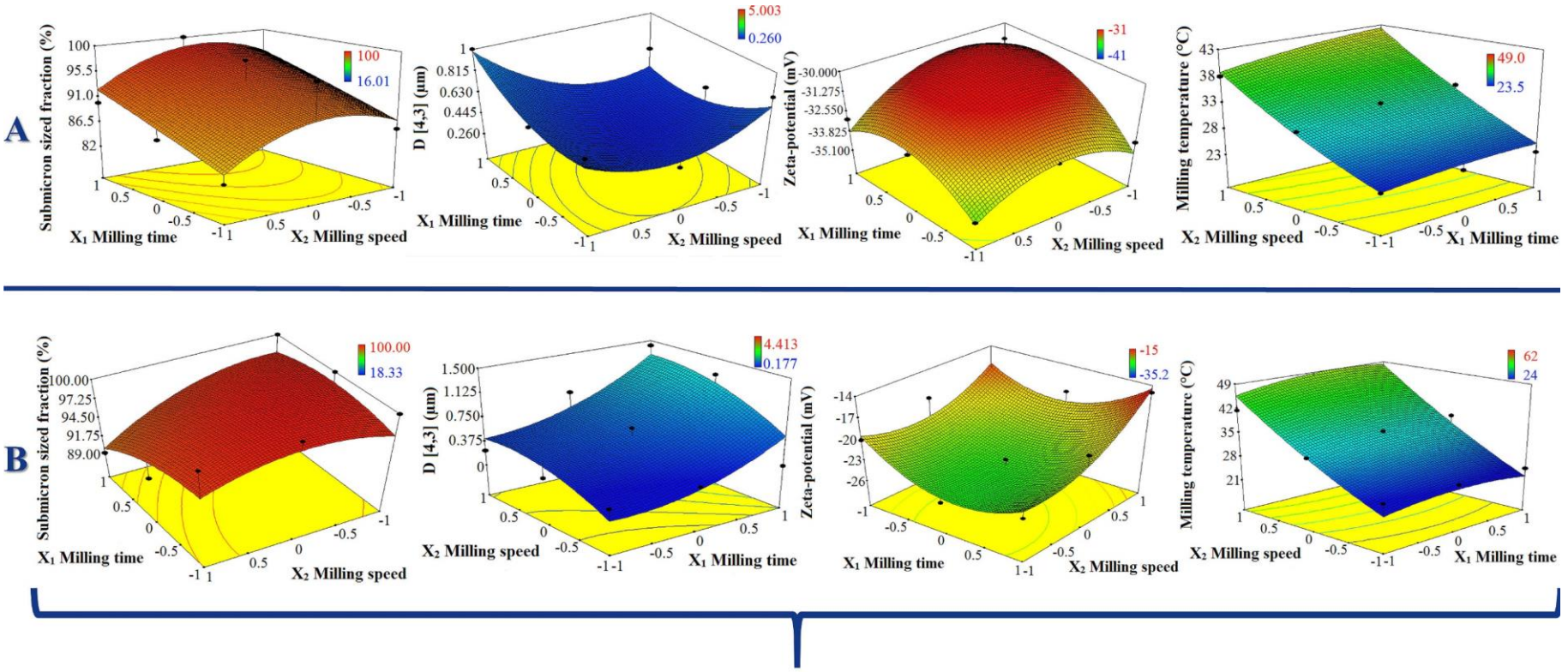

Figure 11. *Demonstration of the effect of milling time, milling speed on particle size distribution parameters and zeta-potential values of milled ABZ suspensions by 3-Dimensional response surface plots at A: 100 ml and B: 200 ml of milling beads applied, n = 5, mean values ± SDs, where X_3: d = 0.1 mm sized zirconia beads*

Thus, prolonged operations are advisable for the development of ABZ nanosuspension by low energy wet bead milling method with the utilization of larger zirconia beads (d = 0.3 mm, d = 1.0 mm) at higher milling speed values. In contrast application of smaller zirconia beads (d = 0.1 mm) are favored at lower to mediocre milling speeds, which yielded ABZ nanosuspension in a shorter process.

Utilization of 200 ml applied volume of milling beads the same aggregation tendency can be registered at higher mechanical energy input for d = 0.1 mm (**Figure 11**) and even for d = 0.3 mm sized beads, resulted in a significant milling temperature escalation from previously measured 39.0 ^{0}C to 49.9 ^{0}C for d = 0.1 mm and 44.5 ^{0}C for d = 0.3 mm sized beads with higher zeta-potential values >-26 mV for d = 0.1 mm and > -33 mV for d = 0.3 mm observed compared to the mean zeta-potential value (< -30.5 mV) at lower amount of beads applied previously. Preset nanosuspension criteria (see end of section 3.3.5. Process parameter optimization of wet-milling) excluded the application of higher amount of zirconia beads, due to higher zeta-potential values of milled ABZ suspensions.

The validation of responses predicted by the design model shall be performed in the final step. This is done by conducting confirmatory trials using RSM (response surface methodology) and the results are critically evaluated. Based on the trial results the optimal process parameters are set for manufacturing of the product [125,155]. Validation trials were performed selecting the borderline points of the highlighted region of the contour plot (**Figure 10**) including the point, which contributed to the optimized formulation parameters.

Maximal relative standard deviation was calculated at verification trial No. 3., between actual and predicted mean span values (11.03%), other noticeable differences were registered at verification trial No. 1., between actual and predicted mean milling temperature values (7.41%), at verification trial No. 5., between actual and predicted mean size values (6.48%) and at verification trial No. 6., between actual and predicted mean zeta-potential values (7.38%) (**Table IX**). The fitted model demonstrated good predictions in overall and could be used for critical process parameter optimization.

Table IX. *Verification of central composite design for the optimization of the critical process parameters for ABZ nanosuspension development by top down wet planetary bead milling method (mean values)*

Trial	Milling time (mins)	Milling speed (rpm)	Size of beads (mm)	Point prediction method	Subm. sized fraction (%)	D [4,3] (µm)	Span	Zeta-potential (mV)	T (^{0}C)
1	20	400	0.1	Predicted	93.35	0.453	2.331	-33.07	37.76
				Actual	97.00	0.400	2.300	-33.1	34.00
2	40	200	0.1	Predicted	92.31	0.584	2.100	-31.19	25.81
				Actual	90.21	0.6	2.100	-31.5	24.00
3	40	400	0.1	Predicted	94.49	0.304	2.252	-30.31	39.15
				Actual	98	0.260	2.180	-31.30	37.00
4	60	400	0.1	Predicted	98.31	0.254	2.175	-30.92	37.07
				Actual	100	0.262	2.150	-31.30	37.00
5	60	200	0.1	Predicted	96.09	0.625	1.962	-31.32	23.13
				Actual	93.69	0.685	2.000	-31.00	24.00
6	30	300	0.1	Predicted	99.41	0.205	0.900	-34.41	28.00
				Actual	100	0.189	0.864	-38.20	26.00

Summarizing optimization results, we can report, that ideal loading consisted of 0.64% (w/w) ABZ, 20.60% (w/w) surfactant solution (containing 0.5% (w/w) Tween 80 solution mixed with 0.01% (v/v) dimethylpolysiloxane as antifoaming agent), including 78.76% (w/w) d = 0.1 mm sized zirconia beads of total mass loading, which was 476.1498 g in stainless container capacity of 500 ml. As for chosen settings, milling speed was 300 rpm with 30 minutes long 5:5 cyclic, milling operation.

Milling temperature at the end of the process was 26.0 ^{0}C, showed a minimal + 6.0 ^{0}C elevation compared to the temperature of starting surfactant solution.

4.3. Comparison of the particle size distribution parameters

Laser diffraction measurements have been performed to validate the mean particle size provided by the supplier (> 90% less, than 30 µm) of raw material albendazole powder after dispersing 3.00% (w/w) ABZ to 0.50% w/w Tween 80 and 0.01% (v/v) dimethylpolysiloxane aqueous-based surfactant solution at a mixing speed of 600 rpm, homogenization time 5 minutes on heatable magnetic stirrer MS-H-S10 at room temperature. Results demonstrated, that the < 30 µm sized fraction was 88.82 ± 0.561% and volume-weighted mean size D [4,3] of 28.787 ± 3.052 µm.

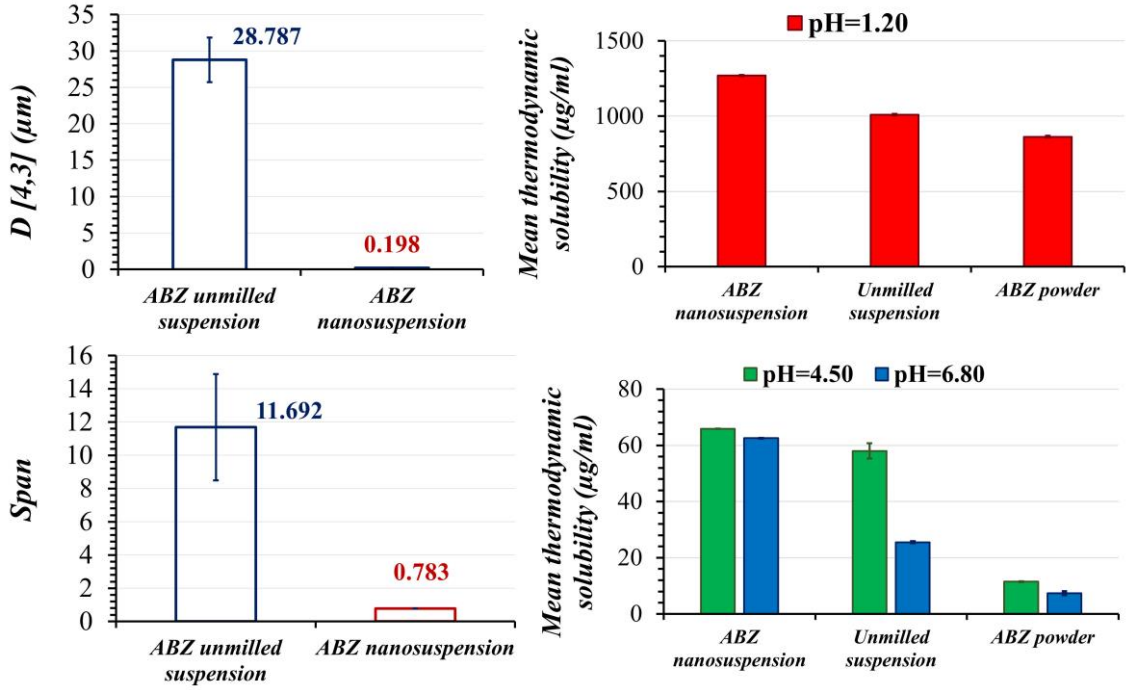

Figure. 12. *Impact of volume weighted mean particle size (D [4,3]) on mean thermodynamic solubility values of ABZ n = 3, mean values ± SDs*

Optimized, milled ABZ nanosuspension formulation yielded ~ 145.39 times reduction in mean size, ~ 14.93 times in mean polydispersity (span value) (**Figure 12**), ~ 18.47 times improvement in specific surface area, ~ 9.55 times boost in submicron sized fraction compared to unmilled ABZ surfactant dispersion.

Freshly prepared end-product was also characterized by DLS and ELS methods as well, confirming the completion of predetermined nanosuspension criteria, with intensity-weighted mean size (Z AVG d) of 173.5 ± 0.97 nm, polydispersity index (PDI) of 0.18 ± 0.012 and zeta-potential of -38.2 ± 0.83 mV (**Table IX**).

4.4. Moisture content and particle size determinations of dried granules

Moisture content values of the granules containing milled and unmilled albendazole were 3.14% (w/w), and 4.00% (w/w) respectively. It has already been reported, that up to ~ 5.6% (w/w) of moisture the MCC characteristics allow the possibility of further processing [142].

Cumulative undersize distributions of solid final products (containing milled and unmilled albendazole) compared to the MCC carrier Vivapur® 12 are slightly altered after the solidification, due to wet granulation, drying and regranulation (**Figure 13**).

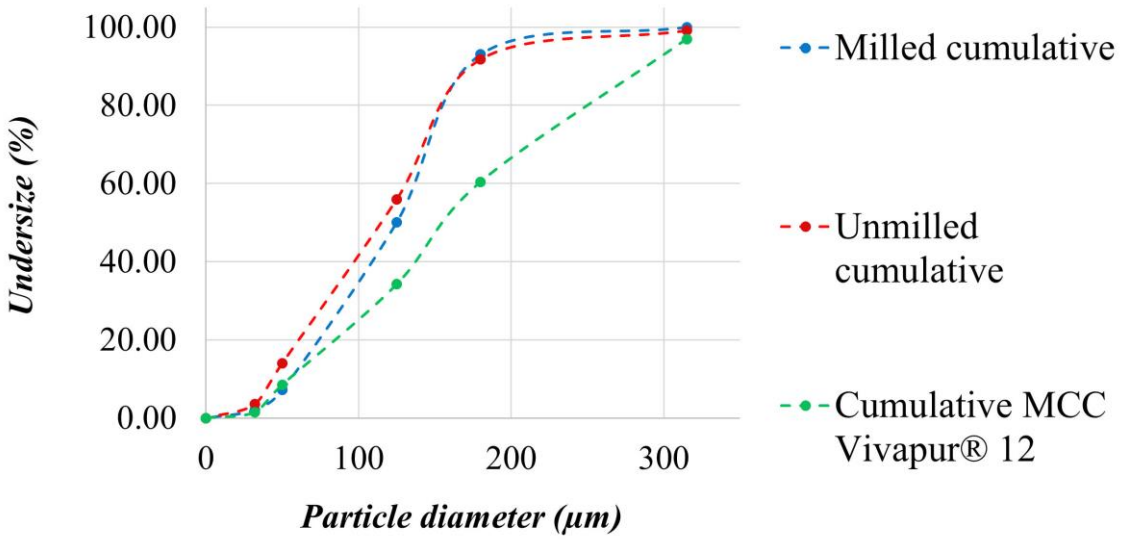

Figure 13. *Cumulative undersize particle size distributions of granules containing milled, unmilled albendazole and solid MCC carrier (Vivapur® 12)*

4.5. PSD parameters and zeta-potential values of reconstituted nanocrystals

Results of the reconstitution studies in every observed media have confirmed, that the particle size distributions of milled albendazole suspensions and released crystals from the dry suspensions were in the nanosized range. Particle size distribution comparisons of milled suspension and dry suspensions have shown the overlapping curves pair-wise measured in different buffer solutions, but there was a slight difference between the particle size distributions of the milled suspensions and the solid suspensions (**Figure 14**).

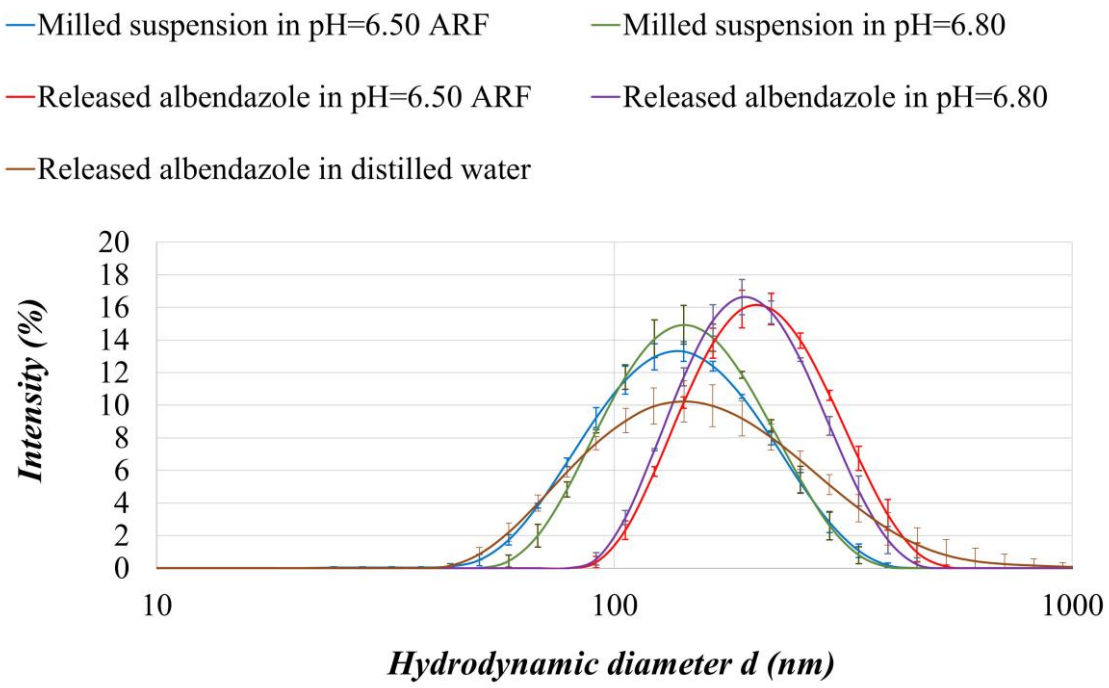

Figure 14. *Comparison of the PSDs by intensities (%) of milled albendazole suspensions and milled albendazole crystals released from Vivapur® 12 dispersions in various pH buffer solutions (n = 5), mean values ± SDs*

Table X. *Results of DLS parameters during reconstitution of ABZ, n = 5*

Sample	***DLS parameters***							
	Z AVG d (nm)				***PDI***			
	Mean	***±***	***SD***	***COV (%)***	***Mean***	***±***	***SD***	***COV (%)***
Milled susp. in pH=6.50	124.2	±	1.40	1.13	0.19	±	0.007	3.78
Milled susp. in pH=6.80	134.2	±	1.06	0.79	0.15	±	0.009	6.03
Released ABZ in pH=6.50	200.4	±	2.32	1.16	0.16	±	0.017	10.56
Released ABZ in pH=6.80	197.2	±	0.21	0.11	0.21	±	0.007	3.37
Released ABZ in distilled water	140.1	±	1.26	0.90	0.24	±	0.01	4.22

Table XI. *Comparison of the DLS parameters during reconstitution, n = 5*

Sample	***DLS parameters***							
	Z AVG d (nm)				***PDI***			
	Mean	***±***	***SD***	***COV (%)***	***Mean***	***±***	***SD***	***COV (%)***
Released compared to suspension in pH = 6.50	162.3	±	53.88	33.20	0.17	±	0.017	9.81
Released compared to suspension in pH = 6.80	165.7	±	44.56	26.90	0.18	±	0.042	23.48

The alterations of particle size distributions cannot be explained by the contrast of the pH values of dispersants, since 100% of ABZ is in neutral form over these pH ranges [92].

Aggregation due to slow tray-drying process could be the main reason of the differences between PSDs, see section 4.9. Short-term stability evaluations of optimized nanosuspension. In this study mean particle size of ABZ nanocrystals increased by ~ 55.04% compared to the sizes of nanocrystals in freshly prepared nanosuspension after 48 hours of storage at room temperature. For industrial feasibility and large scale production of nanosuspensions without solid carriers a rapid removal of dispersant is required at low drying temperature. While freeze-drying can be a suitable method, cost-efficiency of this process is highly questionable. Spray–drying could be mentioned as an alternative. For the manufacturing of post processed nanosuspensions by wet granulation vacuum drying or fluid bed drying can be mentioned.

All samples were measured five times, and the coefficient of variations were calculated for each distribution parameter summarized in **Table X–XI**. For monodisperse samples, where the coefficient of variation (COV < 20%) between DLS parameters and the mean particle size of the suspensions of unaggregated nanoparticles have diameters > 20 nm, the DLS produces highly reproducible and reliable measurements. Polydisperse nanoparticle solutions or stable solutions of aggregated nanoparticles (no visible particulates and no particle settling), typically the DLS measured diameters will be in the 100–300 nm range with a polydispersity index (PDI) of 0.3 or below [156]. According to the referred guide, these samples can be described as stable solutions of aggregated nanoparticles. With lower than 20% coefficient of variations (COV) values between the intensity weighted mean hydrodynamic diameter Z AVG d (nm) and the PDI values. It means, that the analytical method developed and applied to measure particle sizes in these solutions was reliable, reproducible, and have met the built in Zetasizer software's quality criteria.

Prior to wet granulation mean zeta-potential of the milled albendazole suspension was -35.8 ± 0.71 mV, post redispergation value was -24.0 ± 0.58 mV. Mean value increased by + 11.8 mV, probably due to wet granulation, especially tray drying process.

4.6. Comparisons of the thermodynamic solubility values

We have confirmed previous observations of Torrado et al. (1996) [91], that ABZ has pH dependent, poor water solubility, lowest value registered in medium at pH = 6.80, which was 7.4 ± 0.63 µg/ml, due to the dominance of the neutral form of ABZ [92]. Solubilization with 0.50% (w/w) Tween 80 solution enhanced ABZ initial solubility to 25.5 ± 0.27 µg/ml and gained a 2.46-folds boost. Optimized, milled nanosuspension formula further improved performance and showed 62.5 ± 0.05 µg/ml solubility, raised it 1.45-folds compared to unmilled surfactant dispersion. In medium at pH = 4.50 the impact of mean solubility gains were slowly diminishing, initial solubility of raw ABZ powder 11.5 ± 0.16 µg/ml was increased to 58.0 ± 2.71 µg/ml, which was a 4.05-folds boost due to solubilization and optimized milling operation demonstrated 65.9 ± 0.05 µg/ml value, showed a 13.68% boost compared to unmilled dispersion. Least gains in solubility were noticeable in medium at pH = 1.20, where initial solubility of ABZ was maximal, due to the dominance of the cationic form of ABZ [92] 863.4 ± 3.73 µg/ml, which was elevated to 1010.5 ± 2.67 µg/ml, boosted by 17.04% due to solubilization and particle size reduction raised it further to 1269.8 ± 2.43 µg/ml, and gained a 25.66% boost compared to unmilled dispersion (**Figure 12**).

Studies with solidified ABZ dispersion indicated, that in artificial rumen fluid (ARF) at pH = 6.50 initial solubility of ABZ powder was 8.2 ± 0.02 µg/ml, solubilization with the application of Tween 80 in concentration of 0.50% (w/w) improved initial solubility by 4.89 times and 5.97 times in dissolution medium at pH = 6.80. Milling further improved the solubility of dispersions, by 1.98 times in ARF and 1.33 times in medium at pH = 6.8 compared to unmilled dispersions.

Only a small change in solubility was noticeable in pH = 1.20, + 2.55% due to solubilization and + 11.11% to milling (**Figure 15**).

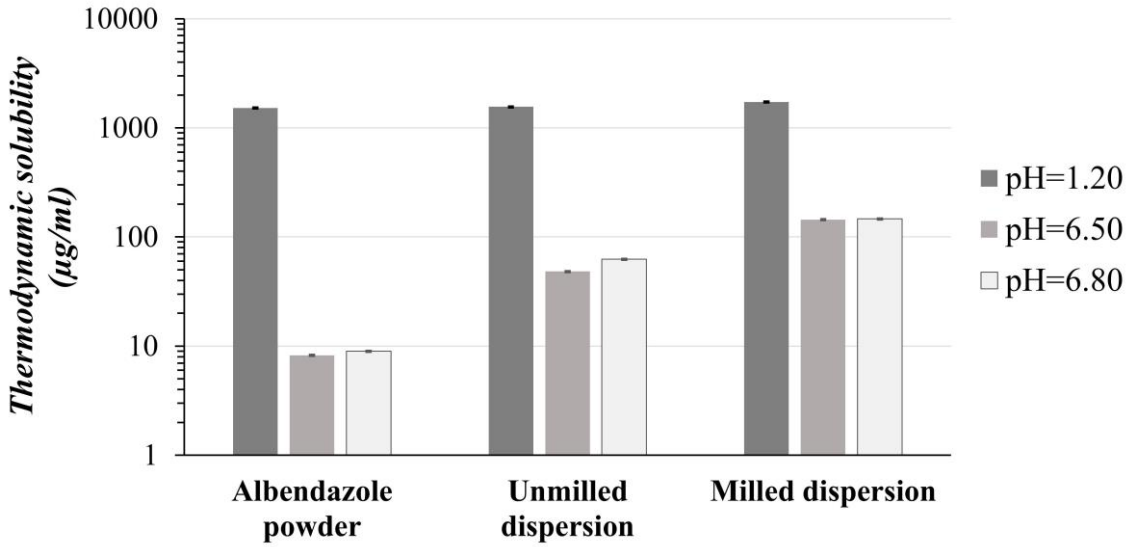

Figure 15. *Mean thermodynamic solubility values of albendazole powder substance, milled and unmilled dispersions in various pH buffer solutions (n = 3)*

4.7. Comparison of the in vitro dissolution profiles

When comparing drug release kinetics from both liquid and solid dosage forms, we have found correlation in ABZ mean solubilities and dissolution rate constants. Comparison of drug release profiles of liquid dosage forms highlighted, that the highest dissolution rate values have been registered, where ABZ initial mean solubility is maximal, in medium at pH = 1.20, solubilization of active boosted it by 1.95-fold, particle size reduction further improved performance by 41.74-folds compare to ABZ powder and 13.50-folds to unmilled suspension. As pH values of dissolution media increased, ABZ solubility values were dropped significantly, so did the dissolution rate constant values, however the influence of surface-active agent and milling was still decisive in all cases. In medium at pH = 4.50 solubilization raised mean dissolution rate constant by 1.01-fold, effect of particle size reduction was conspicuous, indicated a 12.23-folds boost compared to unmilled suspension and a 25.56-folds to ABZ powder. In medium at pH = 6.80 solubilization of ABZ boosted dissolution rate constant by 23.01%, effect of particle size reduction was still potent, showed an 18.70-folds boost compared to unmilled suspension and a 15.01-folds to ABZ powder (**Figure 16**).

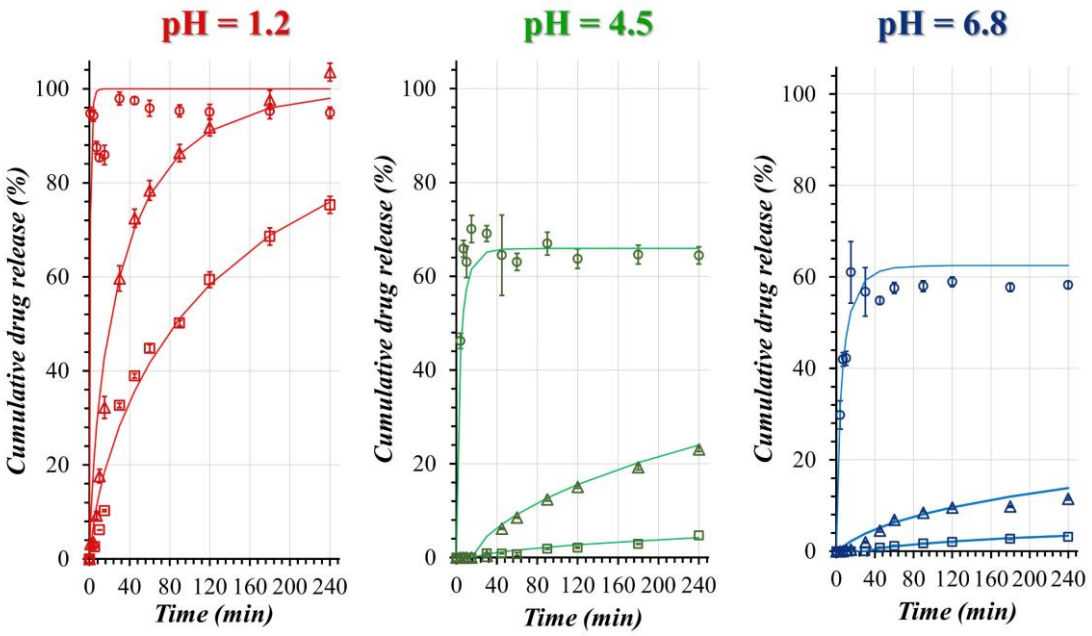

Figure 16. *Comparison of the fitted in vitro dissolution profiles of optimized, milled ABZ nanosuspension (○), surfactant dispersion (Δ) and ABZ powder (□) in various, aqueous based buffer solutions (pH=1.2, pH=4.5, pH=6.8), n = 3, mean values ± SDs*

Table XII. *Influence of particle size reduction and wetting of ABZ on fitted dissolution rate constants (k), n = 3, mean values ± SDs*

Sample	**ABZ powder**			**ABZ Tween 80 dispersion**			**Optimized ABZ nanosuspension**		
Medium	**t_0 (min)**	**k (min^{-1}) ± SD**	**R^2**	**t_0 (min)**	**k (min^{-1}) ± SD**	**R^2**	**t_0 (min)**	**k (min^{-1}) ± SD**	**R^2**
pH = 1.20	0	0.031 ± 0.0034	0.9880	0	0.091 ± 0.0091	0.9806	0	1.321 ± 0.0269	0.9435
pH = 4.50	15.0	0.010 ± 0.0005	0.9719	15.0	0.032 ± 0.0016	0.9878	0	0.425 ± 0.0008	0.9368
pH = 6.80	30.0	0.014 ± 0.0016	0.9962	4.0	0.017 ± 0.0005	0.9740	0	0.272 ± 0.0138	0.9523

The fitted coefficients of determinations (> 0.9) in (**Table XII**) demonstrated, that the dissolution profiles were well fitted to the measurement points and all samples follow first order kinetics.

Peak concentrations registered in media at pH = 4.5 and pH = 6.8 have demonstrated good correlations to mean thermodynamic solubility values of optimized milled ABZ nanosuspension formulas. So ABZ absorption of PES membrane filters were negligible, which ensured appropriate membrane filter selection.

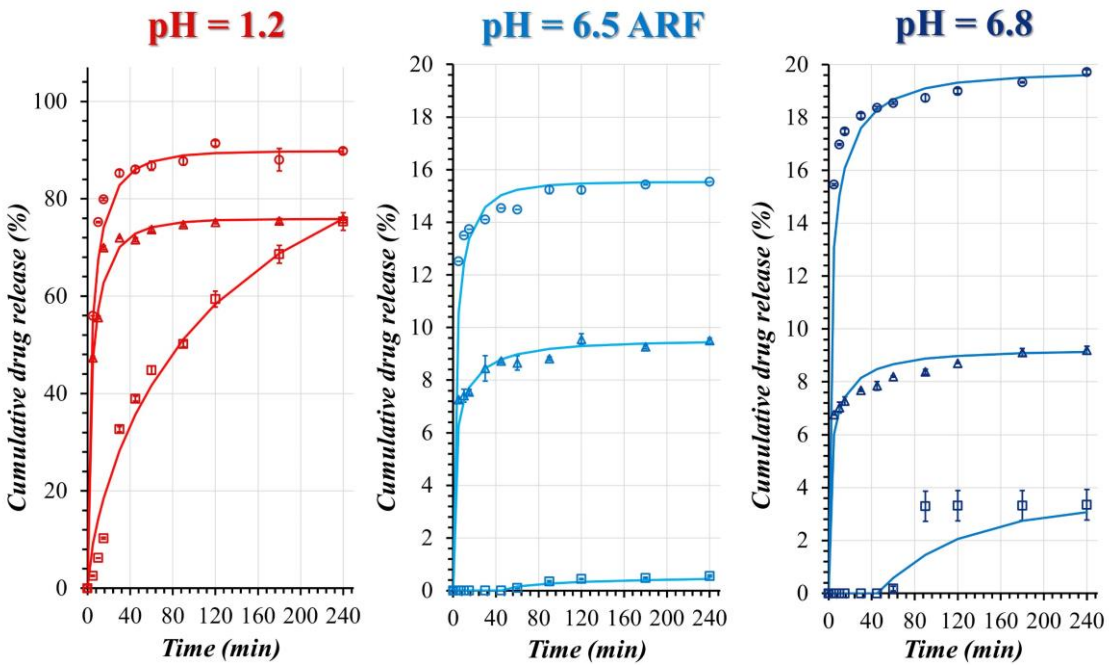

Figure 17. Comparison of the fitted in vitro dissolution profiles of ABZ solid suspensions containing nanocrystals (○), solid suspensions containing unmilled ABZ (Δ) and raw ABZ powder (□) in various, aqueous-based buffer solutions (pH = 1.2, pH = 6.5 ARF, pH = 6.8), n = 3, mean values ± SDs

Comparison of drug release profiles of solid dosage forms in contrast to liquids indicated, that the highest dissolution rate constant values have been registered, where ABZ initial mean solubility was low, in medium at pH = 6.80 (phosphate-buffer) (**Figure 17**).
However, most gains in dissolution rate values were noticeable in medium at pH = 1.2, where solubilization of active raised mean dissolution rate constant by 17.44-folds, effect of particle size reduction was barely noticeable on mean dissolution rate constant, indicated only a 4.82% boost compared to unmilled dispersion and an 18.33-folds to ABZ powder. In medium at pH = 6.5 (ARF), solubilization boosted mean dissolution rate constant by 7.17-folds, particle size reduction further improved performance by 43.88% compared to unmilled dispersion.

In medium at pH = 6.80 (phosphate buffer) mean dissolution rate constant was boosted by 11.07 – folds, due to solubilization, particle size reduction demonstrated a 43.09% improvement compared to unmilled dispersion. The fitted coefficients of determinations (> 0.9) in (**Table XIII**) have also demonstrated, that the dissolution profiles were well fitted to the measurement points and all samples follow first order kinetics.

Table XIII. *Fitted first-ordered dissolution rate constants (k) of milled, unmilled albendazole dispersions and pure albendazole powder (900 ml of ARF at pH = 6.50, at pH = 1.20 and pH = 6.80 dissolution media)*

Sample	$k_{pH=1.20}$ (min^{-1})	$k_{pH=6.50}$ (min^{-1})	$k_{pH=6.80}$ (min^{-1})
milled dispersion	0.174 (R=0.9955)	0.282 (R=0.9843)	0.259 (R=0.9903)
unmilled dispersion	0.166 (R=0.9939)	0.196 (R=0.9678)	0.181 (R=0.9616)
albendazole powder	0.009 (R=0.9819)	0.024 (R=0.9821) *	0.015 (R=0.9825) **

* dissolution started at 51.15 minutes

** dissolution started at 45 minutes

4.8. Drug content and determinations and the effect of beads washing

By simply pouring the optimized ABZ nanosuspension on sieve and separating it from beads, mean ABZ yield was low 60.53 ± 3.485%. It contained 200.00 ± 0.344 mg of ABZ in 5.471 cm^3 volume. Washing the beads after milling operations with different amounts of surface active agent solutions, containing 0.50% (w/w) Tween 80 and 0.01% (v/v) dimethylpolysiloxane antifoaming agent have demonstrated, that increasing amount of Tween 80 added to milled suspensions slightly increased particle size distributions parameters and decreased zeta-potential values, while submicron sized fraction was permanent, which can be explained by the steric stabilizing effect of Tween 80. Best case scenario was the additional 33.33% (w/w) surfactant solution of total mass loading added to milled ABZ suspension, where registered mean zeta-potential value was minimal -51.90 ± 0.465 mV, along with reasonable ABZ yield 83.05 ± 2.783% achieved during our studies. Dilution slightly increased administration volume from 5.47 ± 0.009 cm^3 to

7.09 ± 0.024 cm^3. Registered particle size distribution parameters after dilution with three parallel measurements performed, including volume-weighted mean size (D [4,3]) 0.194 ± 0.005 µm, span 0.923 ± 0.0041, intensity-weighted mean size (Z AVG d) 182.2 ± 1.31 nm and PDI 0.187 ± 0.016 (**Table XIV**). This diluted ABZ nanosuspension was then subjected to short – term physical stability evaluations.

Table XIV. *Influence of beads washing and dilution on final ABZ yield, particle size distribution parameters, zeta-potential values and dose of optimized, milled ABZ nanosuspension, n = 3, mean values ± SDs*

		Washing with additional optimal surfactant solutions of total mass loading (% w/w)			
Parameter	Optimized milled nanosuspension	16.67	2 *X* 16.67	33.33	2 *X* 33.33
Yield (%)	60.53 ± 3.485	70.90 ± 3.245	86.00 ± 2.850	83.05 ± 2.783	86.00 ± 2.670
Z AVG d (nm)	173.5 ± 0.97	183.5 ± 0.17	174.3 ± 1.45	182.2 ± 1.31	178.8 ± 2.70
PDI	0.18 ± 0.012	0.19 ± 0.008	0.18 ± 0.010	0.19 ± 0.016	0.19 ± 0.008
Zeta-potential (mV)	-38.20 ± 0.830	-38.13 ± 0.928	-37.60 ± 0.576	-51.90 ± 0.465	-41.80 ± 0.907
D [4,3] (µm)	0.189 ± 0.0022	0.190 ± 0.0010	0.193 ± 0.0015	0.194 ± 0.0005	0.204 ± 0.0004
Span	0.864 ± 0.0198	0.977 ± 0.0022	0.902 ± 0.0016	0.923 ± 0.0041	1.006 ± 0.0093
Dose (200 mg) in volume (ml)	5.47 ± 0.009	6.37 ± 0.138	6.85 ± 0.067	7.09 ± 0.024	7.98 ± 0.125

For granules containing milled and unmilled albendazole, drug content values were 22.98 ± 0.600% (w/w) and 22.08 ± 1.100% (w/w), respectively.

From the results of our calculations, the mean concentrations of Tween 80 were found to be 3.85% (w/w) for both compositions, since equal amounts of suspensions (milled and unmilled) were added to both carrier systems, while mean MCC (Vivapur® 12) amounts were 70.04% (w/w) and 70.07% (w/w) respectively, regarding to milled and unmilled dispersions.

4.9. Short–term physical stability evaluations of optimized nanosuspension

Short–term physical stability of optimized formula was characterized by recording particle size distribution parameters with both LD and DLS methods at predetermined time points (**Figure 18**). The volume-weighted mean particle size (D [4,3]) and intensity-weighted mean particle size (Z AVG d) values were the most sensitive to aggregation.

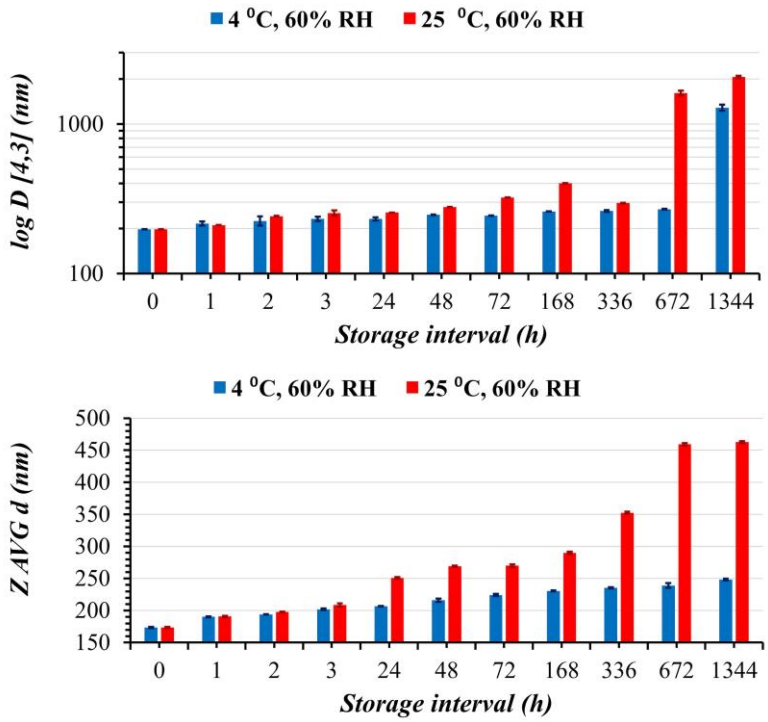

Figure 18. *Influence of storage conditions and time on mean particle size values of optimized, milled ABZ nanosuspensions measured by LD and DLS methods, n = 3, mean values ± SDs*

Results demonstrated, that refrigerated conditions were more suitable for storage of ABZ nanosuspensions, micro sized aggregates have been detected by LD at 56 days of storage, under refrigerated conditions. At room temperature however, micro sized aggregates have been observed much sooner at 28 days of storage.

4.10. Results of solid state characterizations

4.10.1. Comparison of the diffraction patterns

Our experimental PXRD results in agreement with previous ones, performed by Chattah et al. (2015) and Pranzo et al. (2009) [99,100] have demonstrated, that initial material ABZ powder consisted of both polymorphic forms of ABZ, Form I and Form II (**Figure 19**). Most intensive Form I main, characteristic peaks can be identified at 6.9, 11.3, 11.6, 17.9, 24.4, and 27.2 (^{0}2θ) positions. Form II main peaks were also consistent with the literature located at 7.3, 10.7, 14.6, 18.1, 24.7, 25.6 and 30.5 (^{0}2θ) positions. It seemed drying had no effect on ABZ polymorphy, dried, optimized, milled ABZ nanosuspension also contained both forms. We've reached higher milling temperature values at higher amount of milling beads applied (200 ml), especially with the utilization of d = 0.3 mm sized ones during coarse milling programs (involving 600 rpm milling speeds and at least 60 minutes long operations). For demonstration of extreme conditions, a 180 minute long operation was tested in a stainless steel container with capacity of 500 ml among previously described settings, without complete conversion of Form I to Form II registered. So, 50 ^{0}C milling temperature during a 180 minute long session was not enough for the detection of only Form II characteristic peaks. By switching container sizes from 500 ml to 50 ml and therefore, increasing thermal inertia (lowering the total volume of cooling surfactant solution present in the container) milling programs involving various process times (30 minutes, 60 minutes, 180 minutes) were compared. As expected, milling temperature values have massively increased to 60.0 ^{0}C, 65 ^{0}C, and 72 ^{0}C, respectively, which was enough for triggering total conversion of ABZ Form I to Form II in a short amount of time (30 minutes). Conversion was noticeable from the shifted colors of milled suspensions from white to brown.

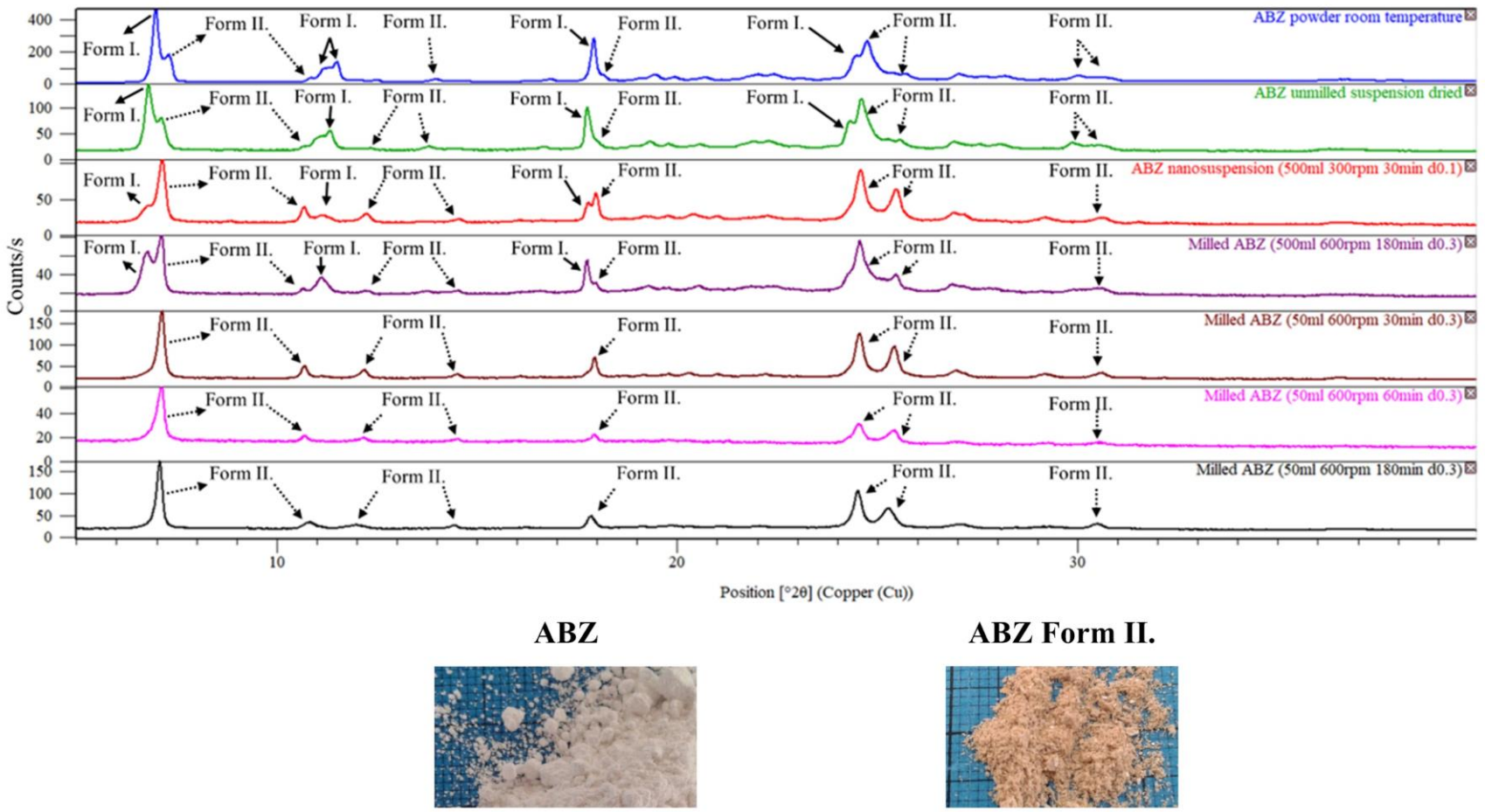

Figure 19. *Comparison of the diffraction patterns of starting material ABZ powder and dried, milled, and unmilled ABZ suspensions*

4.10.2. Comparison of the phase transitions of the solid samples

During the DSC investigations we have found that the melting point of the supplied pure albendazole powder was 197.7 ^{0}C and the enthalpy, that was required for the phase transition was 43.6 mJ/mg. The melting point values of albendazole in unmilled and milled dry suspension formulations were 194.4 ^{0}C and 187.4 ^{0}C, respectively (**Figure 20**). This sifting of the melting point values indicates interactions between the albendazole and the MCC carrier. Also, a major phase transition enthalpy change can be noticed between the solid samples, with the minimal value registered at the milled dispersion (2.00 mJ/mg). This indicated a partial crystalline-amorphous transition of albendazole due to the milling process.

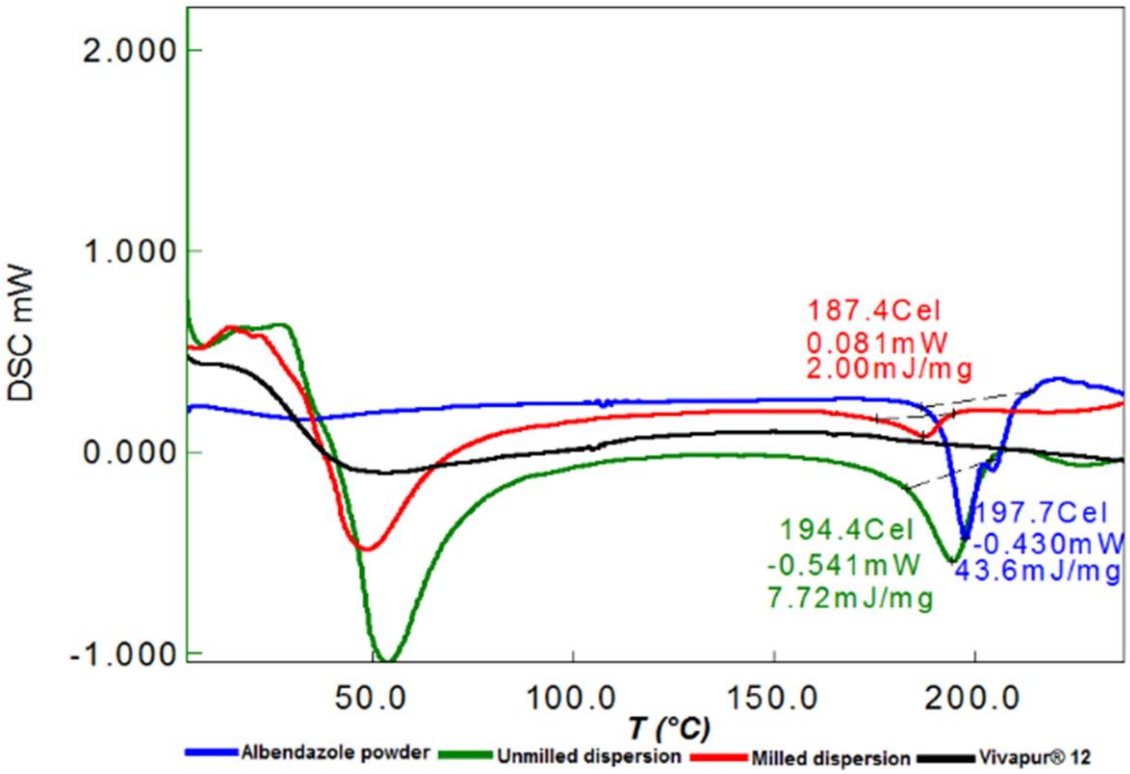

Figure 20. *Comparison of the thermoanalytical behaviors of solid samples*

4.10.3. FT-IR spectral evaluations

The characteristic bands of different structural moieties of albendazole can be easily identified comparing our results to previous investigations of reference materials. A broad band in the spectral range of 3415–3190 cm^{-1}, with peak at 3325, 3319–3317 cm^{-1} positions, due to N-H stretching, from amine groups, over imposed on the vibrations of N-H bond from carbamate moiety. The sharp weak bands due to stretching of alkane-type C-H bonds from the propyl moiety appear around 2956–2865 cm^{-1}. The C=O carbonyl bond bending appear as a sharp band at position 1712–1708 cm^{-1}. The benzoimidazolyl part show two intense closed bands in the 1640–1590 cm^{-1} spectral range, with peaks at 1630 and 1595 cm^{-1} positions. A characteristic band for the aromatic system is the band at position 1523 cm^{-1}, but as well the doublet bands at 1441 and 1422 cm^{-1} positions. Other bands appear in the fingerprint region, below 950 cm^{-1}, but are difficult to be asset to certain moieties. Previous investigations also revealed the spectral differences between the forms of albendazole. When comparing form ABZ I to II, the bands corresponding to the-CH stretching vibration, to C – N stretching, and to-CH deformation appeared slightly shifted. In addition, the bands in the fingerprint region (between 1500 and 600 cm^{-1}) show marked differences between both solid forms, which can be used to identify and distinguish them. In particular, the spectrum of ABZ II shows shifted bands as well as new bands in comparison with that of ABZ I. ABZ I is characterized by bands at positions 885, 863, 850, 805, 759, 728, 611, 597 and 509 cm^{-1}, whereas ABZ II exhibits characteristic bands at positions 881, 866, 846, 767, 755, 732, 597, 588, 520 and 447 cm^{-1} [99,157]. As shown in **Table XV**, our sample consisted of the mixture of both forms of albendazole.

Table XV. *Comparison of the FT-IR absorption bands of various albendazole forms*

Band assignments of albendazole forms	**Wavenumber (cm^{-1})**				
	ABZ I	**ABZ II**	**Albendazole EP**	**Unmilled dispersion**	**Milled dispersion**
-NH stretching	range 3415-3188, peaks at 3325, 3319-3317	3331		3328	3332
Carbonyl group	1712-1708	1711		1711	1713
$-CH_3$ absorption	1443	1443		1444	1445
-CH stretching	2953, 2926	2957, 2912	2959, 2913	2958, 2909	2904
-C=N stretching	1654, 1591	1629, 1578	1616, 1586	1622, 1589	1623, 1588
Aromatic system	1523, and duplet bands at 1441, 1422	1524,1441,1423		1524, 1443, 1426	1525, 1445, 1428
-CH deformation	1373	1377	1374, 1377	1361	1361
Fingerprint region	885, 863, 850, 805, 759, 728, 611, 597, 509	881, 866, 846, 767, 755, 732, 597, 588, 520, 447	887, 864, 847, 770, 755, 730, 598, 513, 449	893, 866, 847, 770, 755, 730, 596, 525, 515, 466, 451	894, 868, 847, 769, 752, 663, 591, 522, 510, 443

When subjected to nanosizing, a slight sifting of the band positions could be registered, nevertheless the recorded absorbance values have significantly decreased compared to albendazole powder, which also indicated a partial crystalline amorphous transition. Spectral analysis of the solid suspensions has also revealed the characteristic bands of MCC as well, masking each other with the vibrational signals of albendazole. From 3600 to 3000 cm^{-1} the stretching of the H-bonded - OH groups of MCC can be registered, masking the N – H stretching of albendazole, the - C–H stretching at position 2900 cm^{-1} is a common band for both MCC and albendazole. The absorbed moisture of MCC at 1640 cm^{-1} is masked by the aromatic system of albendazole. The asymmetric - CH_2 bending and wagging signal of MCC at positions 1440 and 1352 cm^{-1}, finally the - C–O–C - stretching of the β-1,4 glycosidic linkage of MCC at position 1120 cm^{-1} can be observed [158] (**Figure 21**).

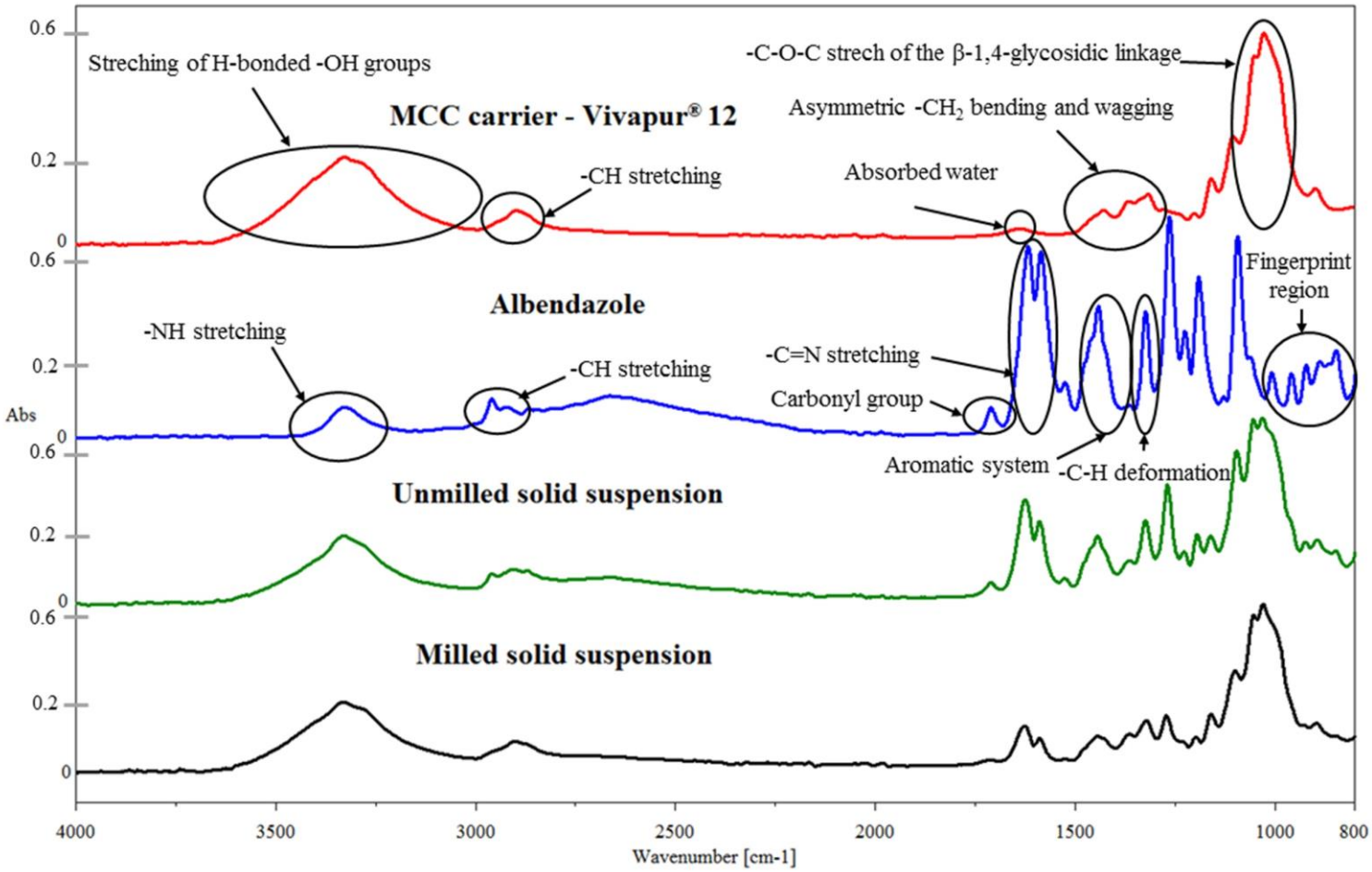

Figure 21. *FT-IR spectral evaluations of MCC (Vivapur® 12) carrier, albendazole powder, and granules containing unmilled and milled albendazole*

4.11. Morphological investigations of solid particulate systems

4.11.1. AFM imaging

Albendazole EP micronized powder contained small lamellar, rhomboid shaped crystals (**Figure 22/A**), which formed ~3 μm sized aggregates with one another (**Figure 22/E**). These small individual crystals could not be detected in the physical mixture formula on the surface of the microcrystalline carrier by AFM (**Figure 22/D**). Close examination of the surface of the granules containing milled ABZ show no signs of nanoparticles (**Figure 22/C, G**). The microcrystalline structure of MCC can be identified (**Figure 22/B, F**), however, a significant change can be detected comparing the surface roughness of the MCC to the granules containing milled ABZ, which can be explained by the effect of the wet granulation process, where the agglomerated wet mass was pushed through a stainless steel sieve with mesh size of d = 180 μm. Regranulation after tray drying was performed using the same sieve. The AFM images of the physical mixture shows recognizable small aggregates related to ABZ and large microcrystalline structures separately, which can be identified as the MCC carrier (**Figure 22/D, H**).

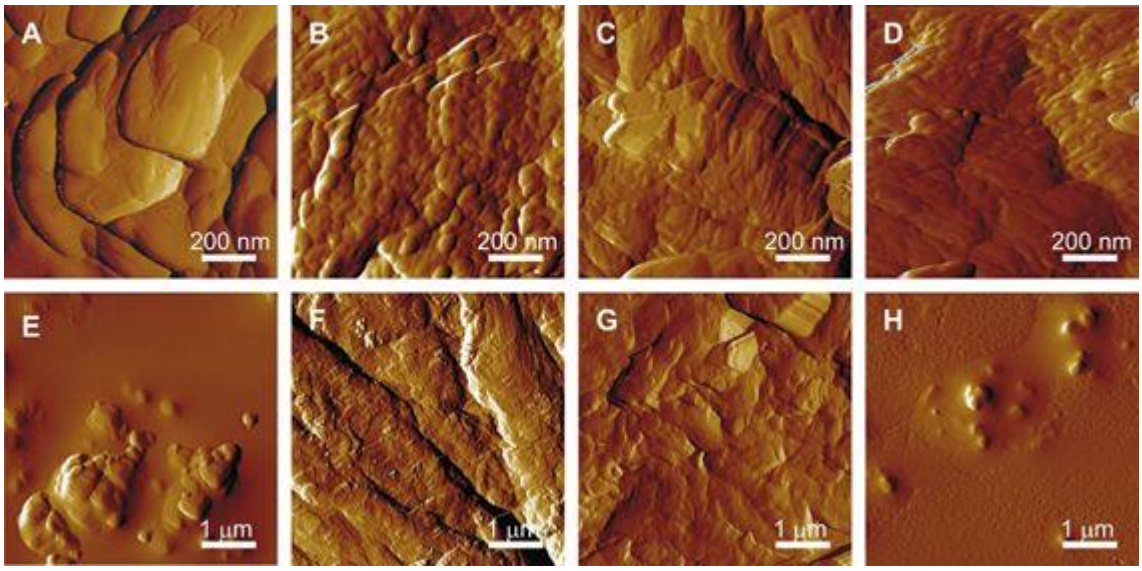

Figure 22. *AFM amplitude-contrast images of microparticulate systems. (A) and (E) albendazole crystals; (B) and (F) Microcrystalline cellulose carrier (Vivapur® 12) powder; (C) and (G) milled albendazole dispersion (solid suspension containing albendazole nanocrystals); (D) and (H) albendazole: MCC 1:3 physical mixture*

4.11.2. SEM imaging

SEM images has revealed albendazole micronized powder particles, which contained ~1 μm sized, lamellar, rhomboid shaped primary and 3–30 μm sized secondary aggregates (**Figure 23/A**). These crystals can be easily detected on the surface of the MCC carrier zooming in to the surface of the physical mixture with SEM (**Figure 23/C**). Also, SEM surface images indicated the change of surface morphology of MCC (**Figure 23/B**) after wet granulation (**Figure 23/D)**. The surface of the granules showed rough, multangular edges compared to the rolled up fibrous structure of the MCC. Wet milled albendazole containing granules showed no sign of albendazole nanocrystals on the surface of the dispersion (**Figure 23/D**). We assume, that ABZ nanocrystals were incorporated in between the fibers of the MCC.

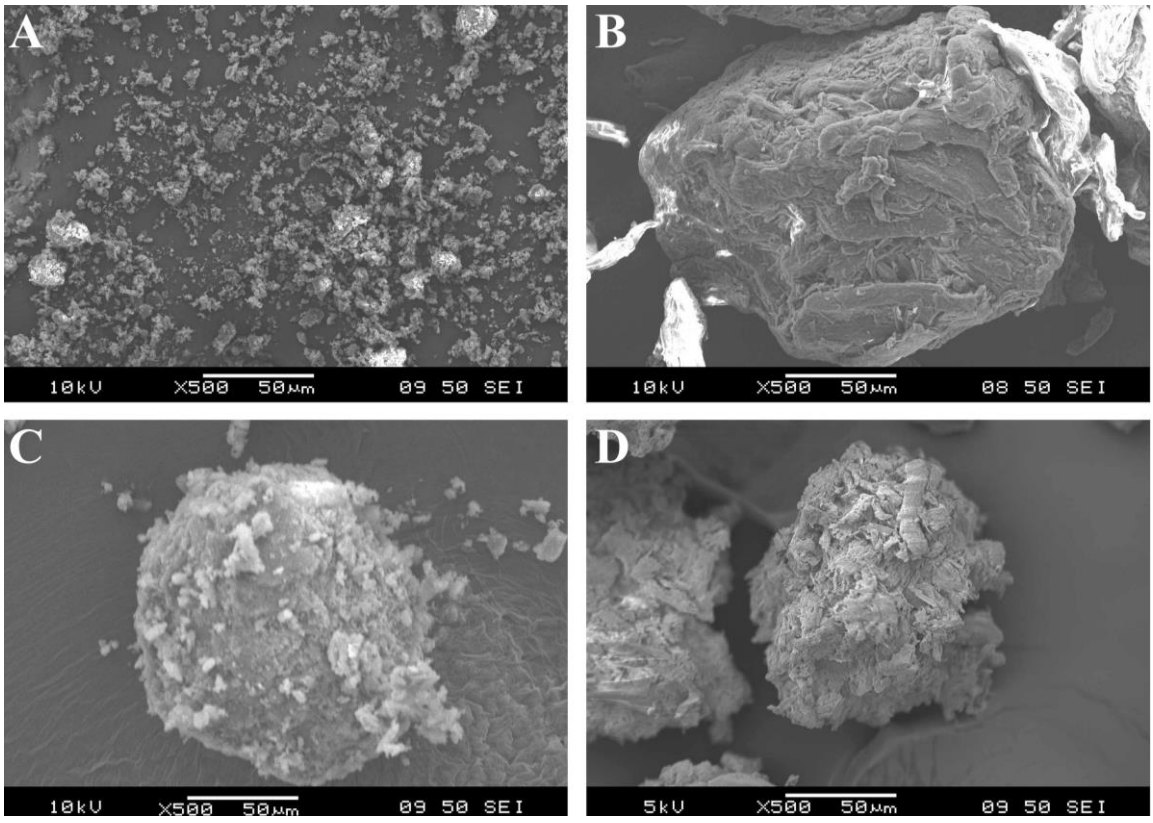

Figure 23. *SEM images of microparticulate systems: (A) albendazole crystals;*
(B) Microcrystalline cellulose carrier (Vivapur® 12) powder;
(C) albendazole: MCC 1:3 physical mixture, (D) milled albendazole dispersion (solid suspension containing albendazole nanocrystals)

5. Conclusions

The main objective of this work was to develop dry nanosuspension drug delivery system containing BCS class II. ABZ active pharmaceutical ingredient to offset the undesirable physicochemical and biopharmaceutical properties of this model drug.

Optimized formula consisted of 0.64% (w/w) ABZ, 20.60% (w/w) surfactant solution (containing 0.5% (w/w) Tween 80 solution mixed with 0.01% (v/v) dimethylpolysiloxane as antifoaming agent), milled with 78.76% (w/w) d = 0.1 mm sized zirconia beads of total mass loading, which was 476.1498 g in stainless container capacity of 500 ml. As for chosen settings, milling speed was 300 rpm with 30 minutes long 5:5 cyclic, milling operation.

Optimized nanosuspension formula has improved thermodynamic solubility of ABZ in all tested media. Maximal gains due to milling were calculated in in phosphate buffer at pH = 6.8 (Ph. Eur. 9), where initial solubility of ABZ was minimal (7.4 ± 0.63 µg/ml), due to the dominance of its neutral form. In this medium particle size reduction raised mean solubility by 1.45-folds compared to unmilled surfactant dispersion. Least gains were noticed in medium at pH = 1.20, where initial solubility of ABZ was maximal (863.4 ± 3.73 µg/ml), due to the dominance of the cationic form of ABZ. Solubility evaluations of solidified, milled suspensions yielded the same results. Torrado et al. (1996). defined the solubility vs. pH profile of ABZ and demonstrated, that minimal solubility was registered in medium at pH = 6.50 in accordance with our results [91]. In medium with this pH value (artificial rumen fluid (ARF)) wet-milling has improved the thermodynamic solubility by 1.98 times and by 1.33 times in phosphate buffer at pH = 6.8 (Ph. Eur. 9) compared to the unmilled dispersion. These observations support the significance of the Ostwald-Freundlich equation.

Dissolution studies have revealed, that as the pH values of dissolution media increased, solubility and dissolution rate constants values of raw bulk ABZ powder were dropped significantly, however the impact of surface-active agent and milling had a direct proportionality with increasing pH of the dissolution media. It seems wetting of ABZ is the main driving force of dissolution and the effect of particle size reduction is more decisive at higher pH values.

Dissolution profiles of nanosuspensions and solidified dispersions were slightly altered probably due to slight aggregation of ABZ nanocrystals during the slow tray drying process. Nevertheless, dissolution profiles of nanocrystal containing formulas (nanosuspension and granules containing milled ABZ) have met the dissolution requirement of immediate release dosage forms (cumulative drug release 80% after 30 minutes of dissolution) [159].

These in vitro results could demonstrate the added value of the developed drug delivery system in the anthelmintic therapy.

Quality control studies have demonstrated the successful reconstitution of ABZ nanocrystals from the solid drug delivery system, with mean particles size of 197.2 ± 0.2 nm and polydispersity index (PDI) of 0.17 ± 0.017 in artificial rumen fluid (ARF) at pH = 6.50 and 140.1 ± 1.3 nm; 0.18 ± 0.042 in phosphate-buffer at pH = 6.8 (Ph. Eur. 9). Solidification of nanosuspensions by wet granulation and subsequent gentle drying process suitable for thermo sensitive compounds (vacuum drying, freeze-drying, fluid bed drying, spray-drying) has been proved to be able to preserve PSDs of nanocrystals and therefore improving shelf-life of products containing nanoparticulates.

Although crystallinity, polymorphs, and structures of ABZ have been thoroughly studied, along with polymorphy inducing factors separately, there are no publications investigating the effect of pearl/bead milling on ABZ crystallinity. This work as a novelty offers the identification of extreme milling conditions, where disadvantageous ABZ Form I → Form II conversion is realized, therefore lowering initial ABZ solubility. This research can give a hint to formulation scientists to avoid these critical conditions during ABZ nanosuspension development by wet planetary bead milling techniques. The influence of process parameters (capacity of the milling container, size of the milling medium, milling speed, milling time) and drying on ABZ polymorphism have been studied. Results have concluded, that there was a full polymorphic conversion of ABZ from Form I to Form II, which was more pronounced with the application of d = 0.3 mm sized zirconia beads, loaded in smaller milling container (50 ml) and with the utilization of coarse milling programs, involving 600 rpm rotation speeds, during 30-180 minute long operations.

6. Summary

Based on QbD approach, ABZ containing nanosuspension was prepared with top-down low energy planetary bead milling. Optimized formula showed less than 200 nm mean size with narrow distribution (PDI < 0.200), which can easily compete with the results of newly developed 'bottom-up' nanoparticle production techniques. Statistical results of optimization suggested the selection of d = 0.1 mm sized zirconia beads in lower (100 ml) volume, at low to mediocre milling speed intervals (200–434 rpm) up to a maximum of 40 minute long milling operations.

Washing the beads after milling with 33.33% (w/w) of total mass loading with surface active agent solutions and mixed with ABZ nanosuspensions have demonstrated reasonable ABZ yield (83.05%), in a relatively low mean dose (200 mg in 7.094 cm^3). Without solidification micrometer sized aggregates have appeared at 28 days of storage at room temperature and at 56 days at refrigerated conditions.

The utilization of ABZ nanocrystals proved to increase thermodynamic solubility values in all tested media, which was most efficient, where initial solubility was minimal. On the contrary improvement of dissolution rate values were the most prominent, where initial solubility was maximal. No lag time values were observed in the dissolution kinetics of the milled formulas in comparison to the unmilled and raw powder samples.

Preparation of dry nanosuspension formulation using MCC (Vivapur® 12) as carrier during wet granulation process was an effective way to preserve the nanocrystalline nature of the wet-milled, poorly water soluble albendazole, which was redispersable after drying.

PXRD studies revealed, that the raw ABZ powder as well as the optimized product contained both polymorphs, so there was no recrystallization due to careful evaluation of loading composition and milling parameters.

Solid state characterization studies of solidified nanosuspension showed partial crystalline–amorphous transition of albendazole during the nanonization process, while the crystalline fraction contained both polymorphic forms of albendazole.

Morphological characterization with AFM and SEM imaging demonstrated the incorporation of albendazole into the microcrystalline cellulose carrier, which also ensured the reconstitution of nanocrystals.

7. Összegzés

A QbD megközelítés alapján ABZ tartalmú nanoszuszpenziót állítottam elő bolygómalomban, nedves őrléssel. Az optimalizált nanoszuszpenzió diszperz fázisa 200 nm alatti átlagos szemcsmérettel és szűk méreteloszlással (PDI < 0,200) jellemezhető, amely felveszi a versenyt az innovatív, felépítéses jellegű előállítási módszerekkel szintetizált nanorészecskékkel. Az optimalizálás statisztikai eredményei alapján összefoglalható, hogy nanoszuszpenzió formulálható kisebb térfogatú (100 ml) d = 0,1 mm méretű cirkónium–dioxid gyöngyök felhasználásával, alacsonytól közepes fordulatszám tartományban (200–434 1/perc), maximum 40 perc hosszú szakaszos őrlési programokkal. Az őrölt szuszpenzió őrlőtestektől való elválasztása után a gyöngytöltetet a teljes töltet tömegének 1/3–ának megfelelő mennyiségű felületaktív anyag és habzásgátló vizes oldatával átöblítve elfogadható hatóanyag kitermelés (83,05% (w/w)) érhető el, alacsony dózis alakítható ki (200 mg/7,094 cm^3).

Igazoltam, hogy az ABZ nanokristályok alkalmazása növelte a termodinamikai oldhatóságot minden vizsgált közegben. Az őrölt minták kioldódási vizsgálatainak kinetikai értékelése során egyik közegben sem tapasztaltam késleltetési időt, a kiindulási ABZ por és az őrlés nélküli szuszpenzió kioldódási profiljaival összehasonlítva.

A mikrokristályos cellulóz (Vivapur® 12) szilárd hordozó segítségével, nedves granulálással és tálcás szárítással kialakított "száraz nanoszuszpenzió" gyógyszerhordozó rendszerből az ABZ nanokristályok rediszpergálás után visszanyerhetők, így alkalmas lehet a szemcsméret-eloszlás állandóságának megőrzésére.

Por-röntgen diffraktometriás vizsgálatok során azonosítottam mind a kiindulási anyagban, mind a végtermékben mindkét polimorfot, így a töltetösszetétel és a kritikus őrlési paraméterek optimalizálása során rekrisztallizáció nem történt.

A "száraz nanoszuszpenzió" gyógyszerhordozó rendszer szilárd fázisú spektroszkópiás vizsgálómódszerekkel történő elemzése alapján megállapítható, hogy a feldolgozás során részleges kristályos amorf átalakulás történt, a kristályos frakcióban pedig mindkét polimorf detektálható.

Morfológiai analízisek (AFM, SEM) pedig szemléltették az ABZ nanokristályok beépülését a mikrokristályos szilárd hordozóba, amely biztosította azok felszabadulását a karrier rendszerből rediszpergálást követően.

8. References

[1] C. Lipinski, American Pharmaceutical Review Poor Aqueous Solubility – an Industry Wide Problem in Drug Discovery, 2003 Am. Pharm. Rev. 1–16.

[2] T. Takagi, C. Ramachandran, M. Bermejo, S. Yamashita, L.X. Yu, G.L. Amidon, A provisional biopharmaceutical classification of the top 200 oral drug products in the United States, Great Britain, Spain, and Japan, 2006 Mol. Pharm. 3 631–643. doi:10.1021/mp0600182.

[3] Y. Kawabata, K. Wada, M. Nakatani, S. Yamada, S. Onoue, Formulation design for poorly water-soluble drugs based on biopharmaceutics classification system : Basic approaches and practical applications, 2011 Int. J. Pharm. 420 1–10.

[4] G.L. Amidon, L. Hans, V.P. Shah, J.R. Crison, A theoretical basis for a Biopharmaceutics Drug Classification: The Correlation of in Vitro Drug Product Dissolution and in vivo Bioavailability, 1995 Pharm. Res. 12 413–420. doi:10.1023/A:1016212804288.

[5] C.A.S. Bergström, C.M. Wassvik, K. Johansson, I. Hubatsch, Poorly soluble marketed drugs display solvation limited solubility, 2007 J. Med. Chem. 50 5858–5862. doi:10.1021/jm0706416.

[6] C.M. Wassvik, A.G. Holmén, R. Draheim, P. Artursson, C.A.S. Bergström, Molecular characteristics for solid-state limited solubility, 2008 J. Med. Chem. 51 3035–3039. doi:10.1021/jm701587d.

[7] X. Pu, J. Sun, M. Li, Z. He, Formulation of Nanosuspensions as a New Approach for the Delivery of Poorly Soluble Drugs, 2009 Curr. Nanosci. 5 417–427.

[8] R.H. Müller, B. Robert, K. Bernd, K. Peters, United States Patent (19) 54, No. 5858410.

[9] C. Prabhakar, K. Bala Krishna, A review on nanosuspensions in drug delivery, 2011 Int. J. Pharma Bio Sci. 2 549–558.

[10] J. Chingunpituk, Nanosuspension Technology for Drug Delivery, 2007 Walailak J Sci Tech. 4 139–153.

[11] P.Y. Cheng, H.K. Schachman, Studies on the validity of the Einstein viscosity law and Stokes' law of sedimentation, 1955 J. Polym. Sci. 16 19–30. doi:10.1002/pol.1955.120168102.

[12] Y. Liu, P. Xie, D. Zhang, Q. Zhang, A mini review of nanosuspensions development, 2012 J. Drug Target. 20 209–223. doi:10.3109/1061186X.2011.645161.

[13] S. Yoel, L.-R. Ganit, T. Ofer, I. Isaac, Nanosuspensions : Emerging Novel Agrochemical Formulations, 2007 Insecticid Des. Using Adv. Technol. 1–39.

[14] B. Van Eerdenbrugh, G. Van den Mooter, P. Augustijns, Top-down production of drug nanocrystals: Nanosuspension stabilization, miniaturization and transformation into solid products, 2008 Int. J. Pharm. 364 64–75.

[15] M.L.A.D. Lestari, R.H. Müller, J.P. Möschwitzer, Systematic screening of different surface modifiers for the production of physically stable nanosuspensions, 2015 J. Pharm. Sci. 104 1128–1140. doi:10.1002/jps.24266.

[16] P.A. Rehbinder, E.D. Shchukin, Surface phenomena in solids during deformation and fracture processs, 1972 Prog Surf Sci. 3 97–104.

[17] A. Monteiro, A. Afolabi, E. Bilgili, Continuous production of drug nanoparticle suspensions via wet stirred media milling : a fresh look at the Rehbinder effect, 2013 39 266–283. doi:10.3109/03639045.2012.676048.

[18] L. Peltonen, Design Space and QbD Approach for Production of Drug Nanocrystals by Wet Media Milling Techniques, 2018 Pharmaceutics. 10 104. doi:10.3390/pharmaceutics10030104.

[19] T. Chaurasia, D. Singh, Nimisha, D. Srivastava, A Review on Nanosuspensionspromising Drug Delivery Strategy., 2012 J. Curr. Pharma Res. 3 764–776. doi:10.33786/jcpr.2012.v03i01.010.

[20] M. George, I. Ghosh, Identifying the correlation between drug/stabilizer properties and critical quality attributes (CQAs) of nanosuspension formulation prepared by wet media milling technology, 2013 Eur. J. Pharm. Sci. 48 142–152. doi:10.1016/j.ejps.2012.10.004.

[21] H. Rachmawati, L. Al Shaal, R.H. Müller, C.M. Keck, Development of Curcumin Nanocrystal: Physical Aspects, 2013 J. Pharm. Sci. 102 204–214. doi:10.1002/jps.23335.

[22] S.W. Musselman, S. Chander, Wetting and adsorption of acetylenic diol based nonionic surfactants on heterogeneous surfaces, 2002 Colloids Surfaces A Physicochem. Eng. Asp. 206 497–513. doi:10.1016/S0927-7757(02)00055-9.

[23] R. Mohammadi, J. Wassink, A. Amirfazli, Effect of surfactants on wetting of super-hydrophobic surfaces, 2004 Langmuir. 20 9657–9662. doi:10.1021/la049268k.

[24] R.H. Muller, C.M. Keck, Challenges and solutions for the delivery of biotech drugs - A review of drug nanocrystal technology and lipid nanoparticles, 2004 J. Biotechnol. 113 151–170. doi:10.1016/j.jbiotec.2004.06.007.

[25] Y. Wang, Y. Zheng, L. Zhang, Q. Wang, D. Zhang, Stability of nanosuspensions in drug delivery, 2013 J. Control. Release. 172 1126–1141. doi:10.1016/j.jconrel.2013.08.006.

[26] B.E. Rabinow, Nanosuspensions in drug delivery, 2004 Nat. Rev. Drug Discov. 3 785–796.

[27] C. Jacobs, R.H. Müller, Production and characterization of a budesonide nanosuspension for pulmonary administration, 2002 Pharm. Res. 19 189–194. doi:10.1023/A:1014276917363.

[28] Y.X. Zhao, H.Y. Hua, M. Chang, W.J. Liu, Y. Zhao, H.M. Liu, Preparation and cytotoxic activity of hydroxycamptothecin nanosuspensions, 2010 Int. J. Pharm. 392 64–71. doi:10.1016/j.ijpharm.2010.03.027.

[29] F. Toziopoulou, M. Malamatari, I. Nikolakakis, K. Kachrimanis, Production of aprepitant nanocrystals by wet media milling and subsequent solidification, 2017 Int. J. Pharm. 533 324–334. doi:10.1016/j.ijpharm.2017.02.065.

[30] Q. Wei, C.M. Keck, R.H. Müller, Solidification of hesperidin nanosuspension by spray drying optimized by design of experiment (DoE), 2018 Drug Dev. Ind. Pharm. 44 1–12. doi:10.1080/03639045.2017.1285309.

[31] Y.Q. Ma, Z.Z. Zhang, G. Li, J. Zhang, H.Y. Xiao, X.F. Li, Solidification drug nanosuspensions into nanocrystals by freeze-drying: A case study with ursodeoxycholic acid, 2016 Pharm. Dev. Technol. 21 180–188. doi:10.3109/10837450.2014.982822.

[32] J. Han, X. Wang, J. Wang, L. Wang, L. Chen, J. Li, W. Li, Quality-by-Design approach to the fluid-bed coating of ginkgo lactone nanosuspensions, 2018 RSC Adv. 8 22136–22145. doi:10.1039/c8ra03288b.

[33] N. Anup, S. Thakkar, M. Misra, Formulation of olanzapine nanosuspension based orally disintegrating tablets (ODT); comparative evaluation of lyophilization and electrospraying process as solidification techniques, 2018 Adv. Powder Technol. 29 1913–1924. doi:10.1016/j.apt.2018.05.003.

[34] B.Y. Gajera, D.A. Shah, R.H. Dave, Investigating a Novel Hot Melt Extrusion-Based Drying Technique to Solidify an Amorphous Nanosuspension Using Design of Experiment Methodology, 2018 AAPS PharmSciTech. 19 3778–3790. doi:10.1208/s12249-018-1189-7.

[35] J.P.K. Tan, Q. Wang, K.C. Tam, Control of burst release from nanogels via layer by layer assembly, 2008 J. Control. Release. 128 248–254. doi:10.1016/j.jconrel.2008.03.012.

[36] R.H. Müller, C. Jacobs, Buparvaquone mucoadhesive nanosuspension: Preparation, optimisation and long-term stability, 2002 Int. J. Pharm. 237 151–161. doi:10.1016/S0378-5173(02)00040-6.

[37] O. Kayser, A new approach for targeting to Cryptosporidium parvum using mucoadhesive nanosuspensions: Research and applications, 2001 Int. J. Pharm. 214 83–85. doi:10.1016/S0378-5173(00)00640-2.

[38] F. Alexis, E. Pridgen, L.K. Molnar, F.C. Omic, Factors Affecting the Clearance and Biodistribution of Polymaric Nanoparticles, 2008 Mol. Pharm. 5 505–515.

[39] J. Lode, Iduna Fichtner, Jörg Kreuter, Antje Berndt, Julia Eva Diederichs, Regina Reszka, Influence of surface-modifying surfactants on the pharmacokinetic behavior of 14C-poly (methylmethacrylate) nanoparticles in experimental tumor models, 2001 Pharm. Res. 18 1613–1619. doi:10.1023/A:1013094801351.

[40] Z. Ning, Wu, D. Da, T.R. L., D. Needham, R. whorton A., M.D. W., Increased Microvascular Permeability Contributes to Preferential Accumulation of Stealth Liposomes in Tumor Tissue, 1993 Cancer Res. 53 3765–3770.

[41] J. Kreuter, V.E. Petrov, D.A. Kharkevich, R.N. Alyautdin, Influence of the type of surfactant on the analgesic effects induced by the peptide dalargin after its delivery across the blood-brain barrier using surfactant-coated nanoparticles, 1997 J. Control. Release. 49 81–87. doi:10.1016/S0168-3659(97)00061-8.

[42] H.M. Ibrahim, H.R. Ismail, A.E.A. Lila, Formulation and optimization pf ocular poly-D, L-lactic acid nano drug delivery system of Amphotericin-B using Box Behnken design, 2012 Int. J. Pharm. Pharm. Sci. 4 342–349.

[43] P. Liu, X. Rong, J. Laru, B. Van Veen, J. Kiesvaara, J. Hirvonen, T. Laaksonen, L. Peltonen, Nanosuspensions of poorly soluble drugs: Preparation and development by wet milling, 2011 Int. J. Pharm. 411 215–222.

[44] A. Maschke, N. Calí, B. Appel, J. Kiermaier, T. Blunk, A. Göpferich, Micronization of insulin by high pressure homogenization, 2006 Pharm. Res. 23 2220–2229. doi:10.1007/s11095-006-9019-0.

[45] E. Merisko-Liversidge, S.L. McGurk, G.G. Liversidge, Insulin nanoparticles: A novel formulation approach for poorly water soluble Zn-insulin, 2004 Pharm. Res. 21 1545–1553. doi:10.1023/B:PHAM.0000041446.14569.e2.

[46] E. Merisko-Liversidge, G.G. Liversidge, E.R. Cooper, Nanosizing: A formulation approach for poorly-water-soluble compounds, 2003 Eur. J. Pharm. Sci. 18 113–120. doi:10.1016/S0928-0987(02)00251-8.

[47] Y. Noguchi, J. Wu, R. Duncan, J. Strohalm, K. Ulbrich, T. Akaike, H. Maeda, Early phase tumor accumulation of Macromolecules: A great difference in clearance rate between tumor and normal tissues, 1998 Japanese J. Cancer Res. 89 307–314. doi:10.1111/j.1349-7006.1998.tb00563.x.

[48] R.K. Jain, Delivery of molecular and cellular medicine to solid tumors, 1998 J. Control. Release. 53 49–67. doi:10.1016/S0168-3659(97)00237-X.

[49] G. Kong, R.D. Braun, M.W. Dewhirst, Hyperthermia enables tumor-specific nanoparticle delivery: Effect of particle size, 2000 Cancer Res. 60 4440–4445.

[50] C.E. Soma, C. Dubernet, G. Barratt, S. Benita, P. Couvreur, Investigation of the role of macrophages on the cytotoxicity of doxorubicin and doxorubicin-loaded nanoparticles on M5076 cells in vitro, 2000 J. Control. Release. 68 283–289. doi:10.1016/S0168-3659(00)00269-8.

[51] Y. Adachi, S. Arii, N. Funaki, H. Higashitsuji, S. Fujita, M. Furutani, M. Mise, W. Zhang, T. Tobe, Tumoricidal activity of Kupffer cells augmented by anticancer drugs, 1992 Life Sci. 51 177–183.

[52] V.B. Junyaprasert, B. Morakul, Nanocrystals for enhancement of oral bioavailability of poorly water-soluble drugs, 2015 Asian J. Pharm. Sci. 10 13–23. doi:10.1016/j.ajps.2014.08.005.

[53] S. Mitragotri, P.A. Burke, R. Langer, Overcoming the challenges in administering biopharmaceuticals: Formulation and delivery strategies, 2014 Nat. Rev. Drug Discov. 13 655–672.

[54] N.S. Zogovic, N.S. Nikolic, S.D. Vranjes-Djuric, L.M. Harhaji, L.M. Vucicevic, K.D. Janjetovic, M.S. Misirkic, B.M. Todorovic-Markovic, Z.M. Markovic, S.K. Milonjic, V.S. Trajkovic, Opposite effects of nanocrystalline fullerene (C60) on tumour cell growth in vitro and in vivo and a possible role of immunosupression in the cancer-promoting activity of C60, 2009 Biomaterials. 30 6940–6946. doi:10.1016/j.biomaterials.2009.09.007.

[55] J. Tulinska, A. Kazimirova, M. Kuricova, M. Barancokova, A. Liskova, E. Neubauerova, M. Drlickova, F. Ciampor, I. Vavra, D. Bilanicova, G. Pojana, M. Staruchova, M. Horvathova, E. Jahnova, K. Volkovova, M. Bartusova, M. Cagalinec, M. Dusinska, Immunotoxicity and genotoxicity testing of PLGA-PEO nanoparticles in human blood cell model, 2015 Nanotoxicology. 9 33–43. doi:10.3109/17435390.2013.816798.

[56] G. Chen, W. Chen, Z. Wu, R. Yuan, H. Li, J. Gao, X. Shuai, MRI-visible polymeric vector bearing CD3 single chain antibody for gene delivery to T cells for immunosuppression, 2009 Biomaterials. 30 1962–1970. doi:10.1016/j.biomaterials.2008.12.043.

[57] R. Yadollahi, K. Vasilev, S. Simovic, Nanosuspension Technologies for Delivery of Poorly Soluble Drugs, 2015 J. Nanomater. 2015 1–13.

[58] R. Shegokar, R.H. Müller, Nanocrystals: Industrially feasible multifunctional formulation technology for poorly soluble actives, 2010 Int. J. Pharm. 399 129–139. doi:10.1016/j.ijpharm.2010.07.044.

[59] E. Joseph, G. Singhvi, Multifunctional nanocrystals for cancer therapy: a potential nanocarrier, Elsevier Inc., . doi:10.1016/b978-0-12-816505-8.00007-2.

[60] M.C.C. Peters, E. dos Santos Neto, L.M. Monteiro, M.N. Yukuyama, M.G.M. Machado, I.F. de Oliveira, M.H.A. Zanin, R. Löbenberg, N. Bou-Chacra, Advances in ophthalmic preparation: the role of drug nanocrystals and lipid-based nanosystems, 2019 J. Drug Target. 0 1–12. doi:10.1080/1061186x.2019.1663858.

[61] A.A. Noyes, W.R. Whitney, The rate of solution of solid substances in their own solutions, 1897 J. Am. Chem. Soc. 19 930–934. doi:10.1021/ja02086a003.

[62] E. Amine, A. Claes, A. Göran, N. Christer, Increased metastable solubility of milled griseofulvin, depending on the formation of a disordered surface structure, 1996 Int. J. Pharm. 136 159–170.

[63] W. Nernst, Theorie der Reaktionsgeschwindigkeit in heterogenen Systemen, 1904 Zeitschrift Für Phys. Chemie. 10 156–157. doi:10.1002/bbpc.19040100904.

[64] E. Brunner, Reaktionsgeschwindigkeit in heterogenen Systemen, 1904 Zeitschrift Für Phys. Chemie. 43 56–102. doi:10.1515/zpch-1904-4705.

[65] K.K. Sawant, M.H. Patel, K. Patel, Cefdinir nanosuspension for improved oral bioavailability by media milling technique: Formulation, characterization and in vitro–in vivo evaluations, 2016 Drug Dev. Ind. Pharm. 42 758–768. doi:10.3109/03639045.2015.1104344.

[66] M. Mosharraf, C. Nyström, The effect of particle size and shape on the surface specific dissolution rate of microsized practically insoluble drugs, 1995 Int. J. Pharm. 122 35–47. doi:10.1016/0378-5173(95)00033-F.

[67] D.M. Oh, R.L. Curl, G.L. Amidon, Estimating the Fraction Dose Absorbed from Suspensions o Poorly Soluble Compounds in Humans: A mathematical Model, 1993 Pharm. Res. 10 264–270. doi:10.1023/A:1018947113238.

[68] G.L.A. Raimar Lödenberg, Modern bioavailability , bioequivalence and biopharmaceutics classification system . New scientific approaches to international regulatory standards, 2000 Eur. J. Pharm. Biopharm. 50 3–12.

[69] J.B. Dressman, D. Fleisher, Mixing-tank model for predicting dissolution rate control of oral absorption, 1986 J. Pharm. Sci. 75 109–116. doi:10.1002/jps.2600750202.

[70] M.J. Grau, O. Kayser, R.H. Müller, Nanosuspensions of poorly soluble drugs — reproducibility of small scale production, 2000 Int. J. Pharm. 196 155–159. doi:10.1016/S0378-5173(99)00411-1.

[71] R.H. Müller, S. Gohla, C.M. Keck, State of the art of nanocrystals - Special features, production, nanotoxicology aspects and intracellular delivery, 2011 Eur. J. Pharm. Biopharm. 78 1–9.

[72] B. Sinha, R.H. Müller, J.P. Möschwitzer, Bottom-up approaches for preparing drug nanocrystals: Formulations and factors affecting particle size, 2013 Int. J. Pharm. 453 126–141. doi:10.1016/j.ijpharm.2013.01.019.

[73] H.K. Chan, P.C.L. Kwok, Production methods for nanodrug particles using the bottom-up approach, 2011 Adv. Drug Deliv. Rev. 63 406–416. doi:10.1016/j.addr.2011.03.011.

[74] C.M. Keck, R.H. Müller, Drug nanocrystals of poorly soluble drugs produced by high pressure homogenisation, 2006 Eur. J. Pharm. Biopharm. 62 3–16. doi:10.1016/j.ejpb.2005.05.009.

[75] M. Eaqub Ali, M. Ullah, S. Bee Abd Hamid, Surfactant-Assisted Ball Milling: a Novel Route To Novel Materials With Controlled Nanostructure -a Review, 2014 Rev. Adv. Mater. Sci. 37 1–14.

[76] J.E. Kipp, J. Chung, T. Wong, M.J. Doty, C.L. Rebbeck, Microprecipitation method for preparing submicron suspensions, Accessed: 22.07.2019.

[77] A.D. Gholap, S.S. Borude, A.M. Mahajan, Smart crystal technology: A review, 2011 Pharmacologyonline. 3 238–243.

[78] GSK Ltd., ZEN/PI/IN/2018/02 Zentel Albendazole Tablets IP / albendazole Oral Suspension IP, https://india-pharma.gsk.com/media/701423/zentel.pdf, [pdf], GlaxoSmithKline plc., India, accessed: 19.07.2019, (n.d.) 1–13.

[79] H. Wen, R.R.C. New, M. Muhmut, J.H. Wang, Y.H. Wang, J.H. Zhang, Pharmacology and efficacy of liposome-entrapped albendazole in experimental secondary alveolar echinococcosis and effect of co-administratration with cimetidine, 1996 Parasitology. 113 111–121.

[80] E. Lacey, The role of the cytoskeletal protein, tubulin , in the mode of action and mechanism of drug resistance to benzimidazoles, 1988 Int. J. Parasitol. 18 885–936.

[81] I. Port, J. Wiley, E. Lacey, Mode of Action of Benzimidazoles, 1990 Parasitol. Today. 6 2–5.

[82] A.D. Dayan, Albendazole, mebendazole and praziquantel. Review of non-clinical toxicity and pharmacokinetics, 2003 Acta Trop. 86 141–159.

[83] US Food and Drug Administration, Prescribing Information Albenza, 2009 4–11. https://www.accessdata.fda.gov/drugsatfda_docs/label/2009/020666s005s006lbl.pdf (accessed May 21, 2020).

[84] European Medicines Agency (EMA) Veterinary Medicines and Inspections, COMMITTEE FOR MEDICINAL PRODUCTS FOR VETERINARY USE ALBENDAZOLE (Extrapolation to all ruminants) SUMMARY REPORT (3). http://www.ema.europa.eu/docs/en_GB/document_library/Maximum_Residue_Limits_-_Report/2009/11/WC500009638.pdf (accessed May 17, 2020).

[85] W.C. Campbell, Benzimidazoles : Veterinary Uses, 1990 Parasitol. Today. 6 130–133.

[86] A. Mckellar, E.W. Scott, The benzimidazole anthelmintic agents - a review, 1990 J. Vet. Pharmacol. Ther. 13 223–247.

[87] L. Ceballos, C. Elissondo, L. Moreno, M. Dopchiz, S. Sánchez Bruni, G. Denegri, L. Alvarez, C. Lanusse, Albendazole treatment in cystic echinococcosis: Pharmacokinetics and clinical efficacy of two different aqueous formulations, 2008 Parasitol. Res. 103 355–362. doi:10.1007/s00436-008-0980-x.

[88] F. Góngora-Rivera, J.L. Soto-Hernández, D. González Esquivel, H.J. Cook, C. Máquez-Caraveo, R. Hernández Dávila, J. Santos-Zambrano, Albendazole trial at 15 or 30 mg/kg/day for subarachnoid and intraventricular cysticercosis, 2006 Neurology. 66 436–438. doi:10.1212/01.wnl.0000195887.63124.dc.

[89] A. Casulli, M.A. Gomez Morales, B. Gallinella, L. Turchetto, E. Pozio, 2-Hydroxypropyl-β-cyclodextrin improves the effectiveness of albendazole against encapsulated larvae of Trichinella spiralis in a murine model, 2006 J. Antimicrob. Chemother. 58 886–890. doi:10.1093/jac/dkl329.

[90] X.Q. Li, A. Björkman, T.B. Andersson, L.L. Gustafsson, C.M. Masimirembwa, Identification of human cytochrome P450s that metabolise anti-parasitic drugs and predictions of in vivo drug hepatic clearance from in vitro data, 2003 Eur. J. Clin. Pharmacol. 59 429–442. doi:10.1007/s00228-003-0636-9.

[91] S. Torrado, S. Torrado, R. Cadorniga, J.J. Torrado, Formulation parameters of albendazole solution, 1996 Int. J. Pharm. 140 45–50.

[92] J. H, M. L, G. L, F. I, M.-E. R, Absorption Studies of Albendazole and Some Physicochemical Properties of the Drug and Its Metabolite Albendazole Sulphoxide, 1998 J. Pharm. Pharmacol. 50 43–48.

[93] PubChem, Compound summary of albendazole, (n.d.). https://pubchem.ncbi.nlm.nih.gov/compound/Albendazole (accessed May 17, 2020).

[94] M.L. Mottier, L.I. Alvarez, M.A. Pis, C.E. Lanusse, Transtegumental diffusion of benzimidazole anthelmintics into Moniezia benedeni : correlation with their octanol – water partition coefficients, 2003 Exp. Parasitol. 103 1–7.

[95] A. Dahan, J.M. Miller, G.L. Amidon, Prediction of Solubility and Permeability Class Membership : Provisional BCS Classification of the World ' s Top Oral Drugs, 2009 AAPS J. 11 740–746.

[96] T. Mukherjee, F.M. Plakogiannis, Development and oral bioavailability assessment of a supersaturated self-microemulsifying drug delivery system (SMEDDS) of albendazole, 2010 J. Pharm. Pharmacol. 62 1112–1120.

[97] J.H. Fagerberg, O. Tsinman, N. Sun, K. Tsinman, A. Avdeef, C.A.S. Bergström, Dissolution rate and apparent solubility of poorly soluble drugs in biorelevant dissolution media, 2010 Mol. Pharm. 7 1419–1430. doi:10.1021/mp100049m.

[98] V. Fülöp, G. Jakab, T. Bozó, B. Tóth, D. Endrésik, E. Balogh, M. Kellermayer, I. Antal, Study on the dissolution improvement of albendazole using reconstitutable dry nanosuspension formulation, 2018 Eur. J. Pharm. Sci. doi:10.1016/j.ejps.2018.07.027.

[99] A.K. Chattah, R. Zhang, K.H. Mroue, L.Y. Pfund, M.R. Longhi, A. Ramamoorthy, C. Garnero, Investigating Albendazole Desmotropes by Solid-State NMR Spectroscopy, 2015 Mol. Pharm. 12 731–741.

[100] M.B. Pranzo, D. Cruickshank, M. Coruzzi, M.R. Caira, R. Bettini, Enantiotropically Related Albendazole Polymorphs, 2010 J. Pharceutical Sci. 99 3731–3742. doi:10.1002/jps.

[101] S. Torrado, M.L. López, G. Torrado, F. Bolás, S. Torrado, R. Cadórniga, A novel formulation of albendazole solution: Oral bioavailability and efficacy evaluation, 1997 Int. J. Pharm. 156 181–187. doi:10.1016/S0378-5173(97)00204-4.

[102] N. Kohri, Y. Yamayoshi, H. Xin, K. Iseki, N. Sato, S. Todo, K. Miyazaki, Improving the Oral Bioavailability of Albendazole in Rabbits by the Solid Dispersion Technique, 1999 J. Pharm. Pharmacol. 51 159–164. doi:10.1211/0022357991772277.

[103] J.L. Delestal, A.I. Alvarez, C. Villaverde, P. Coronel, S. Fabra, J. g. Prieto, Effect of surfactants on Albendazole absorption, 1991 J. Pharm. Biomed. Anal. 9 1161–1164. doi:10.1016/0731-7085(91)80060-M.

[104] J.L. del Estal, A.I. Alvarez, C. Villaverde, A. Justel, J.G. Prieto, Increased systemic bioavailability of albendazol when administered with surfactants in rats, 1994 Int. J. Pharm. 102 257–260. doi:10.1016/0378-5173(94)90063-9.

[105] J.L. del Estal, A.I. Alvarez, C. Villaverde, J.G. Prieto, Comparative effects of anionic, natural bile acid surfactants and mixed micelles on the intestinal absorption of the anthelmintic albendazole, 1993 Int. J. Pharm. 91 105–109. doi:10.1016/0378-5173(93)90329-E.

[106] B. Evrard, P. Chiap, P. DeTullio, F. Ghalmi, G. Piel, T. Van Hees, J. Crommen, B. Losson, L. Delattre, Oral bioavailability in sheep of albendazole from a suspension and from a solution containing hydroxypropyl-β-cyclodextrin, 2002 J. Control. Release. 85 45–50.

[107] K. Awadzi, M. Hero, N. Opoku, D.W. Büttner, P.A. Coventry, M.A. Prime, M.L. Orme, G. Edwards, The chemotherapy of onchocerciasis XVII. A clinical evaluation of albendazole in patients with onchocerciasis; effects of food and pretreatment with ivermectin on drug response and pharmacokinetics., 1994 Trop Med Parasitol. 45 8–203.

[108] M. Homeida, W. Leahy, S. Copeland, M.M.M. Ali, D.W.G. Harron, Pharmacokinetic interaction between praziquantel and albendazole in Sudanese men, 1994 Ann. Trop. Med. Parasitol. 88 551–559. doi:10.1080/00034983.1994.11812903.

[109] H. Lange, R. Eggers, J. Bircher, Increased systemic availability of albendazole when taken with a fatty meal, 1988 Eur. J. Clin. Pharmacol. 34 315–317. doi:10.1007/BF00540964.

[110] J. Nagy, H.G. Schipper, R.P. Koopmans, J.J. Butter, C.J. Van Boxtel, P.A. Kager, Effect of grapefruit juice or cimetidine coadministration on albendazole bioavailability., 2002 Am. J. Trop. Med. Hyg. 66 260–263. doi:10.4269/ajtmh.2002.66.260.

[111] H. Schipper, R. Koopmans, J. Nagy, J. Butter, P. Kager, C. Van Boxtel, Effect of dose increase or cimetidine co-administration on albendazole bioavailability., 2000 Am. J. Trop. Med. Hyg. 63 270–273. doi:10.4269/ajtmh.2000.63.270.

[112] W. Mingjie, X. Shuhua, C. Junjie, L. Bin, F. Cheng, S. Weixia, P. Hotez, Albendazole-soybean oil emulsion for the treatment of human cystic echinococcosis: Evaluation of bioavailability and bioequivalence, 2002 Acta Trop. 83 177–181. doi:10.1016/S0001-706X(02)00096-7.

[113] M.P. Kumar, Y.M. Rao, S. Apte, Improved Bioavailability of Albendazole Following Oral Administration of Nanosuspension in Rats, 2007 Curr. Nanosci. 3 191–194.

[114] W. Li, P. Quan, Y. Zhang, J. Cheng, J. Liu, D. Cun, R. Xiang, L. Fang, Influence of drug physicochemical properties on absorption of water insoluble drug nanosuspensions, 2014 Int. J. Pharm. 460 13–23. doi:10.1016/j.ijpharm.2013.10.038.

[115] M.P. Kumar, Y.M. Rao, S. Apte, Formulation of Nanosuspensions of Albendazole for Oral Administration, 2008 Curr. Nanosci. 4 53–58. doi:10.2174/157341308783591807.

[116] Y. Liu, X.Q. Wang, W.X. Ren, Y.L. Chen, Y. Yu, J.K. Zhang, D. Bawudong, J.P. Gu, X.D. Xu, X.N. Zhang, Novel albendazole-chitosan nanoparticles for intestinal absorption enhancement and hepatic targeting improvement in rats, 2013 J. Biomed. Mater. Res. - Part B Appl. Biomater. 101 B 998–1005. doi:10.1002/jbm.b.32908.

[117] N. Torabi, F. Dobakhti, A. Haniloo, Albendazole and Praziquantel Chitosan Nanoparticles: Preparation, Characterization, and In Vitro Release Study, 2017 Iran. J. Sci. Technol. Trans. A Sci. 42 1269–1275. doi:10.1007/s40995-017-0150-z.

[118] U.S. Department of Health and Human Services (FDA), Guidance for Industry Quality Systems Approach to Pharmaceutical CGMP Regulations, 2006 Pharmacutical CGMP Regul. (ICH Q8). 1–27. https://www.fda.gov/media/71023/download (accessed October 5, 2019).

[119] M.T.C. Tao Feng, Rodolfo Pinal, Process Induced Disorder in Crystalline Materials: Differentiating Defective Crystals from the Amorphous Form of Griseofulvin, 2008 J. Pharm. Sci. 97 3207–3221.

[120] N. Bouvart, R.M. Palix, S.G. Arkhipov, I.A. Tumanov, A.A.L. Michalchuk, E. V. Boldyreva, Polymorphism of chlorpropamide on liquid-assisted mechanical treatment: Choice of liquid and type of mechanical treatment matter, 2018 CrystEngComm. 20 1797–1803. doi:10.1039/c7ce02221b.

[121] A.M. Belenguer, G.I. Lampronti, A.J. Cruz-Cabeza, C.A. Hunter, J.K.M. Sanders, Solvation and surface effects on polymorph stabilities at the nanoscale, 2016 Chem. Sci. 7 6617–6627. doi:10.1039/c6sc03457h.

[122] F. Fischer, A. Heidrich, S. Greiser, S. Benemann, K. Rademann, F. Emmerling, Polymorphism of Mechanochemically Synthesized Cocrystals: A Case Study, 2016 Cryst. Growth Des. 16 1701–1707. doi:10.1021/acs.cgd.5b01776.

[123] D. Hasa, E. Miniussi, W. Jones, Mechanochemical Synthesis of Multicomponent Crystals: One Liquid for One Polymorph? A Myth to Dispel, 2016 Cryst. Growth Des. 16 4582–4588. doi:10.1021/acs.cgd.6b00682.

[124] P. Sharma, Z.D. Zujovic, G.A. Bowmaker, W.A. Denny, S. Garg, Evaluation of a crystalline nanosuspension: Polymorphism, process induced transformation and in vivo studies, 2011 Int. J. Pharm. 408 138–151. doi:10.1016/j.ijpharm.2011.01.032.

[125] V. Nekkanti, A. Marwah, R. Pillai, Media milling process optimization for manufacture of drug nanoparticles using design of experiments (DOE), 2015 Drug Dev. Ind. Pharm. 41 124–130.

[126] A. Billon, B. Bataille, G. Cassanas, M. Jacob, Development of spray-dried acetaminophen microparticles using experimental designs, 2000 Int. J. Pharm. 203 159–168. doi:10.1016/S0378-5173(00)00448-8.

[127] P. Tewa-Tagne, S. Briançon, H. Fessi, Spray-dried microparticles containing polymeric nanocapsules: Formulation aspects, liquid phase interactions and particles characteristics, 2006 Int. J. Pharm. 325 63–74. doi:10.1016/j.ijpharm.2006.06.025.

[128] A. Dévay, K. Mayer, S. Pál, I. Antal, Investigation on drug dissolution and particle characteristics of pellets related to manufacturing process variables of high-shear granulation, 2006 J. Biochem. Biophys. Methods. 69 197–205. doi:10.1016/j.jbbm.2006.03.006.

[129] Stat-Ease » v11 » Optimization Overview » Numerical Optimization » Desirability Function, (n.d.). https://www.statease.com/docs/v11/contents/optimization/desirability-function/ (accessed October 1, 2019).

[130] J. Hao, Y. Gao, J. Zhao, J. Zhang, Q. Li, Z. Zhao, J. Liu, Preparation and Optimization of Resveratrol Nanosuspensions by Antisolvent Precipitation Using Box-Behnken Design, 2014 AAPS PharmSciTech. 16 118–128. doi:10.1208/s12249-014-0211-y.

[131] A.R. Fernandes, N.R. Ferreira, J.F. Fangueiro, A.C. Santos, F.J. Veiga, C. Cabral, A.M. Silva, E.B. Souto, Ibuprofen nanocrystals developed by 22 factorial design experiment: A new approach for poorly water-soluble drugs, 2017 Saudi Pharm. J. 25 1117–1124. doi:10.1016/j.jsps.2017.07.004.

[132] B. Mishra, J. Sahoo, P.K. Dixit, Formulation and process optimization of naproxen nanosuspensions stabilized by hydroxy propyl methyl cellulose, 2015 Carbohydr. Polym. 127 300–308. doi:10.1016/j.carbpol.2015.03.077.

[133] B. Mishra, J. Sahoo, P.K. Dixit, Enhanced bioavailability of cinnarizine nanosuspensions by particle size engineering: Optimization and physicochemical investigations, 2016 Mater. Sci. Eng. C. 63 62–69. doi:10.1016/j.msec.2016.02.046.

[134] D. Medarević, J. Djuriš, S. Ibrić, M. Mitrić, K. Kachrimanis, Optimization of formulation and process parameters for the production of carvedilol nanosuspension by wet media milling, 2018 Int. J. Pharm. 540 150–161. doi:10.1016/j.ijpharm.2018.02.011.

[135] M. Li, M. Azad, R. Davé, E. Bilgili, Nanomilling of drugs for bioavailability enhancement: A holistic formulation-process perspective, 2016 Pharmaceutics. 8. doi:10.3390/pharmaceutics8020017.

[136] M. Li, P. Alvarez, E. Bilgili, A microhydrodynamic rationale for selection of bead size in preparation of drug nanosuspensions via wet stirred media milling, 2017 Int. J. Pharm. 524 178–192. doi:10.1016/j.ijpharm.2017.04.001.

[137] A basic guide to particle characterization, 2015. https://www.malvernpanalytical.com/en/learn/knowledge-center/whitepapers/WP120620BasicGuidePartChar (accessed October 5, 2019).

[138] A. Rawle, Basic principles of particle-size analysis, 2003 Surf. Coatings Int. Part A Coatings J. 86 58–65.

[139] Horiba Instrument Catalog, A Guidebook To Particle Size Analysis, 2014 Horiba Instrum. Cat. 1–32. https://www.horiba.com/fileadmin/uploads/Scientific/Documents/PSA/PSA_Guidebook.pdf (accessed April 10, 2015).

[140] ASTM Standard E799-03, Standard Practice for Determining Data Criteria and Processing for Liquid Drop Size Analysis. doi:10.1520/E0799-03R09.2.

[141] A. Sze, D. Erickson, L. Ren, D. Li, Zeta-potential measurement using the Smoluchowski equation and the slope of the current-time relationship in electroosmotic flow, 2003 J. Colloid Interface Sci. 261 402–410. doi:10.1016/S0021-9797(03)00142-5.

[142] C.C. Sun, Mechanism of moisture induced variations in true density and compaction properties of microcrystalline cellulose, 2008 Int. J. Pharm. 346 93–101.

[143] D.R. Heidemann, P.J. Jarosz, Preformulation Studies Involving Moisture Uptake in Solid Dosage Forms, 1991 Pharm. Res. An Off. J. Am. Assoc. Pharm. Sci. 8 292–297. doi:10.1023/A:1015877011807.

[144] M. Fonteyne, J. Vercruysse, F. De Leersnyder, B. Van Snick, C. Vervaet, J.P. Remon, T. De Beer, Process Analytical Technology for continuous manufacturing of solid-dosage forms, 2015 TrAC - Trends Anal. Chem. 67 159–166. doi:10.1016/j.trac.2015.01.011.

[145] S. Oka, O. Kašpar, V. Tokárová, K. Sowrirajan, H. Wu, M. Khan, F. Muzzio, F. Štěpánek, R. Ramachandran, A quantitative study of the effect of process parameters on key granule characteristics in a high shear wet granulation process involving a two component pharmaceutical blend, 2015 Adv. Powder Technol. 26 315–322. doi:10.1016/j.apt.2014.10.012.

[146] P. Kazemi, M.H. Khalid, J. Szlek, A. Mirtič, G.K. Reynolds, R. Jachowicz, A. Mendyk, Computational intelligence modeling of granule size distribution for oscillating milling, 2016 Powder Technol. 301 1252–1258. doi:10.1016/j.powtec.2016.07.046.

[147] E. Baka, J.E.A. Comer, K. Tak, Study of equilibrium solubility measurement by saturation shake-flask method using hydrochlorothiazide as model compound, 2008 46 335–341.

[148] G. Völgyi, D. Csicsák, K. Takács-novák, Right filter-selection for phase separation in equilibrium solubility measurement, 2018 Eur. J. Pharm. Sci. 123 98–105. doi:10.1016/j.ejps.2018.06.031.

[149] Procedure to make 1 L of artificial rumen fluid, (n.d.). https://www.ecow.co.uk/wp-content/uploads/2014/10/Procedure-for-making-1-L-of-artificial-rumen-fluid.pdf (accessed August 28, 2017).

[150] E. Galia, J. Horton, J.B. Dressman, Albendazole generics - A comparative in vitro study, 1999 Pharm. Res. Res. 16 1871–1875.

[151] I. Antal, R. Zelkó, N. Röczey, J. Plachy, I. Rácz, Dissolution and diffuse reflectance characteristics of coated theophylline particles, 1997 Int. J. Pharm. 155 83–89. doi:10.1016/S0378-5173(97)00161-0.

[152] J. Rouse, S. David, Influence of Surfactants on Microbial Degradation of Organic Compounds, 1994 Crit. Rev. Environ. Sci. Technol. 24 325–370. doi:10.1080/10643389409388471.

[153] X. Guo, Z. Rong, X. Ying, Calculation of hydrophile-lipophile balance for polyethoxylated surfactants by group contribution method, 2006 J. Colloid Interface Sci. 298 441–450. doi:10.1016/j.jcis.2005.12.009.

[154] Stat-Ease » v11 » Fit summary (RSM/MIX Model Selection), (n.d.). https://www.statease.com/docs/v11/contents/analysis/fit-summary/ (accessed October 21, 2019).

[155] Z. Ding, L. Wang, Y. Xing, Y. Zhao, Z. Wang, J. Han, Enhanced Oral Bioavailability of Celecoxib Nanocrystalline Solid Dispersion based on Wet Media Milling Technique: Formulation, Optimization and In Vitro/In Vivo Evaluation, 2019 Pharmaceutics. 11 328. doi:10.3390/pharmaceutics11070328.

[156] Nanocomposix's guide to dynamic light scattering measurement and analysis, (n.d.). http://50.87.149.212/sites/default/files/nanoComposix Guidelines for DLS Measurements and Analysis.pdf (accessed August 30, 2017).

[157] C. Trabdafirescu, F. Borcan, C. Dehelean, Z. Szabadai, M. Nicolov, C. Soica, Study of the Interaction of Albendazole with Study of the Interaction of Albendazole with Benzoic Acid, 2016 Rev. Chim. 67 2370–2374.

[158] K. Das, D. Ray, N.R. Bandyopadhyay, S. Sengupta, Study of the Properties of Microcrystalline Cellulose Particles from Different Renewable Resources by XRD, FTIR, Nanoindentation, TGA and SEM, 2010 J. Polym. Environ. 18 355–363.

[159] U.S. Department of Health and Human Services (FDA), Dissolution Testing and Acceptance Criteria for Immediate-Release Solid Oral Dosage Form Drug Products Containing High Solubility Drug Substances Guidance for Industry, 2018 1074043 FNL. 1–5. https://www.fda.gov/regulatory-information/search-fda-guidance-documents/dissolution-testing-and-acceptance-criteria-immediate-release-solid-oral-dosage-form-drug-products (accessed December 10, 2020).

9. List of publications

9.1. Original publications related to the topic of the Ph.D. thesis

1. Fülöp Viktor, Balogh Emese, Jakab Géza, Antal István, A nanogyógyszerek és nanotechnológia formulálási vonatkozásai I. Bevezetés, biofarmáciai szempontok, 2016 Acta Pharmaceutica Hungarica 86:2 43-52.

2. Fulop V, Jakab G, Bozo T, Toth B, Endresik D, Balogh E, Kellermayer M, Antal I, Study on the dissolution improvement of albendazole using reconstitutable dry nanosuspension formulation, 2018 European Journal of Pharmaceutical Sciences 123, 70-78., https://doi.org/10.1016/j.ejps.2018.07.027

3. Fülöp, V., Jakab, G., Tóth, B., Balogh, E., Antal, I., "Study on Optimization of Wet Milling Process for the Development of Albendazole Containing Nanosuspension with Improved Dissolution, 2020 Periodica Polytechnica Chemical Engineering 64(4), 401-420, https://doi.org/10.3311/PPch.15569

9.2. Co-authored publications

1. Jakab G, Fülöp V, Sántha K, Szerőczei D, Balogh E, Antal I, Önemulgeáló hatóanyag-felszabadító rendszerek, mikroemulziók és nanoemulziók formulálási lehetőségei 2017, Acta Pharmaceutica Hungarica 87:1, 27-34.

2. Jakab Géza, Fülöp Viktor, Bozó Tamás, Balogh Emese, Kellermayer Miklós, Antal István, Optimization of Quality Attributes and Atomic Force Microscopy Imaging of Reconstituted Nanodroplets in Baicalin Loaded Self-Nanoemulsifying Formulations, 2018, Pharmaceutics 10:4, 275., https://doi.org/10.3390/pharmaceutics10040275

10. Acknowledgements

First of all, I would like to thank my supervisor Prof. István Antal for providing me the opportunity to continue my studies by joining the Ph.D. program called “Modern trends in pharmaceutical scientific research” of the Doctoral School of Pharmaceutical Sciences and to conduct my scientific researches at the Department of Pharmaceutics of the Semmelweis University Faculty of Pharmacy. I would like to express my deepest appreciation for the advices and corrections of Emese Balogh Ph.D. and Prof. István Antal, these were very helpful for the development of my data analyzing, summarizing and presentation skills. Special thanks to Prof. István Antal and György Pallós Dr. Pharm. for allowing participation in the development of various veterinary dosage forms, which vastly improved my knowledge on pharmaceutical formulation development and quality control. Also greatly appreciating the help of my colleagues from the department Géza Jakab Dr. Pharm. and Issameddin Aghrabi Dr. Pharm. during the milling experiments. I would like to thank Bence Tóth for giving me a helping hand during the DSC and Géza Jakab Dr. Pharm during the PXRD analysis. I would also like to thank assistant Katalin Jakab for helping me with the preparations of dissolution media and in vitro dissolution studies. To assistants Gabriella Biczók and Katalin Döme for helping me out and supporting me with excipients and membrane filters required for my research. I would like to express my utmost gratitude to Prof. Miklós Kellemayer and Tamás Bozó Ph.D. from the Department of Biophysics and Radiation Biology of the Semmelweis University Faculty of Medicine for helping me with the AFM morphological studies of microparticulate systems. Really appreciating the help of Tamás Igricz from the Department of Organic Chemistry and Technology of the University of Technology and Economics Budapest with the SEM morphological studies. Last, but not least, the love, the support and caring guidance of my family.